Canadian Beaufort Sea - Marine Ecosystem Assessment (CBS-MEA) annual report on the physical system - 2021

Ryan Galley, Andrea Niemi, Jane Eert, Andrew Majewski, and William Williams

Fisheries and Oceans Canada
Freshwater Institute
501 University Crescent
Winnipeg, Manitoba
Canada, R3T 2N6

2026

Canadian Technical Report of
Hydrography and Ocean Sciences 409

Fisheries and Oceans Canada | Pêches et Océans Canada

Canada

Canadian Technical Report of Hydrography and Ocean Sciences

Technical reports contain scientific and technical information of a type that represents a contribution to existing knowledge but which is not normally found in the primary literature. The subject matter is generally related to programs and interests of the Oceans and Science sectors of Fisheries and Oceans Canada.

Technical reports may be cited as full publications. The correct citation appears above the abstract of each report. Each report is abstracted in the data base *Aquatic Sciences and Fisheries Abstracts.*

Technical reports are produced regionally but are numbered nationally. Requests for individual reports will be filled by the issuing establishment listed on the front cover and title page.

Regional and headquarters establishments of Ocean Science and Surveys ceased publication of their various report series as of December 1981. A complete listing of these publications and the last number issued under each title are published in the *Canadian Journal of Fisheries and Aquatic Sciences*, Volume 38: Index to Publications 1981. The current series began with Report Number 1 in January 1982.

Rapport technique canadien sur l'hydrographie et les sciences océaniques

Les rapports techniques contiennent des renseignements scientifiques et techniques qui constituent une contribution aux connaissances actuelles mais que l'on ne trouve pas normalement dans les revues scientifiques. Le sujet est généralement rattaché aux programmes et intérêts des secteurs des Océans et des Sciences de Pêches et Océans Canada.

Les rapports techniques peuvent être cités comme des publications à part entière. Le titre exact figure au-dessus du résumé de chaque rapport. Les rapports techniques sont résumés dans la base de données *Résumés des sciences aquatiques et halieutiques*.

Les rapports techniques sont produits à l'échelon régional, mais numérotés à l'échelon national. Les demandes de rapports seront satisfaites par l'établissement auteur dont le nom figure sur la couverture et la page de titre.

Les établissements de l’ancien secteur des Sciences et Levés océaniques dans les régions et à l'administration centrale ont cessé de publier leurs diverses séries de rapports en décembre 1981. Vous trouverez dans l'index des publications du volume 38 du *Journal canadien des sciences halieutiques et aquatiques*, la liste de ces publications ainsi que le dernier numéro paru dans chaque catégorie. La nouvelle série a commencé avec la publication du rapport numéro 1 en janvier 1982.

Canadian Technical Report of
Hydrography and Ocean Sciences 409

2026

CANADIAN BEAUFORT SEA – MARINE ECOSYSTEM ASSESSMENT (CBS-MEA) ANNUAL REPORT ON THE PHYSICAL SYSTEM – 2021

by
Ryan Galley, Andrea Niemi, Jane Eert, Andrew Majewski, and William Williams

Fisheries and Oceans Canada
Freshwater Institute
501 University Crescent
Winnipeg, Manitoba
Canada, R3T 2N6

Cat. No. Fs.97-18/409E-PDF ISBN 978-0-660-97986-1 ISSN 1488-5417

Correct Citation for this publication:

Galley, R., Niemi, A., Eert, J., Majewski, A., and Williams, W. 2026. Canadian Beaufort Sea - Marine Ecosystem Assessment (CBS-MEA) annual report on the physical system - 2021. Can. Tech. Rep. Hydrogr. Ocean Sci. 409: ix + 103 p.

CONTENTS

List of Figures

List of Tables

ABSTRACT

Galley, R., Niemi, A., Eert, J., Majewski, A., and Williams, W. 2026. Canadian Beaufort Sea - Marine Ecosystem Assessment (CBS-MEA) annual report on the physical system - 2021. Can. Tech. Rep. Hydrogr. Ocean Sci. 409: ix + 103 p.

The Beaufort Regional Environmental Assessment – Marine Fishes Project (BREA-MFP, 2012-2014), and more recently the Canadian Beaufort Sea – Marine Environmental Assessment (CBS-MEA) program (2017-present), seek to create and annually augment regional ecological knowledge, with the support and collaboration of Inuvialuit communities and the Inuvialuit Game Council. CBS-MEA integrates physical oceanography with marine food web parameters on an annual basis, with the long-term goal of characterizing interannual variability and change in the ecosystem. Conductivity-Temperature-Depth (CTD) data from August and September 2021 reveal the end-of-summer physical oceanographic characteristics in the region based on profiles of temperature, salinity, potential density, Brunt-Väisälä frequency squared (N^2), temperature-salinity plots, and temperature and salinity sections, as well as derived surface mixed layer depth and the ocean heat content and freshwater content in the surface mixed layer at 49 stations. We further set these oceanographic observations in the context of the annual evolution of air temperature, sea level pressure, winds, and sea ice concentration and motion in the region. Anomalously warm winter air temperatures and anomalous atmospheric forcing in winter enhanced sea ice transport into the region in 2021, and contributed to significant sea ice mobility and lead presence in Amundsen Gulf. Old sea ice was advected into the region from the north through spring, reducing negative total sea ice concentration anomalies along the Mackenzie shelf and in southern and eastern Amundsen Gulf in spring. Summer was relatively cool with sea ice import-favorable atmospheric forcing, dynamically slowing summer sea ice loss. Anomalously warm air temperatures and export-favorable atmospheric forcing in autumn continually removed new locally-forming sea ice from the region, delaying both freeze up and thickening of sea ice in place.

RÉSUMÉ

Galley, R., Niemi, A., Eert, J., Majewski, A., and Williams, W. 2026. Canadian Beaufort Sea - Marine Ecosystem Assessment (CBS-MEA) annual report on the physical system - 2021. Can. Tech. Rep. Hydrogr. Ocean Sci. 409: ix + 103 p.

Le projet d'évaluation environnementale régionale de Beaufort – Poissons marins (BREA-MFP, 2012-2014) et, plus récemment, le programme canadien d'évaluation environnementale marine de la mer de Beaufort (CBS-MEA) (2017-présent) visent à créer et à enrichir chaque année les connaissances écologiques régionales, avec le soutien et la collaboration des communautés inuvialuites et du Conseil inuvialuit de la chasse et de la pêche. Le programme CBS-MEA intègre chaque année l'océanographie physique et les paramètres du réseau trophique marin, dans le but à long terme de caractériser la variabilité interannuelle et les changements dans l'écosystème. Les données de conductivité, de température et de profondeur (CTD) recueillies en août et septembre 2021 révèlent les caractéristiques océanographiques physiques de fin d'été dans la région, sur la base des profils de température, de salinité, de densité potentielle, fréquence de Brunt-Väisälä au carré (N^2), des graphiques de température-salinité et des sections de température et de salinité, ainsi que de la profondeur dérivée de la couche de mélange superficielle et de la teneur en chaleur et en eau douce de l'océan dans la couche de mélange superficielle à 49 stations. Nous avons ensuite replacé ces observations océanographiques dans le contexte de l'évolution annuelle de la température de l'air, de la pression au niveau de la mer, des vents, ainsi que de la concentration et du mouvement de la glace de mer dans la région. Les températures hivernales anormalement élevées et les forces atmosphériques inhabituelles pendant l'hiver ont favorisé le transport de la glace de mer vers la région en 2021 et ont contribué à une mobilité importante de la glace de mer et à la présence de chenaux dans le golfe d'Amundsen. La vieille glace de mer a été transportée dans la région depuis le nord tout au long du printemps, réduisant ainsi les anomalies négatives de la concentration totale de glace de mer le long du plateau Mackenzie et dans le sud et l'est du golfe Amundsen au printemps. L'été a été relativement frais, avec un forçage atmosphérique favorable à l'importation de glace de mer, ce qui a ralenti de manière dynamique la perte de glace de mer estivale. Les températures de l'air anormalement chaudes et le forçage atmosphérique favorable à l'exportation en automne ont continuellement éliminé la nouvelle glace de mer qui se formait localement dans la région, retardant à la fois le gel et l'épaississement de la glace de mer en place.

1. Introduction

In 2021, the Arctic continued to warm at a rate far exceeding that of temperate latitudes. The average Arctic surface air temperature in 2021 was in the top ten all time to that point, and the Arctic multiyear sea ice volume post-winter 2021 was very low. Recent work sought to explain anomalous Arctic sea ice transport in 2020 and 2021, indicating extremely high sea level pressure over the central Arctic forced highly positively anomalous wind forcing that advected old sea ice from the central Arctic into the Beaufort Sea (Mallet et al., 2021) where it is prone to melt (e.g., Perovich and Richter-Menge, 2009). Winter (December-January-February) of 2020-2021 had the second highest sea level pressure north of 60°N since 1979 (Mallet et al., 2021), creating forcing that flushed first-year sea ice out of the Beaufort Sea to the west, and imported multiyear sea ice into the Beaufort from the north (Moore et al., 2022). This resulted in 23.5% of the entire Arctic's multiyear sea ice residing in the Beaufort at the end of winter 2021, the largest proportion of the Arctic's multiyear sea ice in the Beaufort Sea at the end of winter since 1984 (Mallet et al., 2021).

Fisheries and Oceans Canada (DFO) continues to help build marine ecosystem-based approaches to marine measures and resource management through comprehensive assessment of the biology and habitats of the Beaufort Sea and Amundsen Gulf in the Inuvialuit Settlement Region. The Canadian Beaufort Sea – Marine Ecosystem Assessment (CBS-MEA) program (2017-present), provides an increasingly complete understanding of spatial and temporal processes affecting and controlling the regional ecosystem, following on from the Beaufort Regional Environmental Assessment - Marine Fishes Project (BREA-MFP) in 2012-2014 and earlier ArcticNet work in the region. The CBS-MEA program pursues understanding of linkages within the regional physical system, as well as physical-biological linkages inter-annually and in the long-term. The CBS-MEA provides information relevant to the six Inuvialuit Settlement Region communities in the area, including variables related to elements of the regional marine food web, from phytoplankton to belugas and bowhead whales.

In this report, we present atmospheric and sea ice information over an annual cycle to provide context for physical oceanographic observations recorded in August and September of 2021. We explain basic physical forcing and processes over one year in a study region that broadly encompasses the Canadian Beaufort Sea, the Mackenzie Shelf, and Amundsen Gulf, roughly bounded by longitudes -145°E to -110°E and latitudes 68°N to 75°N. The study region overlaps the Inuvialuit Settlement Region, and includes the Anguniaqvia niqiqyuma (Niemi et al., 2020) and Tarium Niryutait (DFO, 2010) Marine Protected Areas, as

well as a number of ecologically and biologically significant areas (EBSAs, e.g. DFO, 2014), and the Cape Bathurst Flaw Lead Polynya Complex (see for e.g. Stirling, 1980).

2. Data and Methods

This assessment of physical conditions and drivers in the Inuvialuit Settlement Region of Canada's western Arctic during 2021 includes air temperature, sea level pressure, winds, and solar radiation at the ocean surface, reanalysis products, sea ice concentration and motion data, and the ship-based oceanographic data of the CBS-MEA program. Climatological averages (over the period 1983-2010) were calculated to determine how anomalous the conditions were in 2021. CTD data collected in August and September of 2021 in the region were used to identify the surface salinity and temperature, calculate the thickness of the ocean surface mixed layer at sampling stations, and to determine the ocean heat and freshwater content of that layer. These CTD profile data were also used to create the cross-sectional oceanographic plots presented.

2.1 Environmental Forcing

European Centre for Medium-range Weather Forecasts (ECMWF) Reanalysis v5 (ERA5) data, specifically 2-m air temperature, sea level pressure, 10-m u- and v- winds, and surface solar radiation downwards (SSRD) data at six-hourly intervals from January 1, 1983 to December 31, 2021 (Hersbach et al., 2018) were obtained from the Copernicus Climate Change Service Climate Data Store (https://cds.climate.copernicus.eu/cdsapp#!/dataset/reanalysis-era5-pressure-levels?tab=overview). Monthly averages of 2-m air temperature, sea level pressure, and 10-m wind speed and direction were created for each of the 4089 grid cells in the study region for each month of 39 years (1983-2021). Monthly climatological standard normals (i.e. averages) for 2-m air temperature, sea level pressure, 10-m winds were produced from all the data in each month in 1983-2010 (28 years; note 28 years are employed for this period ending in 2010 in order to maintain consistency with the sea ice data which begins in 1983. See below for further explanation). Monthly anomalies in 2021 were calculated using the monthly climatological standard normal:

$$T_{a\ anomaly} = T_a - T_{a\ clim} \quad (1)$$

where $T_{a\ anomaly}$ is the air temperature anomaly in a month in a year, T_a is the average air temperature in a month in a year, and $T_{a\ clim}$ is the climatological average air temperature for the month (for 1983-2010). Positive anomalies occur when the monthly average air temperature is greater than the climatological

standard normal for that month, negative anomalies occur when the monthly average is lower than the climatological standard normal for the month.

2.2 Sea Ice Concentration and motion

Monthly average sea ice concentration maps for 1983-2021 were created by downloading and gridding regional Canadian Ice Service (CIS) digital archive data for the western Arctic freely available at https://iceweb1.cis.ec.gc.ca/Archive/page1.xhtml?lang=en at 1-km resolution on the CIS Lambert conformal conic projection (https://www.canada.ca/en/environment-climate-change/services/ice-forecasts-observations/latest-conditions/archive-overview/information-about-data.html). Analysis of the CIS data was initiated no earlier than 1983 because the CIS data is broken down by consistent source data and preparation method eras, and the quality index prior to 1983 is reduced (please see Tivy et al., 2011 for detailed information on the CIS data quality indices). Using all the available CIS charts in each month in each year, the monthly mean total sea ice concentration (in tenths) and mean partial concentrations (tenths) for old ice (a superset of second year and multiyear sea ice), first-year sea ice, and new-plus-young sea ice (i.e. all sea ice < 30 cm thick) stages of development were computed at 1-km resolution (see Fequet, 2005 for details on sea ice stages of development). Monthly climatological averages for total sea ice concentration as well as old sea ice, first-year sea ice, and new-plus-young sea ice were calculated by averaging all the data in each month between 1983 and 2010 inclusive. Monthly anomalies in each year for total, old, first-year, and new-plus-young ice concentrations were created by subtracting the months' climatological (1983-2010) average sea ice concentration from the corresponding monthly average concentration for each stage of development.

Monthly average sea ice velocity and direction in the Beaufort Sea from 1983 to 2021 were calculated from the National Snow and Ice Data Centre Polar Pathfinder Daily 25-km EASE-grid sea ice motion vector data (Version 4) for the northern hemisphere, freely available at https://nsidc.org/data/NSIDC-0116 (Tschudi et al., 2019). Climatological monthly averages were created using the u- and v- vector components for each month between 1983 and 2010 (inclusive). Monthly anomalies for each year were created by subtracting the monthly climatological average u- and v- components of the sea ice motion from the monthly average sea ice motion u- and v- components in each year.

2.3 Sea ice-adjusted Surface Solar Radiation Downwards

ECMWF ERA5 surface solar radiation downwards (SSRD, in J m^{-2}) data at six-hourly intervals between 1983 and 2021 (inclusive) was employed for this analysis. SSRD is the amount of shortwave radiation (including

both diffuse and direct radiation) that reaches a horizontal plane at the surface of the earth; it is the model equivalent of the amount of shortwave radiation a pyranometer would measure at the surface. In this case in particular, SSRD may be thought of as light energy from the sun that turns to heat energy if it is absorbed by the surface, either melting surrounding sea ice, or contributing to increased water temperatures. The SSRD must be adjusted for sea ice cover to approximate the amount of solar radiation incident on the ocean surface in the Arctic marine environment (unimpeded by sea ice). In each month of each year between 1983-2021, the CIS monthly mean total sea ice concentration grid was downscaled to the same resolution of the ERA5 grid, divided by 10 to obtain a fractional coverage, and then subtracted from unity to obtain the monthly fractional open water area in each grid cell. The fractional open water area in a month was multiplied by the mean SSRD for the month to obtain the sea-ice adjusted SSRD ($J\ m^{-2}$) incident on the ocean surface in each grid cell. Monthly climatological averages over the period 1983-2010 were calculated using the sea-ice adjusted monthly mean SSRD, and monthly anomalies of sea-ice adjusted SSRD were calculated for each month in each year between 1983 and 2021.

2.4 The CBS-MEA Sampling

Physical oceanographic sampling in the region was undertaken between 5 August and 3 September 2021 from *FV Frosti* at stations in central Amundsen Gulf, Darnley Bay, Dolphin and Union Strait, Prince Albert Sound, Minto Inlet, Jesse Bay, De Salis Bay, and approaching the community of Ulukhaktok, N.W.T. Conductivity, temperature, and depth (CTD) measurements were made using a Seabird SBE 911plus deployed as part of the ships' CTD-Rosette system. Average salinity (PSS-78) and temperature (ITS-90, °C) over 1 decibar (approximately one meter) increments were output after the CTD data underwent quality assurance and control (bottle salinity samples were collected with the rosette and used as part of data QA/QC process, and salinity is considered to be accurate within ±0.003). An altimeter was employed for water depth measurements, and the noted depth at each station was the median of the deepest two meters recorded. In the absence of altimetric measurements at a station, the deepest depth measured by the CTD was used.

Potential density referenced to the surface ((σ, θ), minus 1000 $kg\ m^{-3}$) and N^2 (the square of the buoyancy frequency, (s^{-2})), were calculated for each depth using the OCE package (Kelley, 2018) for R (R Core Team, 2022). The topmost surface value of temperature and salinity at 49 stations in 2021 were mapped. The depth of maximum N^2 was identified in each profile, and that value was used to connote the bottom of the surface layer of the ocean column. The N^2-maximum surface layer depth at each of the 49 stations was used to integrate the total freshwater content (FWC, in meters) and the total ocean heat content

(OHC, in kilojoules), in a 1 m^2 column of water to the depth of the surface layer. The FWC was calculated at each decibar depth interval of the column specified by the maximum N^2 depth:

$$FWC = \frac{S_o - S}{S_o} \quad (2)$$

where S_o is the reference salinity of 34.8, and S is the salinity at each depth interval and the FWC at each depth were summed. The OHC relative to 0°C was calculated at each decibar depth interval of the column specified by the maximum N^2 depth:

$$OHC = c_{sw} \times \rho \times \Theta \quad (3)$$

where c_{sw} is the specific heat capacity of seawater (set to 4 kJ $kg^{-1}K^{-1}$ for the observed temperature and salinity ranges after Sharqawy et al., 2010), ρ is seawater density (kg m^{-3}) calculated using absolute salinity and conservative temperature, and Θ is conservative temperature (°C). The OHC at each depth interval in the surface layer was then summed.

3. Results and Discussion

Air temperature, sea level pressure (SLP), wind, sea ice concentration and motion, and sea-ice-adjusted surface solar radiation results and discussion are presented by season with winter (January February, March), spring (April, May, June), and summer (July, August, September), summarizing key processes and physical drivers prior to and during the CBS-MEA cruise, 5 August - 3 September 2021. Finally, autumn (October, November, December) conditions are presented to provide the full annual perspective of temperature, SLP, sea ice concentration and motion, and solar radiation during freeze up and consolidation of the ice pack.

3.1 Winter

In January, February, and March of 2021, most of the study region was warmer than -25 °C, except for Banks and Victoria Islands (Figure 1). The 2-m air temperature anomalies for winter 2021 show that much of the region was more than 5 °C warmer than the climatological average (1983-2010) (Figure 2). Winter in the region is typically characterized by low sea level pressure (SLP) in the southwest as one advances towards the Aleutian Low, and high SLP in the northwest (i.e. the Beaufort High), and high SLP over the north continental coast. In January and March 2021, the SLP pattern in the region (Figure 3) was very

similar to the climatological mean (Figure 4), while in February 2021 the SLP departed from the climatological pattern with low SLP in the northeast over M'Clure Strait, and high SLP over the mainland coast west of the Mackenzie River (Figures 3, 4). Following on from the regional SLP, the wind speed and direction in the region in winter 2021 varied little from the climatological average in January and March (Figure 5). However, the wind field was highly anomalous in February 2021, when high velocity westerly winds occurred in the region (Figure 5, 6).

In winter 2021, as in all winters, the study region was completely covered by sea ice, which was mobile in the Canadian Beaufort Sea and all of Amundsen Gulf (Figure 7). Landfast sea ice ($10/10^{ths}$ concentration) covered Dolphin and Union Strait, a small band along the Mackenzie Shelf, and the smaller coastal bays surrounding Amundsen Gulf (Figure 7). Mobile sea ice in the Beaufort Sea in winter 2021 was composed of mostly old ice in the northwest, and mostly first-year sea ice in the southeast on the shelf and into Amundsen Gulf. New-plus-young sea ice (< 30cm thick), representing areas of divergence in the regional sea ice cover, was found mostly in the Cape Bathurst Flaw Lead Polynya complex (Figure 7). Sea ice anomalies (compared to the 1983-2010 period) indicate that there was more old ice than average in the south and east edges of the old ice pack and consequently less first-year sea ice in those areas than in the long-term average (Figure 8). The sea ice anomaly maps for winter 2021 also indicate increased presence of new-plus-young sea ice in the flaw lead along the Mackenzie Shelf, in the circumference of Amundsen Gulf, and along the west coast of Banks Island (Figures 7, 8). This is likely owing to the wind direction and speed in January (Figures 5, 6) and substantiating that sea ice was mobile within the entirety of Amundsen Gulf in winter 2021. Regional sea ice motion indicated substantial positive velocity anomalies in January 2021, rapidly exporting sea ice westward through the southern part of the study area (Figures 15, 16), likely contributing to sea ice divergence that generated substantial areas of new-plus-young sea ice in January 2021. In February typical anticyclonic (clockwise) sea ice motion slowed to below climatologically average velocities (Figures 15, 16), allowing some areas of new-plus-young sea ice to thicken to the first-year stage of development (Figure 7).

3.2 Spring

The study region warmed through spring 2021 (April, May, and June), resulting in below-freezing temperatures over the marine portions of the region and Banks and Victoria Islands, while the mainland warmed from below -15 °C to > 6 °C on average in June (Figure 1). In spring, much of the study region was colder than the climatological averages for April, May and June (Figure 2) with the exception of an area near the mouth of the Mackenzie River in June. This warm anomaly corresponds geographically with a

reduction in total sea ice concentration in June in the same area which would have allowed heat from the relatively warm ocean into the atmosphere. In June, land areas in the region became warmer than the marine areas (Figure 1). In spring 2021, the SLP pattern over the region experienced departure from the climatological average; in April and May, low SLP bookended the region in the southwest and northeast, while the highest regional SLP was in the northwest (Figure 3). In June, the location of the High shifted from its climatological typical position in the Beaufort Sea to the east over Victoria Island (Figure 3). Spring winds were slower than the 1983-2010 average in April, blowing from the northeast over the western part of the study area, anomalously blowing from the northwest into Amundsen Gulf over the eastern half of region (Figures 5, 6). In May 2021, the wind direction (Figure 5) was more typical of the climatological average, but the wind speed was positively anomalous over most of the study area (Figure 6). In June 2021, the SLP pattern gave rise to an uniquely anomalous wind direction field (Figure 5) from a ridge that divided the region from northwest to southeast across the Beaufort; climatologically the June wind field is anticyclonic, blowing out of Amundsen Gulf. So, the June 2021 wind anomalies were significant (Figure 6).

The regional sea ice cover was complete in April, save for the aforementioned small area of reduced concentration on-shelf just west of the Mackenzie River mouth (Figure 9). As a result of this total sea ice concentration reduction, this small area showed sea ice-adjusted surface solar radiation downwards (SSRD) at the ocean surface for the first time in 2021 in April (Figure 17). In May, it is notable that an anomalous decrease in the ice concentration in the Canada Basin northwest of Amundsen Gulf occurred, and persisted into June (Figures 9, 10), likely caused by divergence resulting from anomalously strong winds in May (Figure 5). Break-up began in the Cape Bathurst Flaw Lead Polynya complex in May and continued into June 2021 (Figure 9). Break-up was earlier than the climatological average in 2021 and negative total sea ice concentration anomalies occurred along much of the continental coast and in western Amundsen Gulf (Figure 10). Anomalous new-plus-young ice concentration was present in May 2021 in the flaw lead areas along the Mackenzie Shelf and west of Banks Island, and in eastern Amundsen Gulf (Figures 9, 10) due to early break-up and air temperatures that were still favorable for ice formation (Figure 1). Early break-up in 2021 exposed open water areas in the Canada Basin and in the Cape Bathurst Flaw Lead Polynya complex to substantial positive sea ice-adjusted SSRD anomalies in May and June (Figures 17, 18). In April 2021, sea ice motion was relatively quiescent in the region (Figure 15), moving anticyclonically at velocities slower than the climatological average (Figure 16). However, in May sea ice motion velocities increased substantially while maintaining their climatologically average anticyclonic pattern in the region with enhanced, larger than average westward export velocities from the region

compared to import velocities from the north (Figures 15, 16). This likely contributed to the observed early break-up (Figures 9, 10) in 2021. In June, an area of anomalously high sea ice velocity was observed in the predominantly old sea ice pack (Figures 15, 16), moving that ice east toward the coast of Banks Island and toward the mouth of Amundsen Gulf faster than ice in the southern end of the region could be exported to the west. This convergent scenario near the mouth of Amundsen Gulf caused accumulation of first-year sea ice in the area during June (Figure 9, 10).

3.3 Summer

July, August, and September (summer) 2-m air temperatures indicate that July had the highest temperatures in 2021, but that much of the marine area of the study region remained colder than the terrestrial area until September (Figure 1). Much of the region, both marine and terrestrial, experienced cooler than average air temperatures in July, August and September (Figure 2); warm anomalies were not pervasive, though they did occur at the Mackenzie River mouth and eastern Amundsen Gulf in July, the Mackenzie River mouth and Dolphin and Union Strait in August, and the northwest corner of the study region in the Beaufort Sea in September (Figure 2).

The SLP was anomalous in July 2021. Instead of the typical Beaufort High over the northwest of the region, the highest SLP was in the southwest near the mouth of the Mackenzie River, with low pressure in the north and northeast (Figures 3, 4). July 2021, SLP reversal is clearly indicated in the anomaly map (Figure 4). The anomalous SLP pattern in July 2021 resulted in westerly and northwesterly winds throughout the region (Figure 5), which were anomalous in both speed and direction (Figure 6) compared to the 1983-2010 period. In August and September 2021, the Beaufort High was located in a more climatologically typical position, with lower SLP in the northeast and southwest corners of the study region (Figure 3). In August 2021, observed westerly winds were typical in their direction, while their velocities were greater than average (Figure 5, 6). In September 2021, winds in the region were much faster than average and their direction was generally from the northwest to the southeast (Figure 5). These winds varied substantially from the climatological average (Figure 6) especially in the eastern half of the study region.

Regional sea ice break-up and melt continued into summer 2021 (Figure 11), with below normal total sea ice concentrations along the Mackenzie Shelf and in Amundsen Gulf in July (Figure 12). In contrast, positive total sea ice anomalies occurred in the Canada Basin and within the typical zone of transition from the old ice pack in the northwest to the predominantly first-year sea ice areas in the south and east (Figures 11, 12). Positive total sea ice anomalies at the edges of the summer ice pack in the Beaufort were composed

of lower than normal concentrations of old ice which were more than offset by higher than average first-year sea ice concentrations (Figure 12). Negative total sea ice anomalies along the Mackenzie Shelf and in Amundsen Gulf in July corresponded to enhanced positive anomalous sea ice-adjusted SSRD in July (Figures 17, 18), while positive total sea ice anomalies along the west coast of Banks Island corresponded to negative SSRD anomalies in the same month (Figure 18). Despite cooler than average air temperatures in September 2021, very little sea ice was left in the region (Figure 11). In July 2021 the pattern and velocity of sea ice motion was similar to June (Figure 15), concentrating old ice against the coast of Banks Island, and maintaining high concentrations of first-year sea ice at the southeast edge of the Beaufort Sea ice pack (Figure 11). As a result, there were negative anomalies in sea ice-adjusted SSRD along the west coast of Banks Island, and near the mouth of Amundsen Gulf in July (Figure 18). In August 2021, the sea ice-adjusted SSRD in the region was lower than the climatological (1983-2010) mean values (Figure 18); less solar energy than average reached the ocean surface in much of the study region in August 2021.

In order to relate some indication of the potential for solar energy accumulation in the ocean surface prior to and during the physical oceanographic observations in August and September 2021, the (i) mean sea ice-adjusted SSRD in each month in 2021 from January to August and (ii) the anomaly of the accumulated sea ice-adjusted SSRD compared to the 1983-2010 period were calculated for each grid cell in the study region (Figure 19). Prior to September, the open water areas in the southern arm of the Cape Bathurst Flaw Lead Polynya Complex and much of eastern Amundsen Gulf had the opportunity to accumulate substantial and positively anomalous amounts of solar energy that may have heated the upper ocean (Figure 19). This energy was mostly received by open water in May, June, and July (Figure 18). However, these sea ice-adjusted SSRD accumulation results for the Jan-Aug 2021 period (Figure 19) also indicate that the ocean surface west of Banks Island and across the mouth of Amundsen Gulf received less solar energy between January and August 2021 than the climatological average amount, shown by negative accumulated sea ice-adjusted SSRD anomalies (Figure 19). However, in September 2021, the sea ice motion pattern changed to westerly movement (Figure 15) at anomalously high velocities (Figure 16) that drove the southern tip of a longitudinal band of high concentration old and first-year sea ice westward across the region from the southwest corner of Banks Island and completely cleared Amundsen Gulf of sea ice (Figure 11). This ice motion scenario led to positively anomalous sea ice-adjusted SSRD along the west coast of Banks Island in September (Figures 17, 18).

3.3.1 Summer ocean conditions

Oceanographic sampling at the end of summer (5 August - 3 September 2021) occurred at the stations in Figure 21. The lowest ocean surface temperature in the Amundsen Gulf region was <1 °C at the north end of the CPY transect (station CPY_ICE01, Figure 22a) due to melting sea ice in the immediate vicinity acting to cool the surface of the ocean. At this location, a cool surface layer 8 m deep overlaid a much warmer water layer (12-15 m thick) with a maximum temperature of more than 3 °C (See Appendix A, page 96 for CPY_ICE01 profile). CTD data at CPY-ICE01 indicated that the water column was warm from the surface to a depth > 20 m prior to sea ice entering the area and was cool at the very surface only. The maximum sea surface temperature in the region was 6.60 °C in the southwest corner of Prince Albert Sound (PAS_05A) (Figure 22a, Table 1). The mean sea surface temperature in the Amundsen Gulf region in 2021 was 4.48 °C (standard deviation = 1.35). End-of-summer surface salinity was lowest in De Salis Bay (22.20, Figure 22b), and highest (29.85) offshore of Ulukhaktok at station ULU_8.1 (Figure 22b, Table 1). The mean surface salinity in 2021 was 27.36, (standard deviation = 1.78). Appendix A contains profile plots of salinity, temperature, potential density and N^2, along with T-S plots and locations for each of the stations in 2021.

The surface layer depth (the depth of the N^2 maximum) in the Amundsen Gulf region was variable at the end of summer 2021, ranging between 2 m near Ulukhaktok to 38 m at the east end of Dolphin and Union Strait (Figure 23a) (mean = 15.8 m, standard deviation = 8.5 m). Relatively thin surface layers occurred in shallow, coastal areas including the Ulukhaktok section, Minto Inlet, Jesse Bay, and De Salis Bay, as well as at the two deeper central Amundsen Gulf (AMG) stations (Figure 23a). Unsurprisingly, the station with the thinnest surface layer (ULU_8.2) contained the least ocean heat content in 2021 (Figure 23b, Table 1). The greatest ocean heat content in the defined surface layer, 886 kJ, occurred at the east end of Dolphin and Union Strait at station DUS_11 where the surface layer was the thickest (Figure 23a, b, Table 1). The mean ocean heat content in the defined surface layer in the region in 2021 was 269 kJ, with a standard deviation of 207.8 kJ. Once reason the surface layer ocean heat content is important because that is the amount of heat the ocean must lose to the atmosphere prior to ice formation in the autumn, substantially affecting freeze-up timing and end-of-winter sea ice thickness in the next spring. Stations ULU_8.2 and MTI_03 also contained the least amount of freshwater in the defined surface layer (Figure 23c, Table 1) while DUS_11 contained the greatest freshwater content (6.03 m) in the defined surface layer (Figure 23c, Table 1). The mean freshwater content in the defined surface layer in 2021 in the region was 2.67 m, with a standard deviation of 1.59 m.

Salinity and temperature across Dolphin and Union Strait (DUS) from west to east are presented in section view in Figure 24 for the full depth (Figure 24a, c) and for the top 50 m (Figure 24b, d). The mean N^2-defined surface layer across Dolphin and Union Strait is 20 m, though it is more shallow in the center of the Strait (6 m at DUS_06), and deeper closer to both the continental coast in the west (23 m at DUS_01), and the coast of Victoria Island in the east (38 m at DUS_11). In the full depth section (Figure 24a, c), the summer surface mixed layer overlies Pacific Water (salinity 31 to 33.5), which overlies water of Atlantic origin (salinity > 33.8). Upon closer inspection of the near-surface (<50-m deep) waters (Figure 24 b, d), the surface layer was between 4-6 °C with a salinity of 28.5-30. The warm, fresh water at the surface is thickest at the coasts, and thinner in the middle of the Strait – it is especially thick at the eastern end of the section (DUS_11), which may be due to local westerly winds prior to and/or during the oceanographic survey of the area.

Prince Albert Sound contained three sections in 2021 (Figure 21a), a section from south-to-north on the west end of the Sound (Figure 25), a south-to-north section at the east end of the Sound (Figure 26), and a section from the mouth of the Sound in the west into the Sound toward Victoria Island (Figure 27). The mean N^2-derived surface layer depth was 23.2 m across the mouth of Prince Albert Sound from south to north; the maximum surface layer thickness was 33 m at the south end of the section (PAS_05a). The surface layer was between 5-6 °C with salinity of 28-30 (Figure 25). Accumulation of fresh, warm water was also observed at the south end of this section, proximal to same at the east end of the Dolphin and Union section (Figure 24), though the thickness of the surface water was much more uniform in west Prince Albert Sound (Figure 25). Across inner Prince Albert Sound from south to north (Figure 26), the N^2-derived surface layer was much thicker at the south end of the section (22 m at PAS_11) than at the north end of the section (9 m at PAS_09) (Table 1). Heat in the surface layer in inner Prince Albert Sound was relatively evenly distributed with a subtle accumulation at the south end (Figure 26c), while the salinity was heterogeneously distributed (Figure 26b). Salinity was 29 or greater at the south end of the section, while freshwater accumulated at the north end the section where the salinity was < 24 (Figure 26b). The mean N^2-derived surface layer from west to east into Prince Albert Sound was 10.3 m, from 20 m at PAS_02 at the mouth of Prince Albert Sound to 3 m at PAS_10 in the center of the inner S-N section. Heat was distributed relatively uniformly from west to east in the surface layer that was 4-6 °C (figure 27d), while the salinity was lowest (~23.5) in the center of the section at PAS_HC4 and much higher (>28) at the west and east ends of this section (Figure 27b).

A short (~10 km) section (Figure 28) composed of four stations (ULU 08, ULU_8.3, ULU_8.2, ULU_8.1) (Figure 21a) from south to north was undertaken south of Ulukhaktok, N.W.T. The N^2-derived surface layer was deepest at ULU_08 (15 m) and ULU_8.1 (10 m) at the south and north ends of the section, and much thinner (3 and 2 m) in the two middle stations (Table 1). These surface layer thickness values reflect the distribution of near-surface freshwater and heat (Figure 28). At the south end of the section, the deep surface layer was relatively less saline (~28) than the rest of the section and was 3-5 °C (Figure 28b, d). In the center of the section there was little heat or freshwater at the surface. At the north end of the section closest to Ulukhaktok, there was heat but little freshwater in the 10 m surface layer (Figure 28, Table 1).

In Minto Inlet (Figure 21a) five stations over ~17 km from south to north were sampled in 2021, and their mean N^2-derived surface layer thickness was 7 m (range 5-10 m) (Table 1). However, CTD data in Minto Inlet are presented with the caveat that much if not all the data above the surface layer thickness is missing due to quality control/quality assurance (Figure 29, profiles in Appendix A). Despite this limitation, it is obvious that Minto Inlet contained substantial heat down to 15-20 m depth that was relatively evenly distributed from south to north (Figure 29d), and contained some freshwater at the surface (salinity < 27) at the north end of the section (Figure 29b).

Two shallow stations were sampled in Jesse Bay on the east coast of Banks Island near the mouth of Prince of Wales Strait, yielding a N^2-derived surface layer depths of 7 m and 9 m moving southeast out of the Bay. The surface waters of Jesse Bay were relatively fresh, and became fresher moving away from Banks Island where the 9 m surface layer was less saline than 24 (Figure 30a). Heat was concentrated in the N^2-derived surface layer across Jesse Bay though not to the magnitude of the stations further south (Table 1). Shallow stations in De Salis Bay on the southeast coast of Banks Island had thinner surface layers (6 and 5 m), and the temperature of the water in the surface water of De Salis Bay was fresher (Figure 31a) and much warmer (Figure 31b) than in Jesse Bay. On the southwest coast of Banks Island, four Cape Bathurst stations were sampled in 2021 (Figure 21a, Table 1) from south to north. In section, the CTD data from the Cape Bathurst stations showed freshwater accumulation near the coast of Banks Island (Figure 32a, b), and substantial heat (3-5 °C) in the N^2-derived surface layer that thickened towards the coast of Banks Island (Figure 32c, d).

In central Amundsen Gulf, the two stations sampled (AMG_03 in the south and AMG_HC01 in the north) had N^2-derived surface layer thicknesses of 14 and 10 m, respectively. A small increase in salinity occurred from south to north as the surface layer thinned (Figure 33b), while heat content increased from south to

north in this section with water temperatures > 5 °C closest to the coast of Banks Island, and cooler surface layer temperatures moving away from the coast (Figure 33c, d, Table 1).

In Darnley Bay, there were three Bennett Point (BPT) stations sampled in 2021 (Figure 21a) where the N^2-derived surface layer was relatively thick (19-22 m) over a narrow range. From west to east, the lower salinity surface layer (salinity ~28) was homogenous across Darnley Bay, as was the temperature (>5 °C) (Figure 33). However, the surface water closest to Cape Parry on the west end of Darnley Bay was fresher (though not really low in the context of the whole region), and slightly cooler than elsewhere across the section (Figure 34).

Working from south to north along the Cape Parry (CPY) section/stations (Figure 21a, Figure 35), the two stations closest to Cape Parry had N^2-derived surface layer thicknesses of 31 m and 21 m (Table 1). The thick surface layer at the south end of the Cape Parry section was more saline (Figure 35a, b) than the thinner surface layer depths northward, though the temperature of the top 30 m at the south end of the section was very warm (4-6 °C). The two CPY stations farther north offshore had thinner surface layers due to the presence of sea ice that had obviously cooled the very surface at those stations, affecting the stratification and more specifically the temperature with depth (Figure 35c, d).

3.4 Autumn

In autumn 2021 (October, November, and December) air temperatures in the study region cooled steadily (Figure 1). Banks and Victoria Islands experienced the coldest air temperatures, while summer open water areas experienced the warmest air temperatures (Figure 1), likely in part due to the heat transferred to the atmosphere by autumn oceanic cooling (Figure 13). Positive 2-m air temperature anomalies over the study region in autumn 2021 (Figure 2) indicate that most of the region was much warmer in 2021 than the climatological (1983-2010) average.

In autumn 2021, the SLP in the region was characterized by high SLP in the north and northeast, with lower pressure in the southwest, similar to the climatological average pattern in October and November. As a result, the wind direction over those months in 2021 was similar to the climatological average, albeit with anomalously enhanced speeds (Figures 5, 6). However, in December 2021 the SLP was greatest in the northeast over M'Clure Strait, straying from its climatological average position in the northwest in that month (Figure 3). This resulted in a December 2021 wind field composed primarily of easterly winds (Figure 5), which lack the typical anticyclonic nature of the wind climatology for December (Figure 6).

Sea ice formation began in autumn 2021 within relatively high total sea ice concentration areas in the northwest where old ice remained after summer (first-year sea ice that survives through September is re-categorized as old ice on October 1). Positive new-plus-young sea ice anomalies were spatially coincident with negative old ice anomalies in October (Figure 14); new-plus-young sea ice filled areas that were typically covered in old ice. Reduced sea ice in October 2021 resulted in positively anomalous sea ice-adjusted SSRD at the open water surface (Figure 18) though the absolute values of October SSRD were relatively low (Figure 17) due to seasonal constraint on the total amount of sun the region may receive late in the year. As regional air and water temperatures cooled in November, new and young sea ice formation continued across the region in areas devoid of sea ice, rapidly covering much of the region with 7-10/10^{ths} sea ice (Figure 13), and progressing almost entirely from new-plus-young sea ice in November to first-year sea ice in December (Figure 13). In November, highly positive new-plus-young sea ice anomalies combined with negative first-year sea ice anomalies over much of the southern and eastern parts of the region highlight delayed freeze-up in the region (Figure 14). In December 2021, the region was completely ice covered with mobile ice in the Beaufort Sea and the entirety of Amundsen Gulf disconnected from the adjacent landfast sea ice by the Cape Bathurst Flaw Lead Polynya (Figure 13). The polynya system is evidenced by the positively anomalous new-plus-young sea ice concentration in December (Figure 14) which indicates consistent sea ice motion, i.e. if the sea ice was immobile, those areas would have grown thicker into the first-year stage of development. When the sea ice-adjusted SSRD for each month of 2021 were accumulated (Figure 20), the results are very similar to those from the January-August period. This makes sense given that the total insolation wanes considerable in September-December. However, the total sea ice-adjusted SSRD in the flaw lead area along the Mackenzie Shelf and within eastern Amundsen Gulf was augmented compared to the cumulative value at the end of August (Figure 19), likely due to positively anomalous sea ice-adjusted SSRD in these areas in October 2021 (Figure 17, 18). These results also indicate that the annual accumulation of sea ice-adjusted SSRD in the study region was affected very little by the addition of September and October values, highlighting the importance of months surrounding the summer solstice (e.g. Figure 18) when downwelling shortwave radiation is highest annually. In autumn 2021, the pattern of sea ice motion in the study region was anticyclonic, similar to the long-term (1983-2010) climatological average for those months, however the speeds in autumn 2021 were positively anomalous in October and November (Figure 15, 16). This likely delayed the formation of a high concentration sea ice cover in the region in October (Figure 13) by exporting sea ice from the area faster than it could be formed and thickened. This also resulted in the anomalous predominance of new-plus-young sea ice throughout much of the southern portion of the

study region in November (Figures 13, 14). In December 2021 the sea ice velocities slowed to anomalously low values (Figure 16), the region became ice covered and much of the new-plus-young sea ice formed in November was able to grow thicker in place rather than being exported, resulting in the prevalence of first-year sea ice in the southern portion of the Beaufort Sea and in Amundsen Gulf (Figure 13).

4. Conclusions

Winter 2021 was warmer than the long-term climatological average, with deviation from the climatological average SLP in February, leading to anomalous high velocity westerly winds. Positively anomalous old sea ice concentrations at the south periphery of the Beaufort pack occurred in winter 2021, and positively anomalous new-plus-young sea ice concentrations occurred in the Cape Bathurst flaw lead polynya complex due to rapid wind-driven export westward in January and March. As a result, Amundsen Gulf was largely covered by mobile sea ice in winter 2021.

Spring was anomalously cold, with anomalous and variable SLP. Significant departure from climatological average wind direction and speed occurred in all three spring months as a result. The Cape Bathurst flaw lead polynya began to break up much earlier than average, but despite anomalous dynamic removal of sea ice, cold air temperatures still produced new sea ice in May 2021. Early breakup also exposed large areas of open water leading to large positive sea ice-adjusted SSRD anomalies in spring. Sea ice was exported westward in May, while in June 2021 sea ice from the north was moved southward faster than sea ice could be exported west, accumulating sea ice at the mouth of Amundsen Gulf.

Summer 2021 was characterized by negatively anomalous air temperatures, and an anomalous SLP reversal in July with the Beaufort High much farther south than its average position. Climatologically normal SLP patterns occurred in August and September, but with atypical wind directions and greater than average speeds in September indicating perhaps that the regional wind field was driven by larger scale SLP patterns than those presented here. Negative sea ice anomalies occurred along the Mackenzie Shelf and in Amundsen Gulf, and positive sea ice anomalies occurred along the west coast of Banks Island and at southern periphery of the summer Beaufort pack until September when ice motion switched to western export from the area, clearing Amundsen Gulf and the west coast of Banks Island of sea ice.

Autumn 2021 was warmer than the climatological average, with open water areas likely keeping air above those areas warmer than elsewhere. SLP and wind direction were similar to the climatological averages in October and November, with enhanced wind speed. Positively anomalous new and young sea ice concentrations occurred along the periphery of the old ice pack in October, and large positive new-plus-

young sea ice anomalies and large negative first-year sea ice anomalies in November indicated a shift in sea ice formation timing in the region to later in the year. Anomalous easterly winds due to movement of the Beaufort High over M'Clure Strait occurred in December 2021 kept sea ice in Amundsen Gulf mobile, creating positively anomalous new-plus-young sea ice in the flaw lead in December.

5. Acknowledgements

We thank the Inuvialuit Game Council, the Fisheries Joint Management Committee, and the Western Arctic Marine Protected Area steering committee for supporting this work and providing valuable input into study objectives. We are grateful to the Canadian Coast Guard and crew of the *CCGS Sir Wilfrid Laurier* for logistical support. And finally, thanks to the crew and management team of the *F/V Frosti* for their tireless service and professionalism.

Funding for the 2021 field year was provided by various DFO sources including the National Conservation Plan, Aquatic Climate Change Adaptation Services Program, the Arctic Science Fund, the Competitive Science Research Fund, the Results Fund, and Marine Planning and Conservation.

6. References

DFO. 2010. Monitoring indicators for the Tarium Niryutait Marine Protected Area (TNMPA). DFO Can. Sci. Advis. Sec. Sci. Advis. Rep. 2010/059.

DFO. 2014. Re-evaluation of Ecologically and Biologically Significant Areas (EBSAs) in the Beaufort Sea. DFO Can. Sci. Advis. Sec. Sci. Advis. Rep. 2014/052.

Fequet, D., 2005. MANICE: Manual of Standard Procedures for Observing and Reporting Ice Conditions, Meteorological Service of Canada. Canada.

Häkkinen, S., and A. Proshutinsky, 2004. Freshwater content variability in the Arctic Ocean, Journal of Geophysical Research, 109, C3, doi: 10.1029/2003JC001940.

Hersbach, H., Bell, B., Berrisford, P., Biavati, G., Horányi, A., Muñoz Sabater, J., Nicolas, J., Peubey, C., Radu, R., Rozum, I., Schepers, D., Simmons, A., Soci, C., Dee, D., Thépaut, J-N. 2018. ERA5 hourly data on single levels from 1959 to present. Copernicus Climate Change Service (C3S) Climate Data Store (CDS). (Accessed June 2022), 10.24381/cds.adbb2d47

Kelley, D. E. 2018. Oceanographic analysis with R. Springer, New York, NY. ISBN: 978-1-4939-8844-0, doi: 10.1007/978-1-4939-8844-0, 290pp+xxi.

Mallet, R. D. C., Stroeve, J. C., Cornish, S. B., Crawford, A. D., Lukovich, J. V., Serreze, M. C., Barrett, A. P., Meier, W. N., Heorton, H. D. B. S., Tsamados, M. 2021. Record winter winds in 2020/21 drove exceptional Arctic sea ice transport, Communications Earth and Environment, 2, article number 149, https://doi.org/10.1038/s43247-021-00221-8.

Moore, G. W. K., Steele, M., Schweiger, A. J., Zhang, J., Laidre, K. L.. 2022. Thick and old sea ice in the Beaufort Sea during summer 2020/21 was associated with enhanced transport. Communications Earth and Environment, 3, article number 198, https://doi.org/10.1038/s43247-022-00530-6.

Niemi, A., Majewski, A., Eert, J., Ehrman, A., Michel, C., Archambault, P., Atchison, S., Cypihot, V., Dempsey, M., de Montety, L., Dunn, M., Geoffroy, M., Hussherr, R., MacPhee, S., Mehdipour, N., Power, M., Swanson, H., Treau de Coeli, L., Walkusz, W., Williams, W., Woodard, K., Zimmerman, S., Reist, J. 2020. Data from the BREA-MFP and CBS-MEA research programs describing the Anguniaqvia niqiqyuam Marine Protected Area (ANMPA) ecosystem. Can. Data Rep. Fish. Aquat. Sci. 1316: ix + 90 p.

Perovich, D. K., and Richter-Menge, J. A. 2009. Loss of sea ice in the Arctic. Annu. Rev. Mar. Sci. 2009, 1:417-441, doi: 10.1146/annurev.marine.010908.163805.

R Core Team, 2022. R: A language and environment for statistical computing. R Foundation for Statistical Computing, Vienna, Austria. https://ww.R-project.org/

Sharqawy, M. H., Lienhard V, J.. H., Zubair, S. M. 2010. Thermophysical properties of seawater: a review of existing correlations and data, Desalination and Water Treatment, 16: 354-380, doi: 10.5004/dwt.2010.1079.

Stirling, I. 1980. The biological importance of Polynyas in the Canadian Arctic. Arctic, 33(2), 303-315.

Tschudi, M., Meier, W. N., Stewart, J. S., Fowler, C., Maslanik, J. 2019. Polar Pathfinder Daily 25 km EASE-Grid Sea Ice Motion Vectors, Version 4. [1983-2021]. Boulder, Colorado USA. NASA National Snow and Ice Data Center Distributed Active Archive Center. doi: https://doi.org/10.5067/INAWUWO7QH7B. [June 2022].

Tivy, A., Howell, S. E. L., Alt, B., McCourt, S., Chagnon, R., Crocker, G., Carrieres, T., Yackel, J. J. 2011. Trends and variability in summer sea ice cover in the Canadian Arctic based on the Canadian Ice Service Digital Archive, 1960-2008, and 1968-2008. Journal of Geophysical Research, Oceans, 116(C3), doi: 10.1029/2009JC005855.

7. Figures

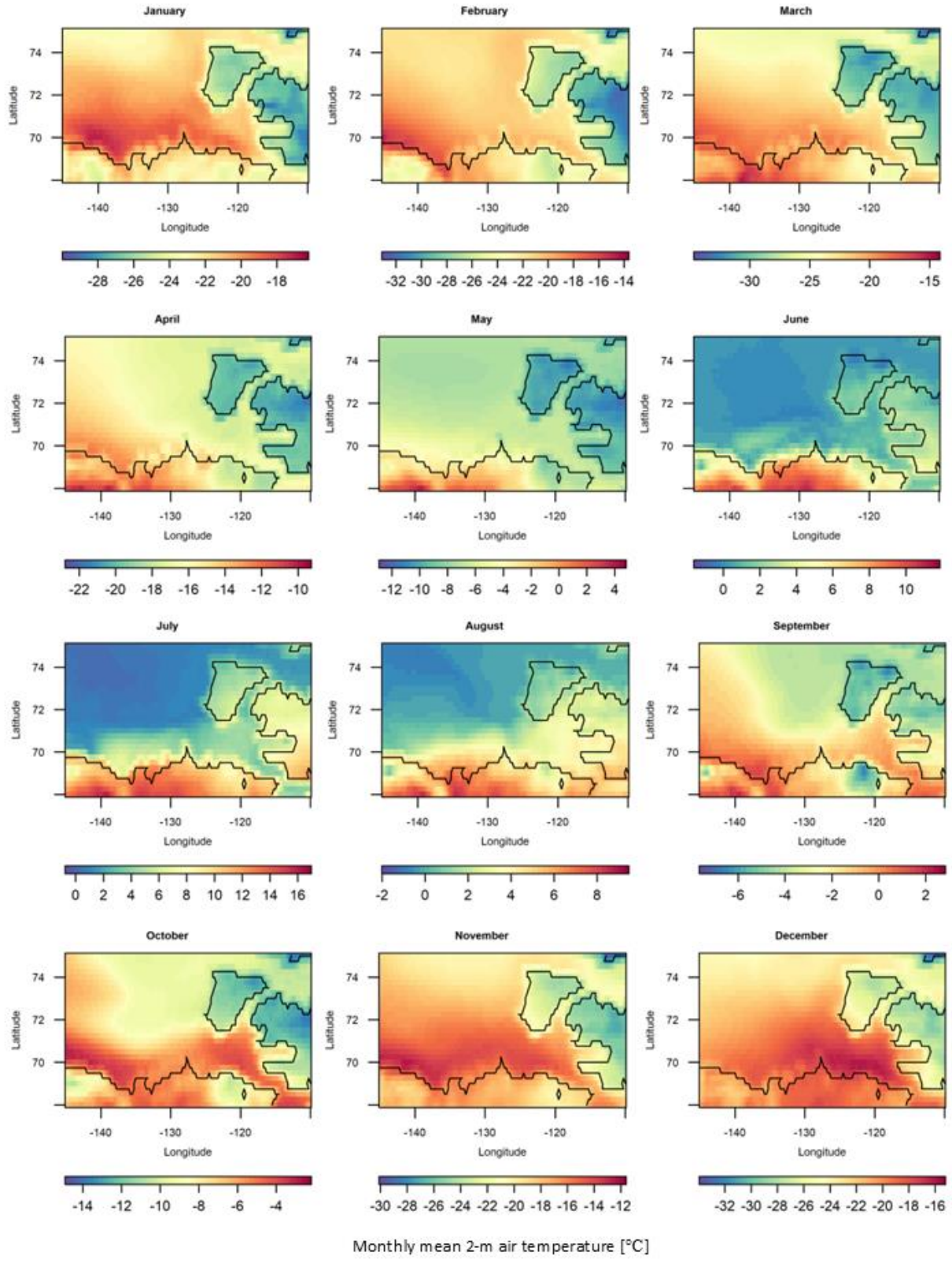

Figure 1. Monthly mean 2 m air temperature (°C) in 2021 over the Beaufort Sea and Amundsen Gulf.

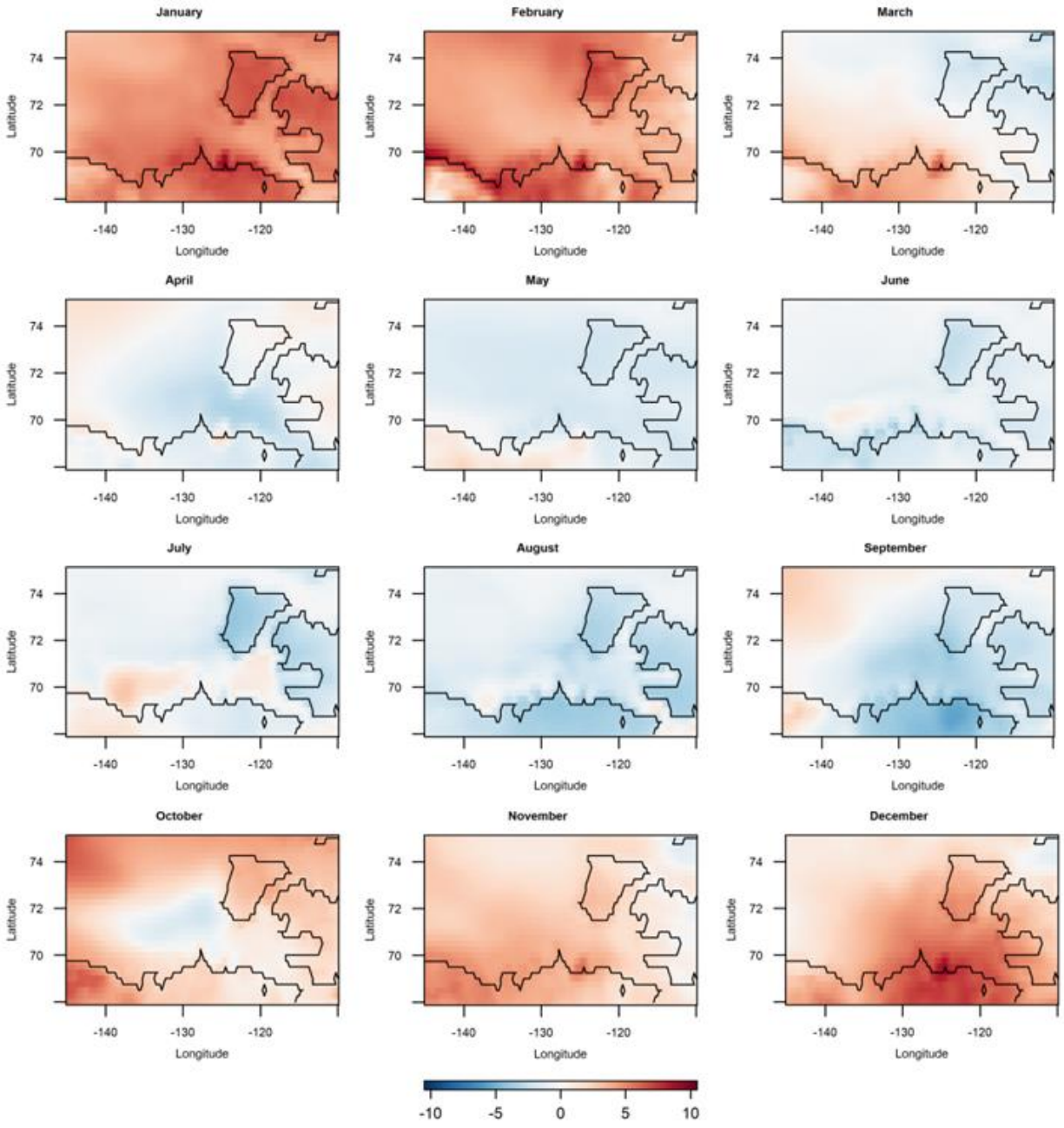

Figure 2. Monthly 2 m air temperature anomalies (°C) in 2021 from the climatological average period 1983-2010 in the Beaufort Sea and Amundsen Gulf.

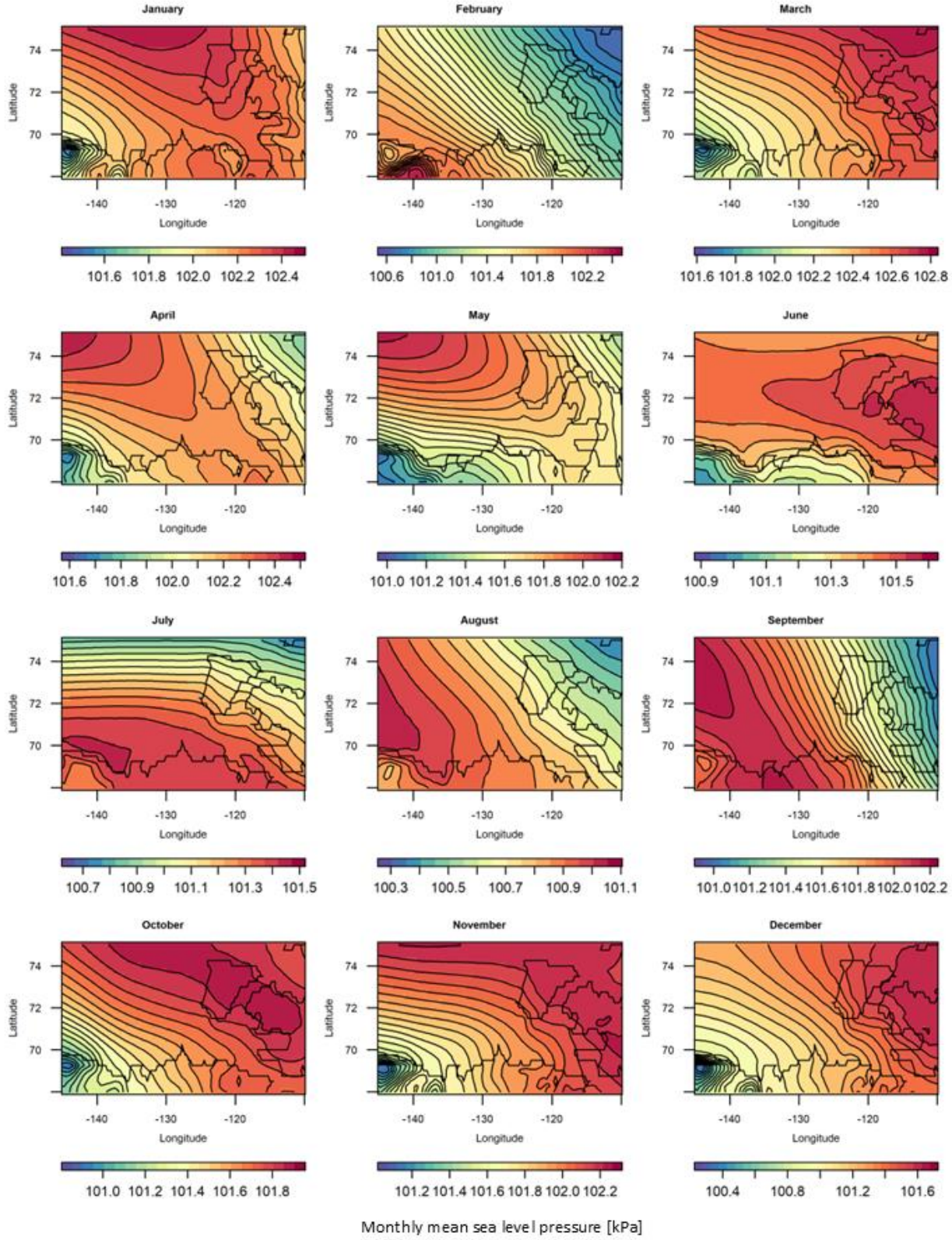

Figure 3. Monthly sea level pressure (kPa) over the Beaufort Sea and Amundsen Gulf in 2021.

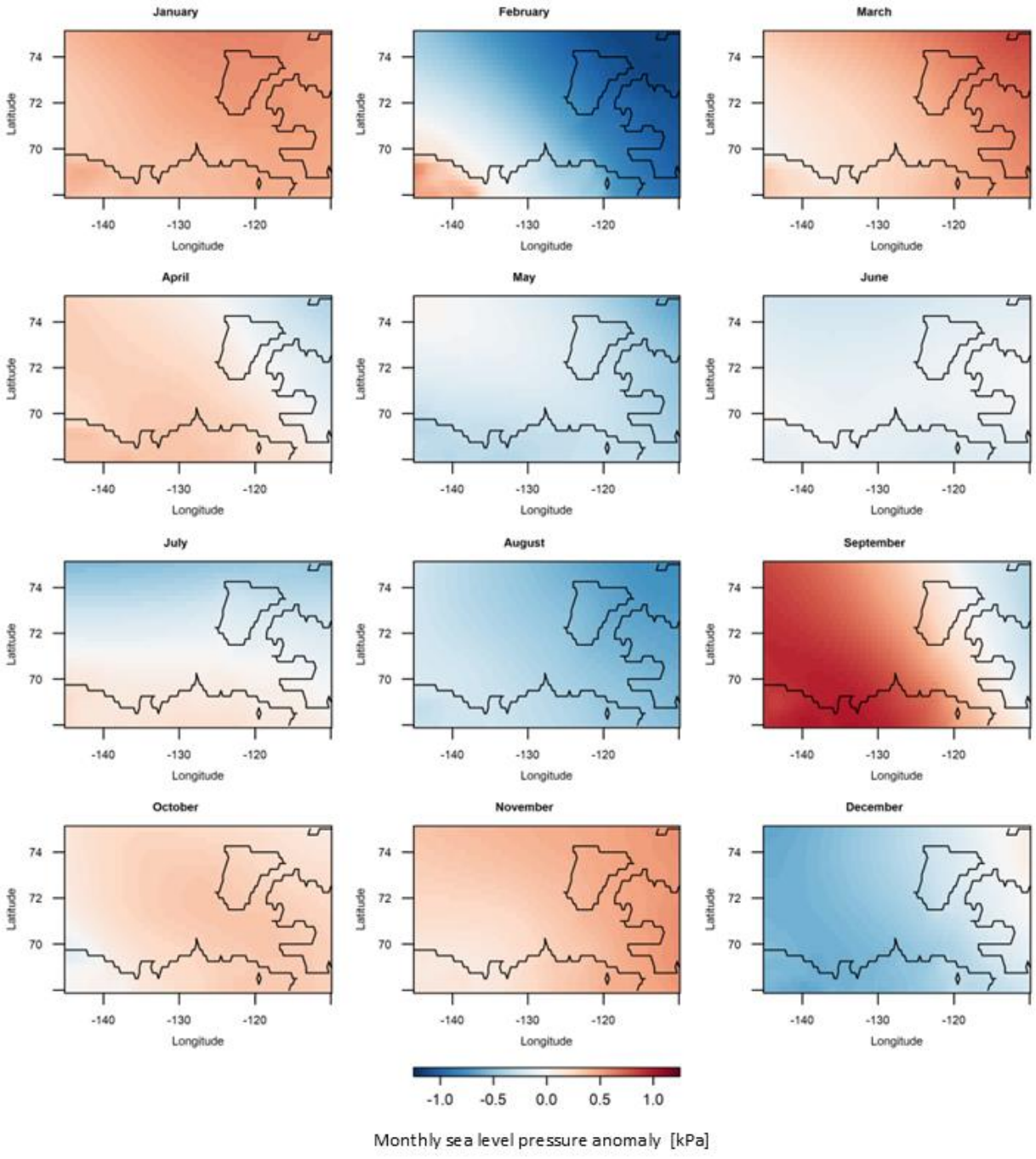

Figure 4. Monthly sea level pressure anomalies (kPa) in 2021 from the climatological average period 1983-2010 in the Beaufort Sea and Amundsen Gulf.

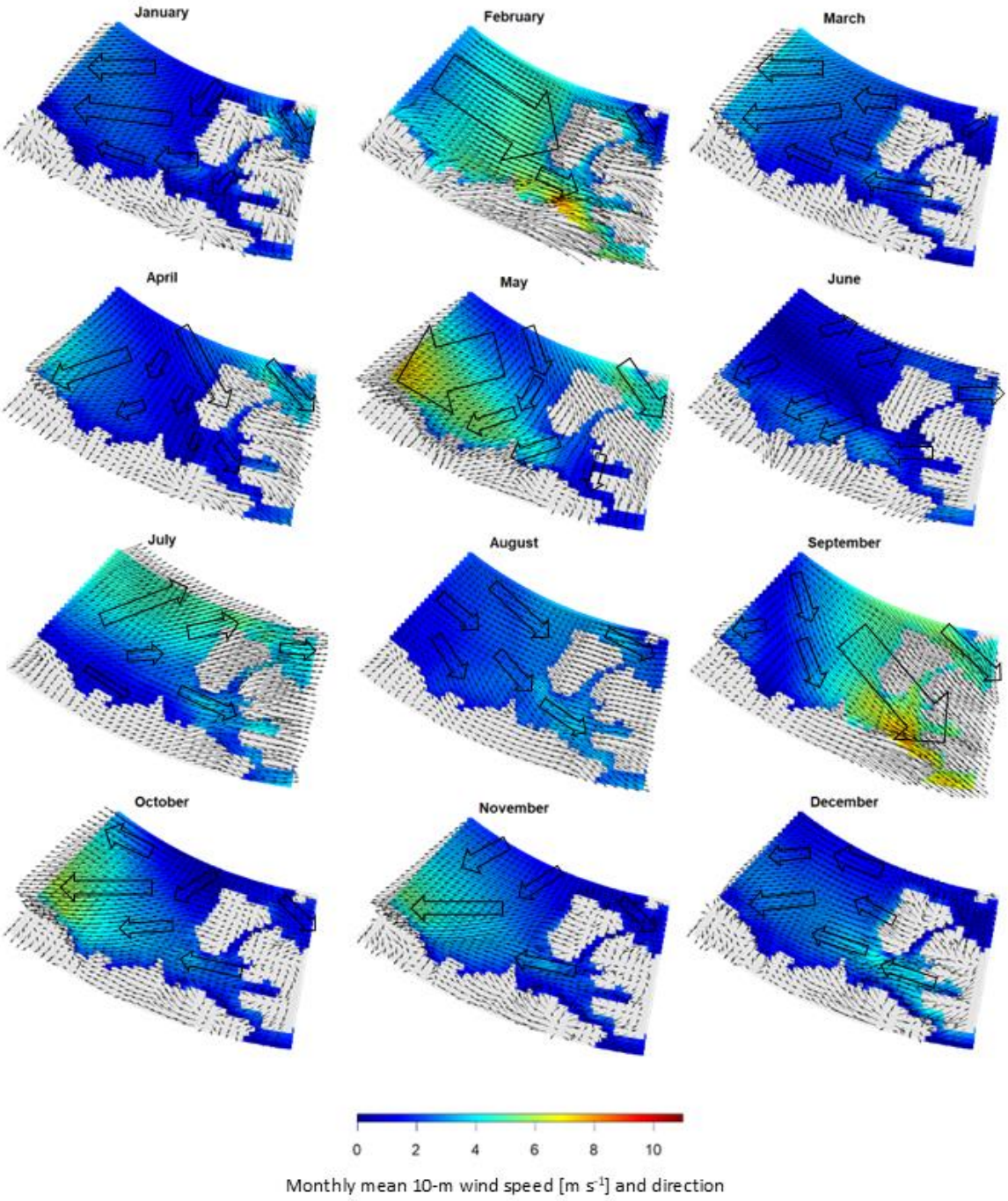

Figure 5. Monthly mean 10 m wind speed (m s^{-1}) and direction in 2021 in the Beaufort Sea and Amundsen Gulf.

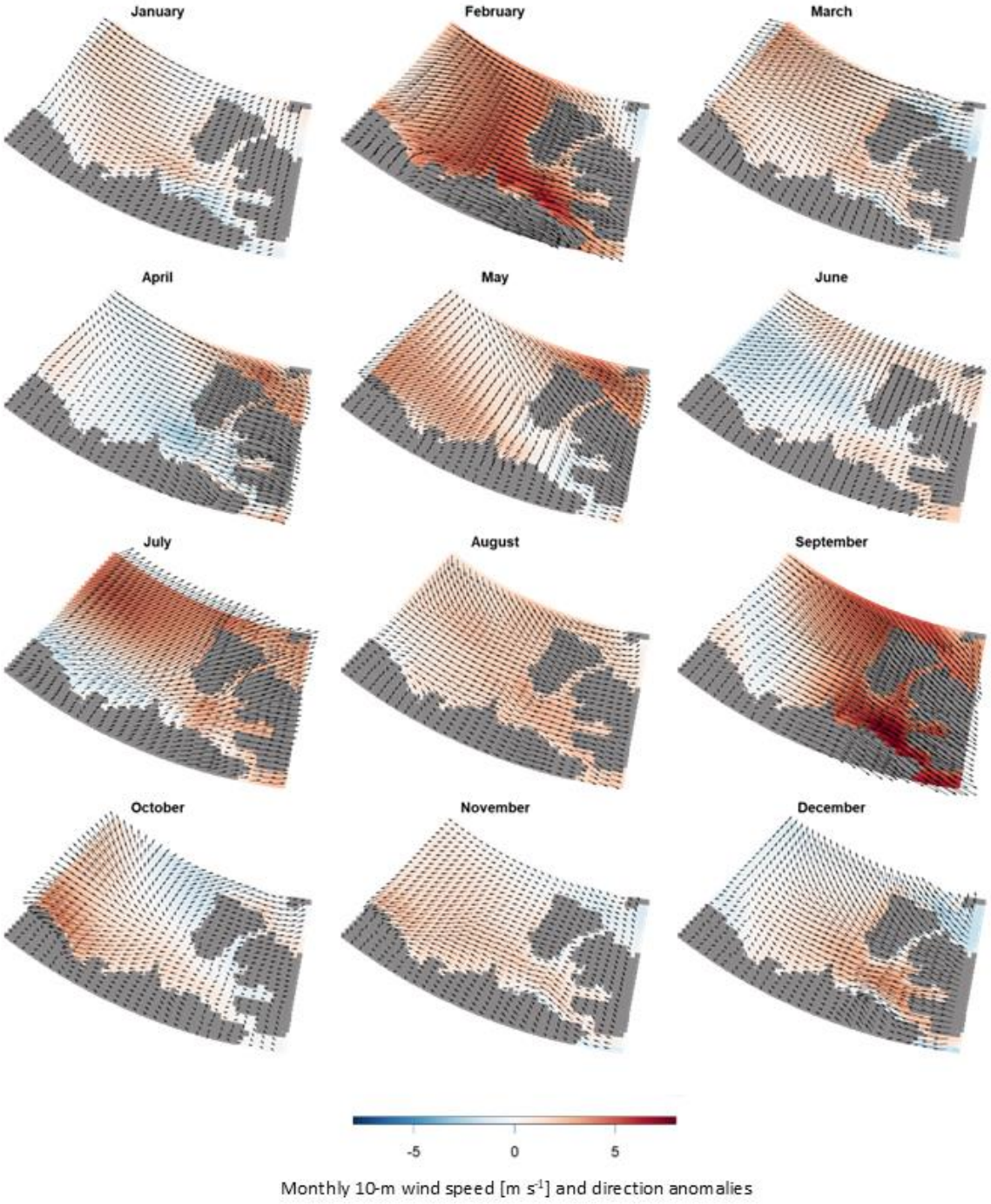

Figure 6. Monthly 10 m wind speed (m s^{-1}) and direction anomalies from the climatological average period 1983-2010 in the Beaufort Sea and Amundsen Gulf in 2021.

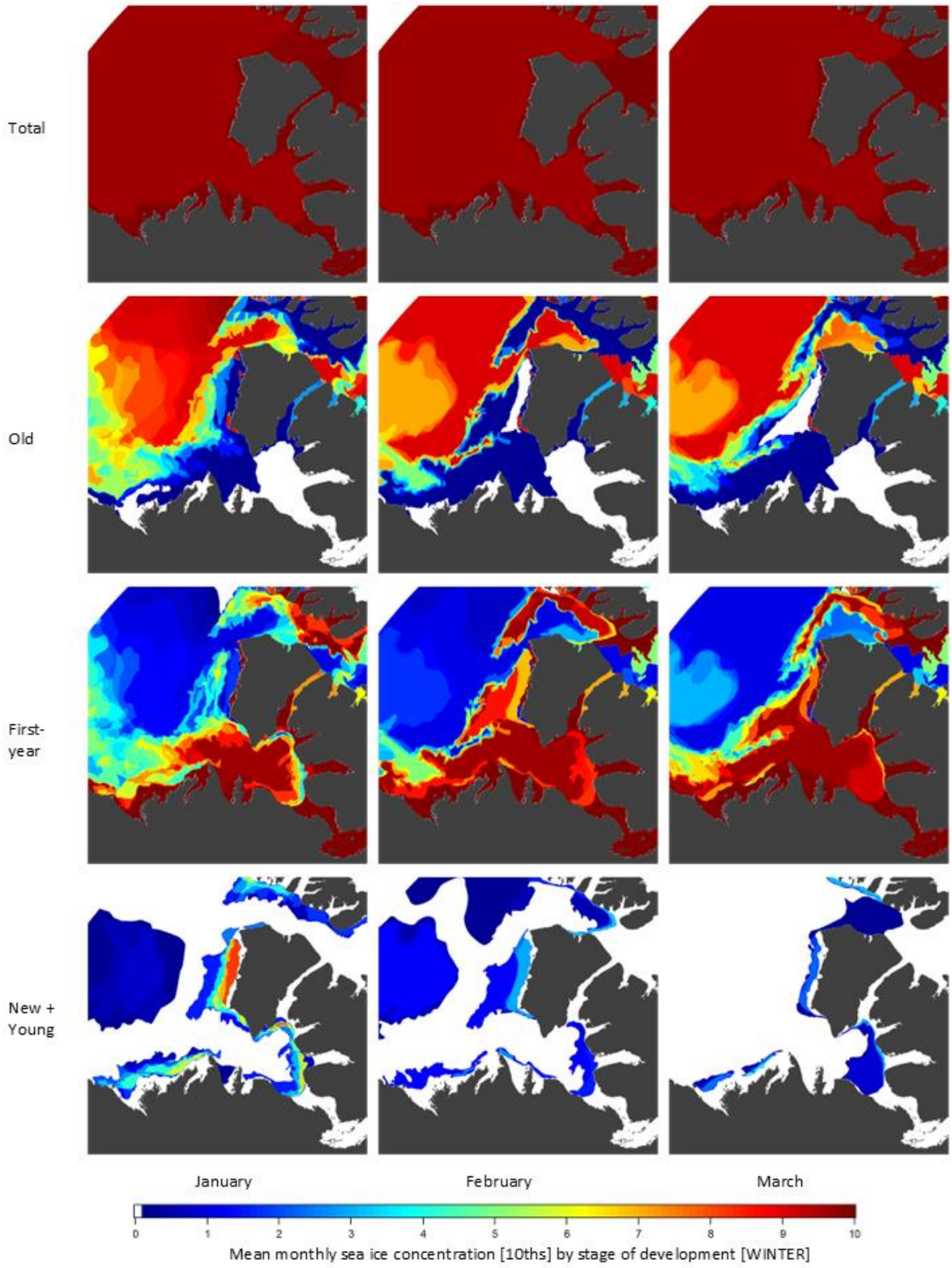

Figure 7. Mean monthly sea ice concentration (10^{ths}) for total sea ice and three stages of development (old, first-year, and young + new ice) for January, February, and March [winter] 2021.

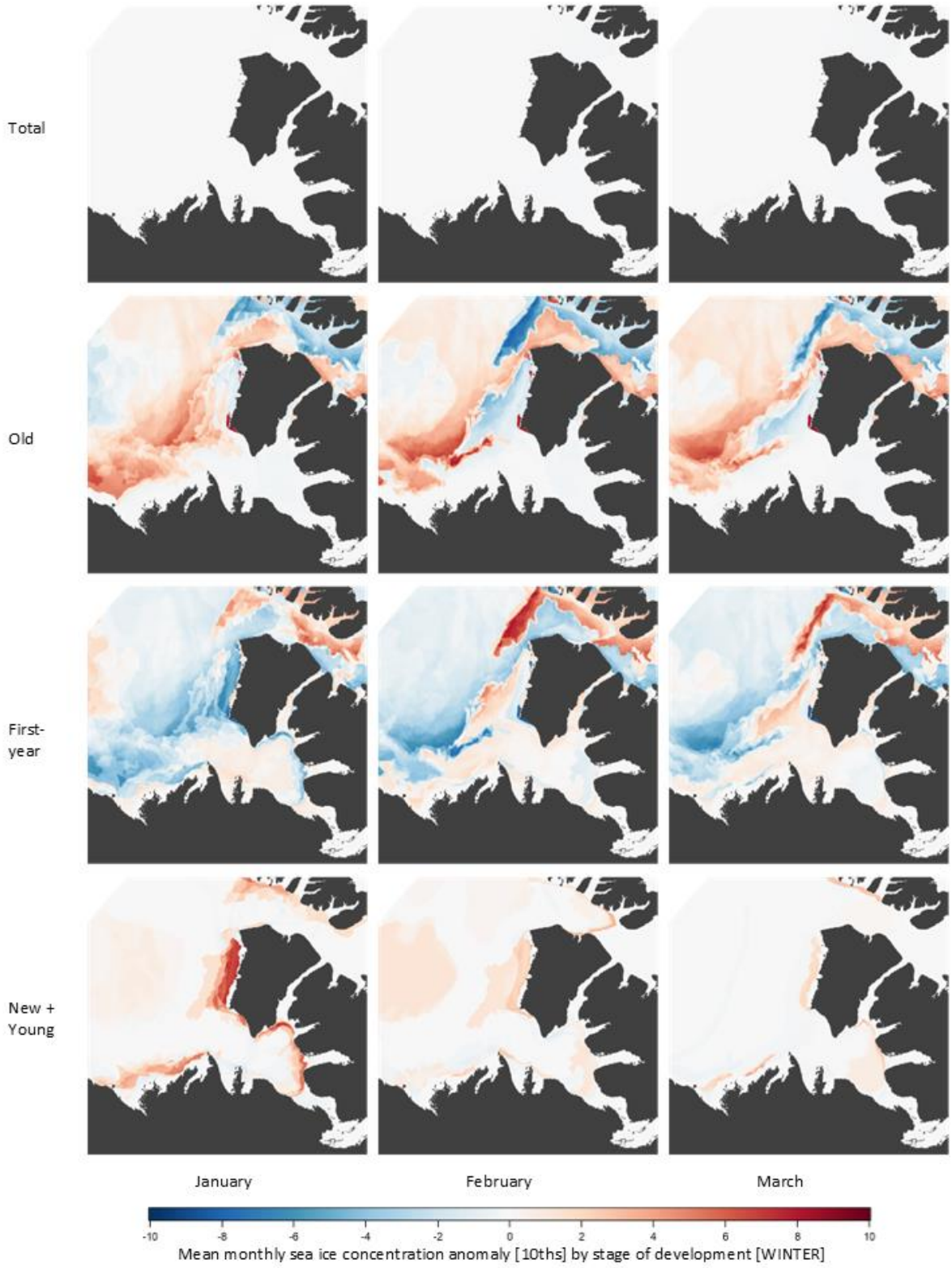

Figure 8. Mean monthly sea ice concentration anomalies (10^{ths}) for total sea ice and three stages of development (old, first-year, and young + new ice) for January, February, and March [winter] 2021.

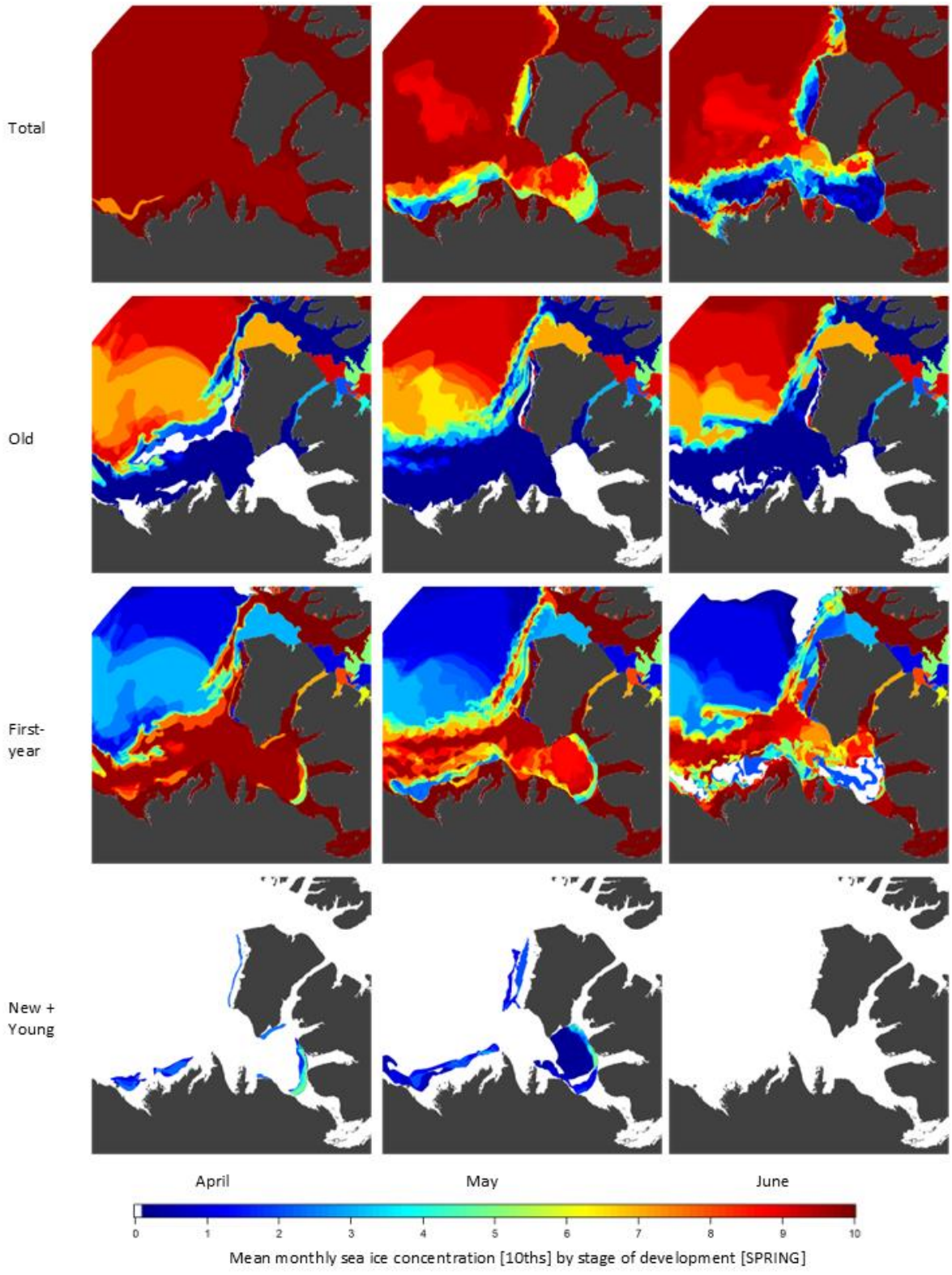

Figure 9. Mean monthly sea ice concentration (10^{ths}) for total sea ice and three stages of development (old, first-year, and young + new ice) for April, May, and June [spring] 2021.

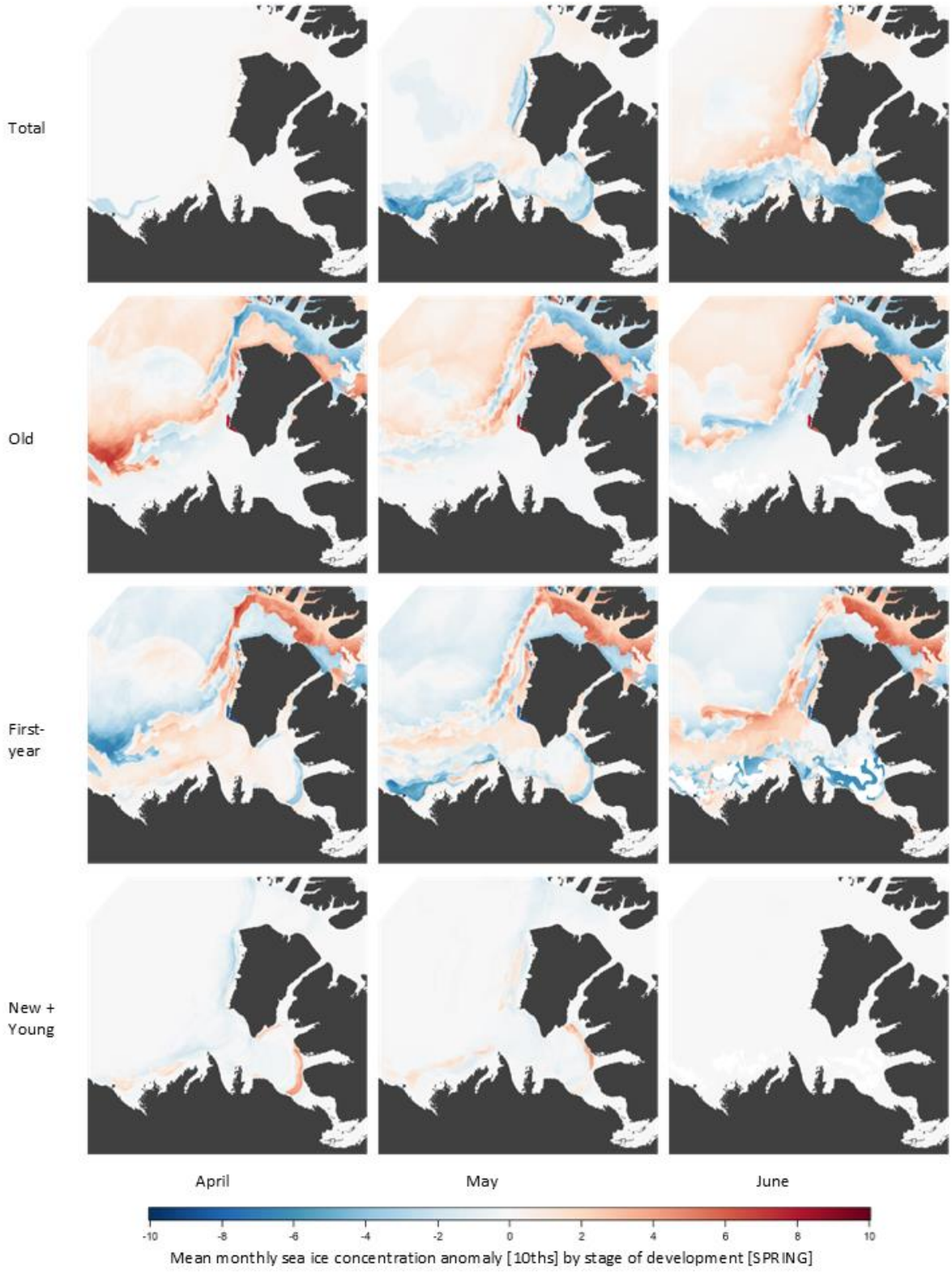

Figure 10. Mean monthly sea ice concentration anomalies (10^{ths}) for total sea ice and three stages of development (old, first-year, and young + new ice) for April, May, and June [spring] 2021.

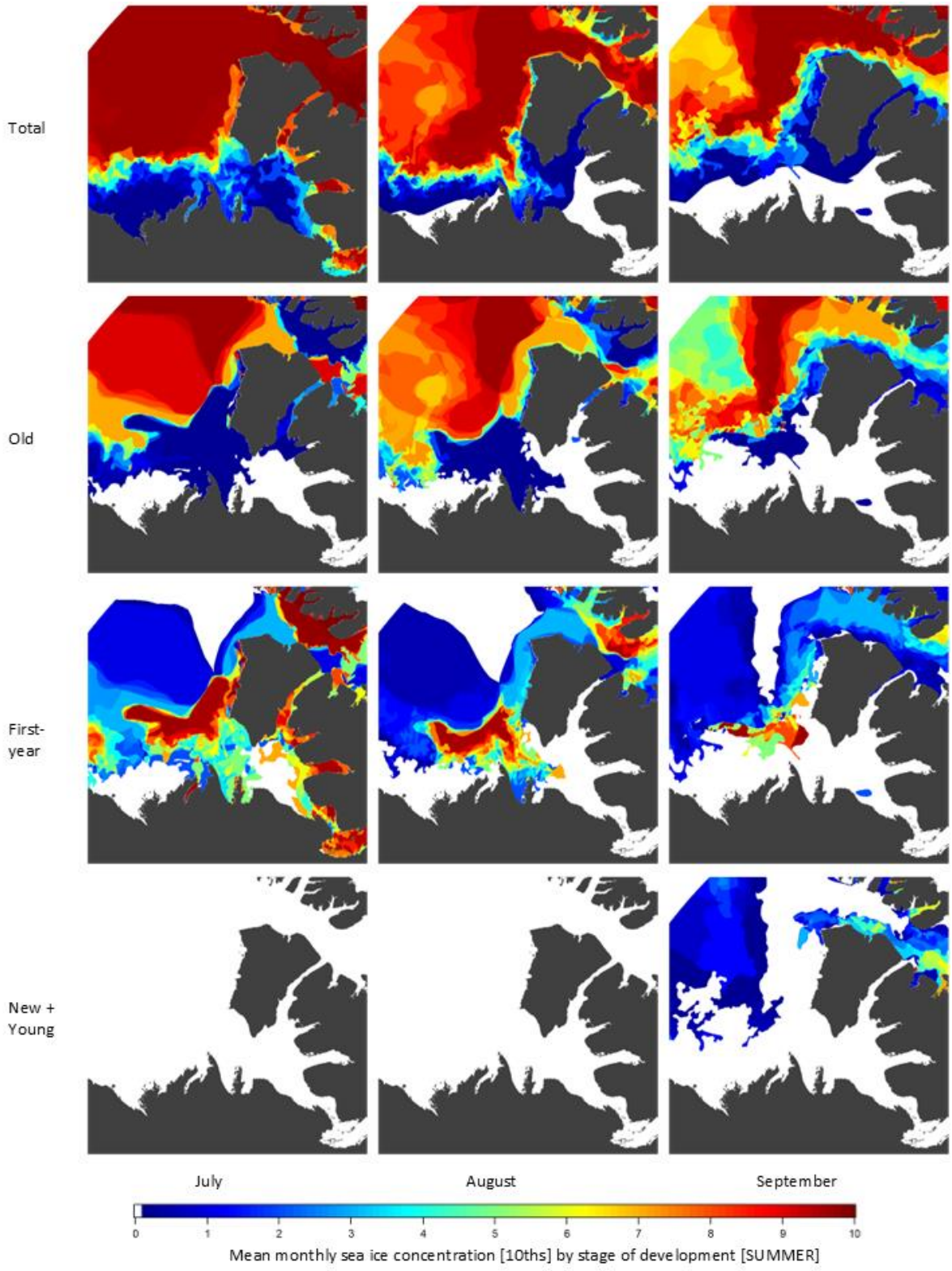

Figure 11. Mean monthly sea ice concentration (10^{ths}) for total sea ice and three stages of development (old, first-year, and young + new ice) for July, August, and September [summer] 2021.

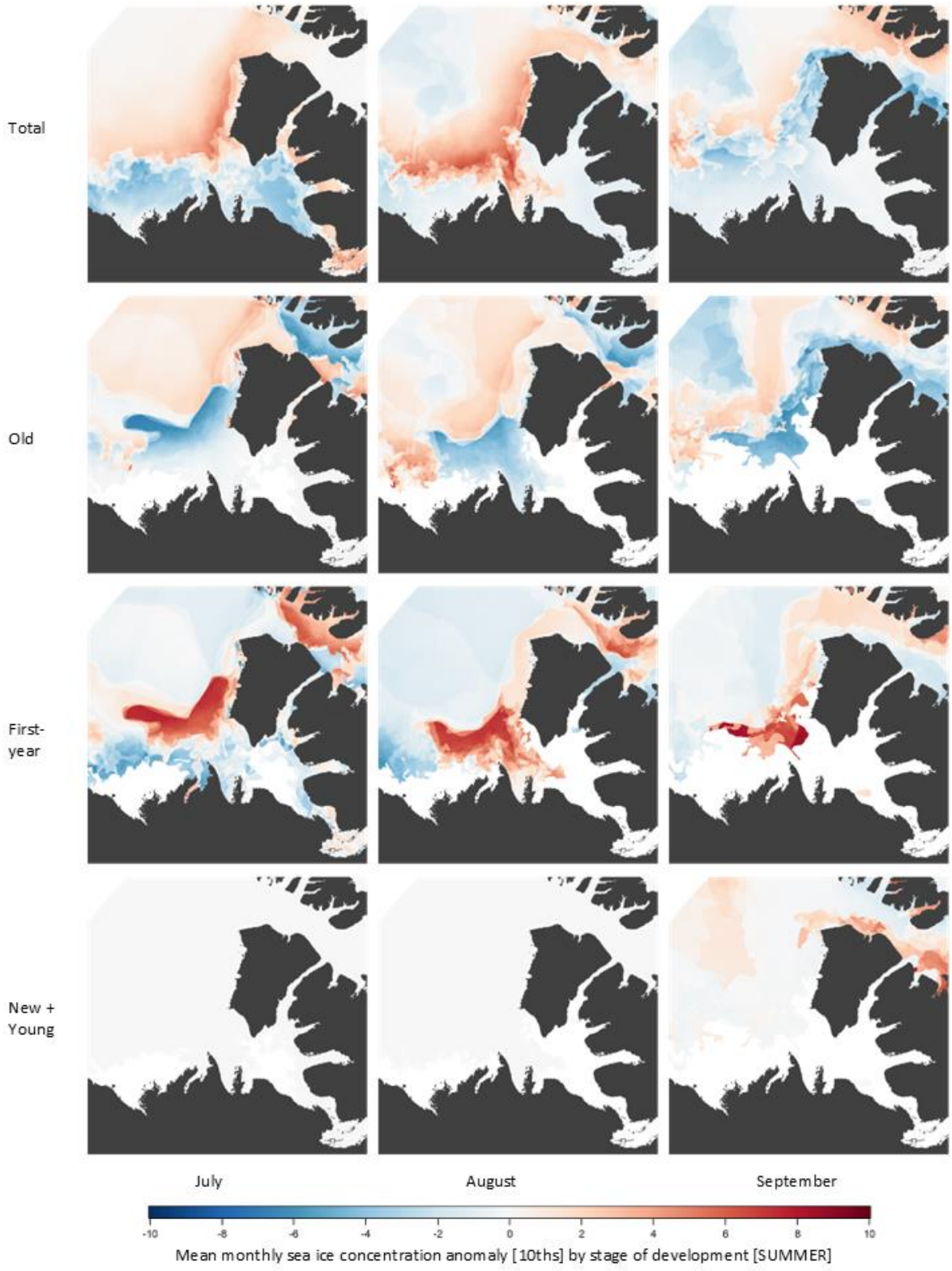

Figure 12. Mean monthly sea ice concentration anomalies (10^{ths}) for total sea ice and three stages of development (old, first-year, and young + new ice) for July, August, and September [summer] 2021.

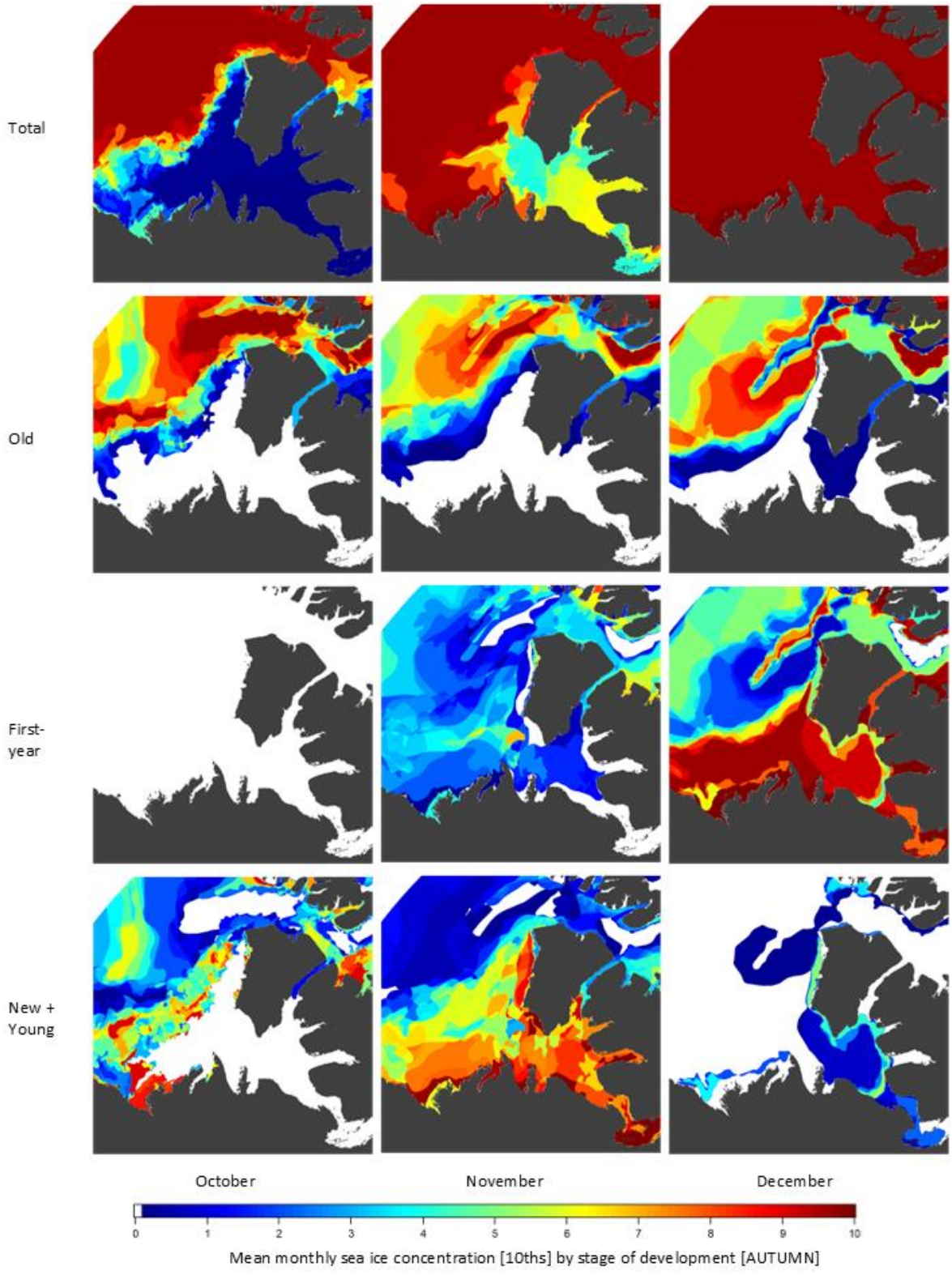

Figure 13. Mean monthly sea ice concentration (10^{ths}) for total sea ice and three stages of development (old, first-year, and young + new ice) for October, November, and December [autumn] 2021.

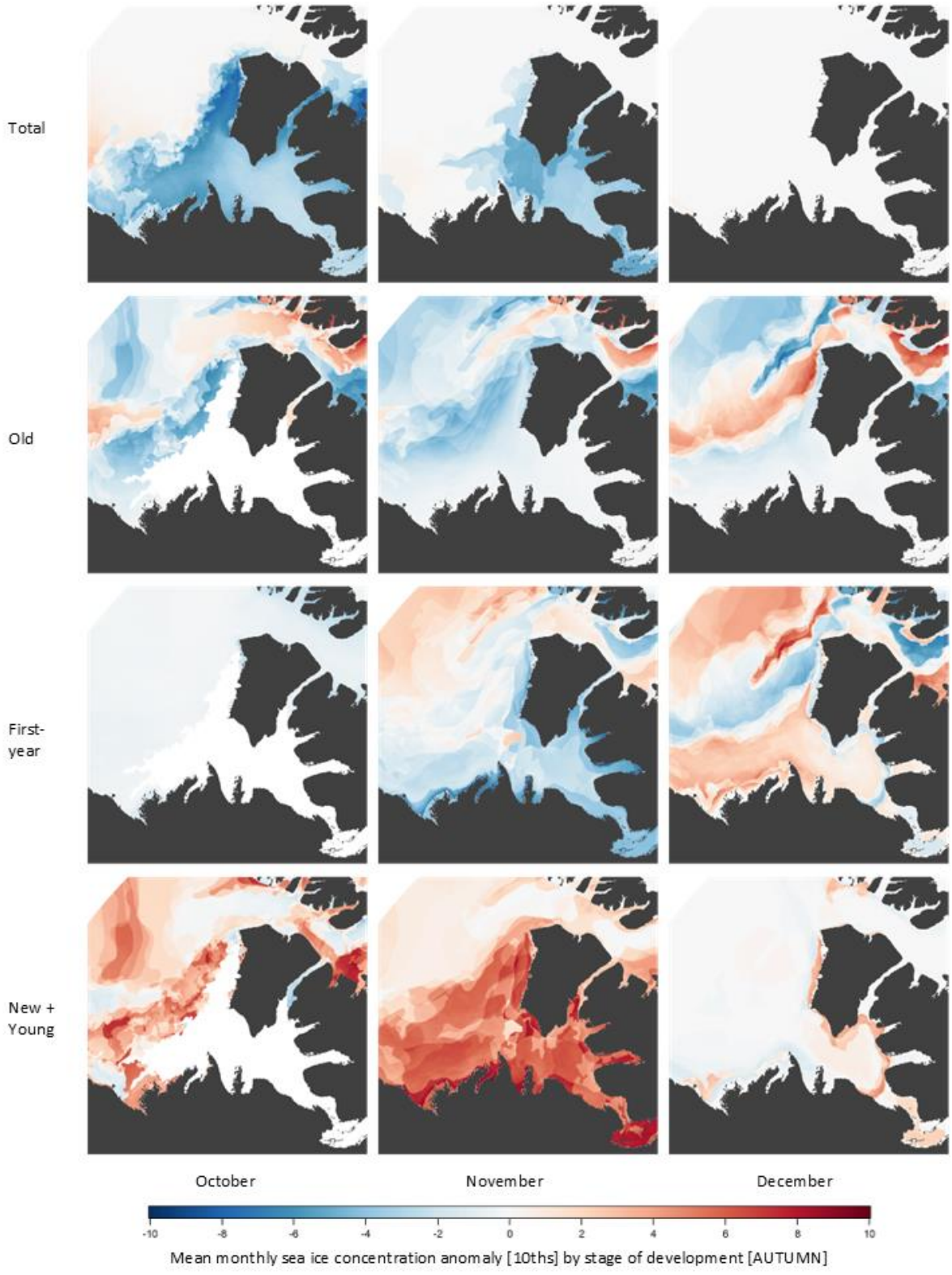

Figure 14. Mean monthly sea ice concentration anomalies (10^{ths}) for total sea ice and three stages of development (old, first-year, and young + new ice) for October, November, and December [autumn] 2021.

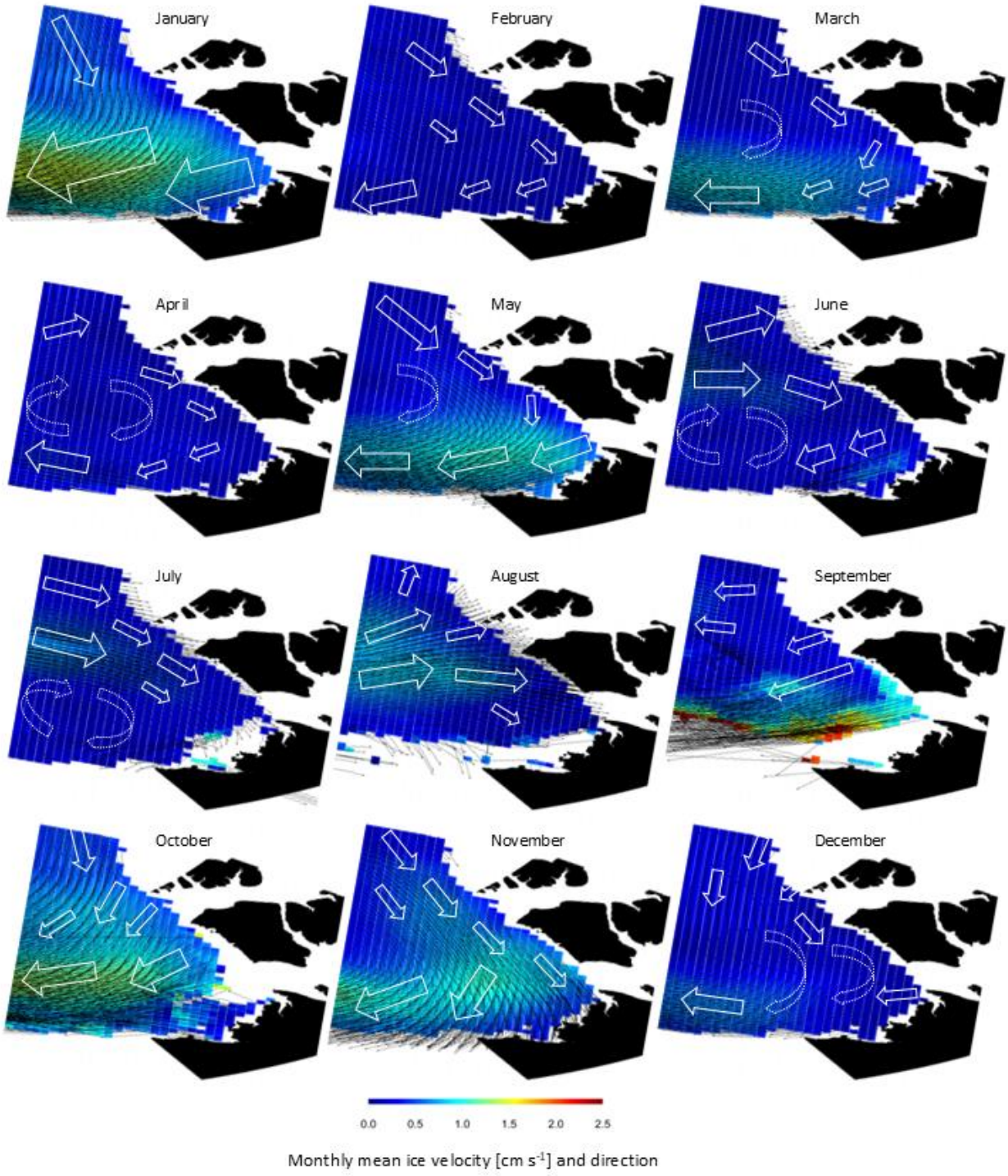

Figure 15. Monthly mean sea ice velocity (cm s^{-1}) and direction in 2021 in the Beaufort Sea and Amundsen Gulf.

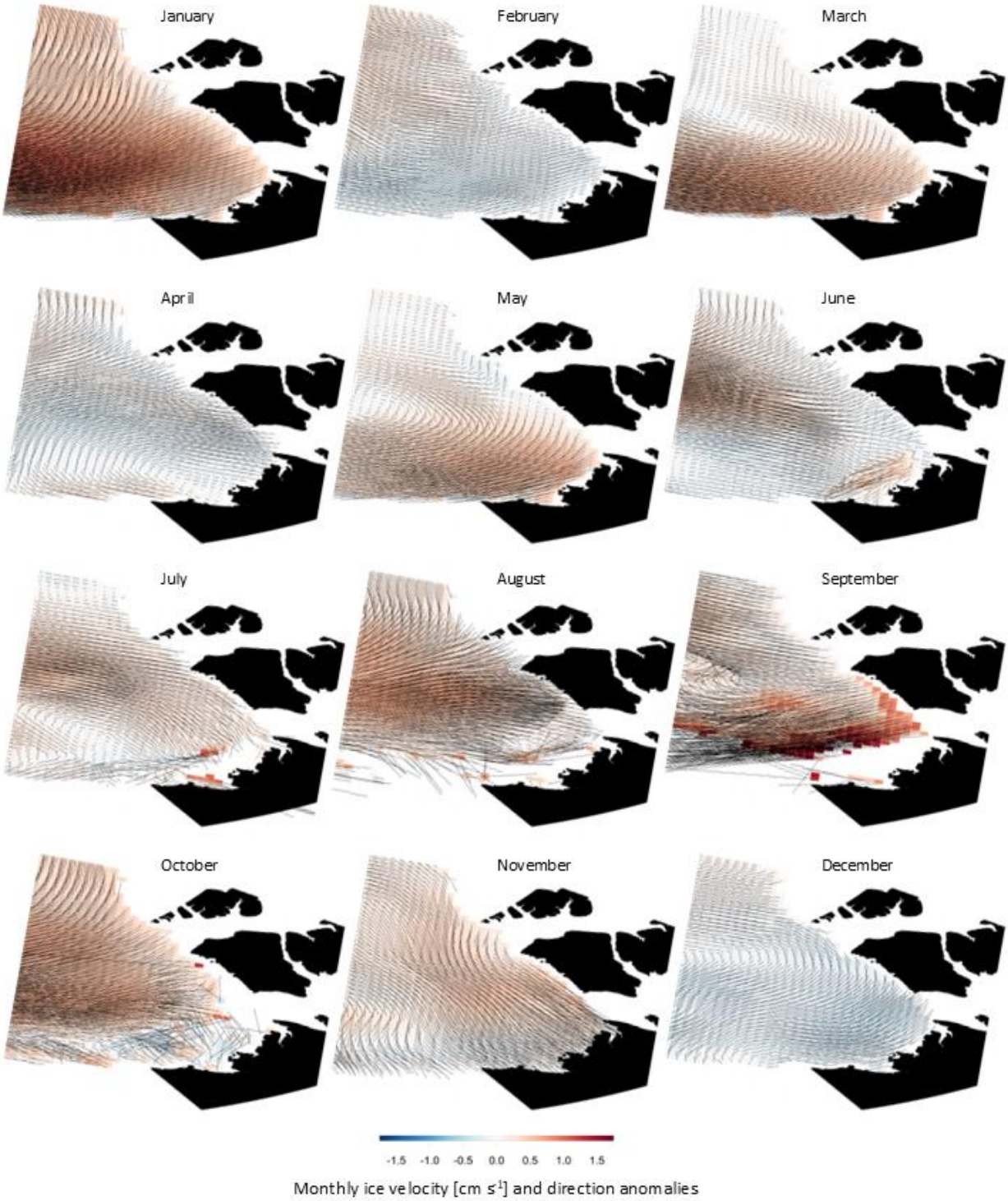

Figure 16. Monthly sea ice velocity (cm s^{-1}) and direction anomalies in 2021 from the climatological mean period 1983-2010 in the Beaufort Sea and Amundsen Gulf.

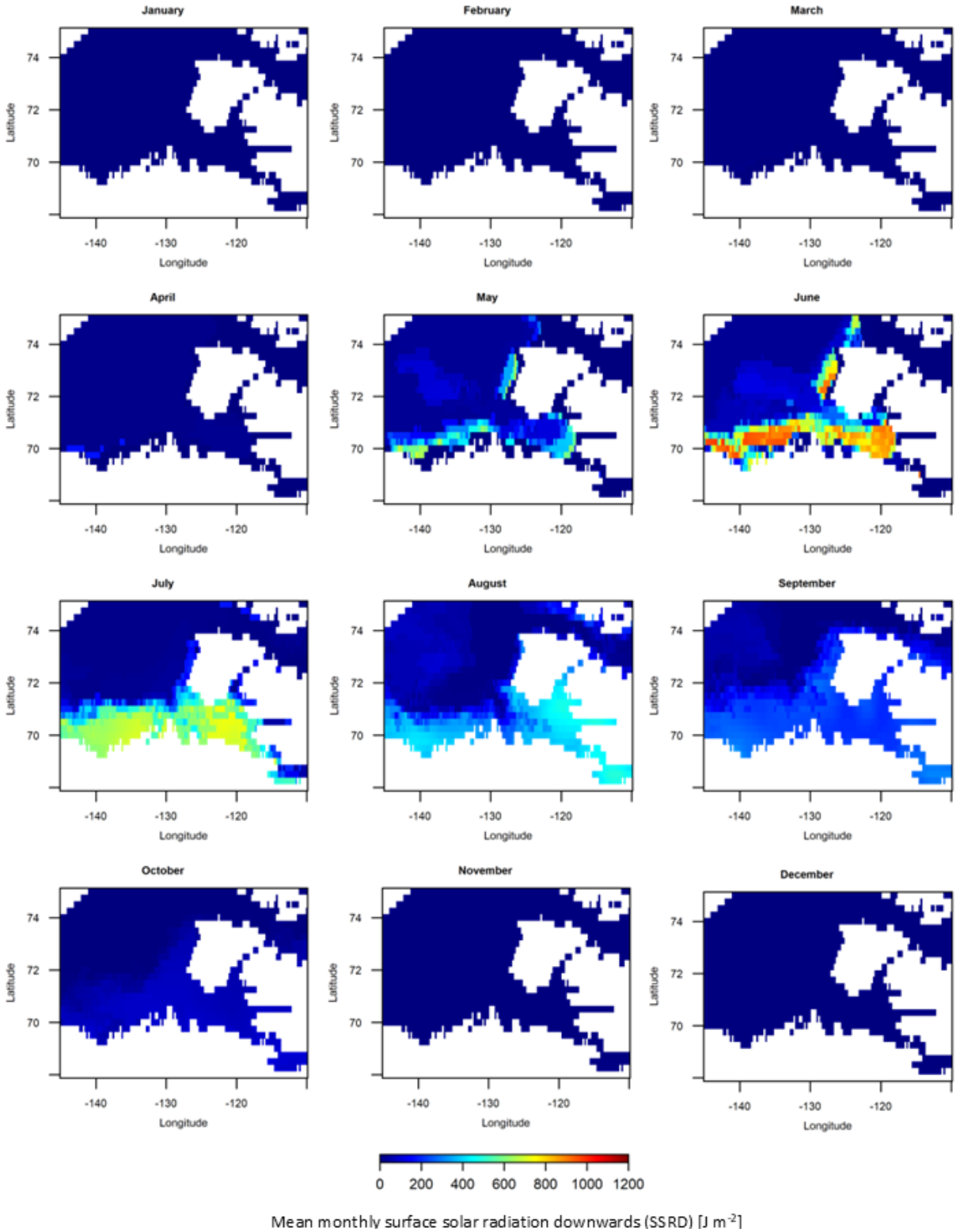

Figure 17. Mean monthly sea ice-adjusted surface solar radiation downwards (J m^{-2}) in 2021 in the Beaufort Sea and Amundsen Gulf.

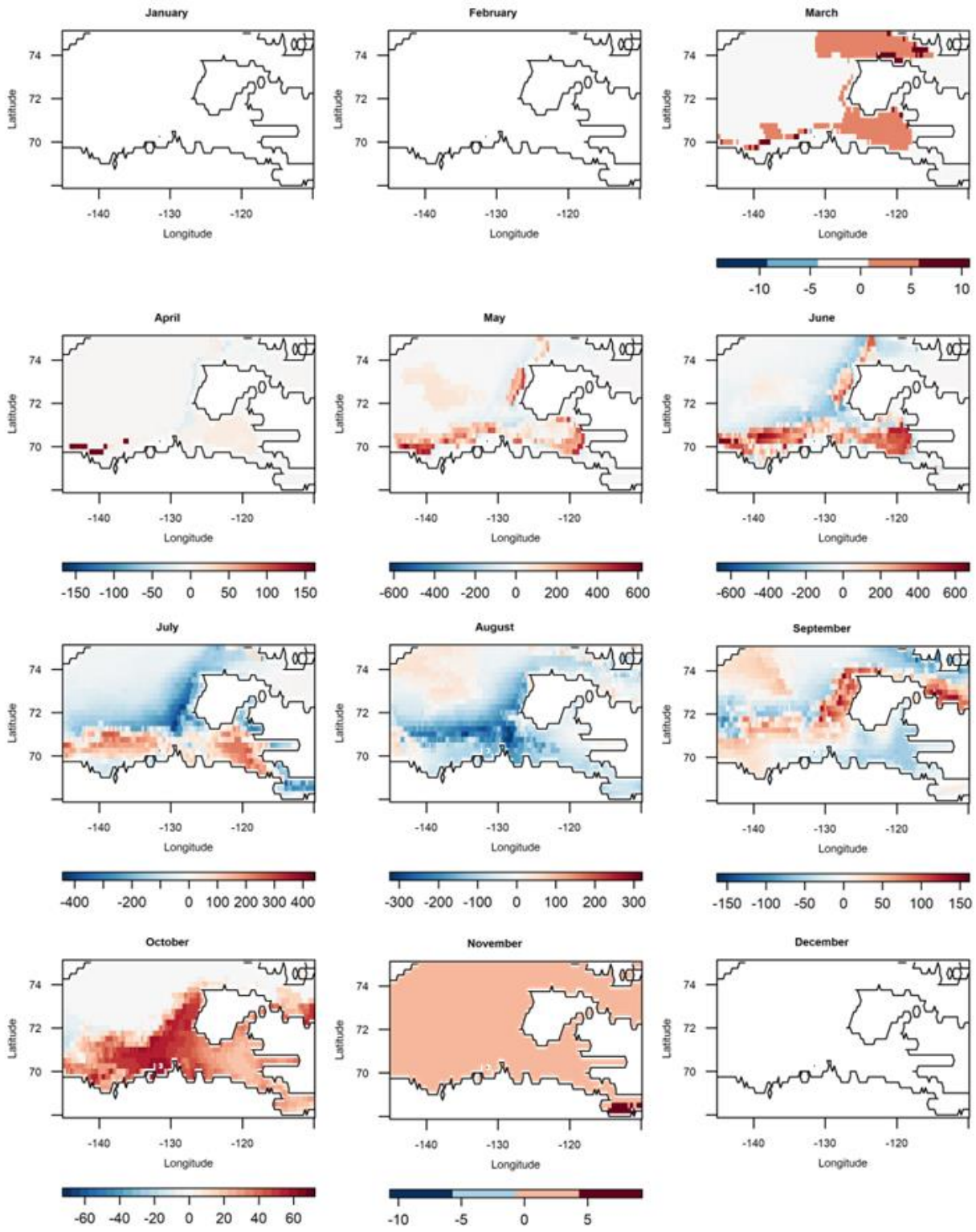

Figure 18. Monthly sea ice-adjusted surface solar radiation downwards anomalies (J m^{-2}) in 2021 compared to the climatological average period 1983-2010 in the Beaufort Sea and Amundsen Gulf.

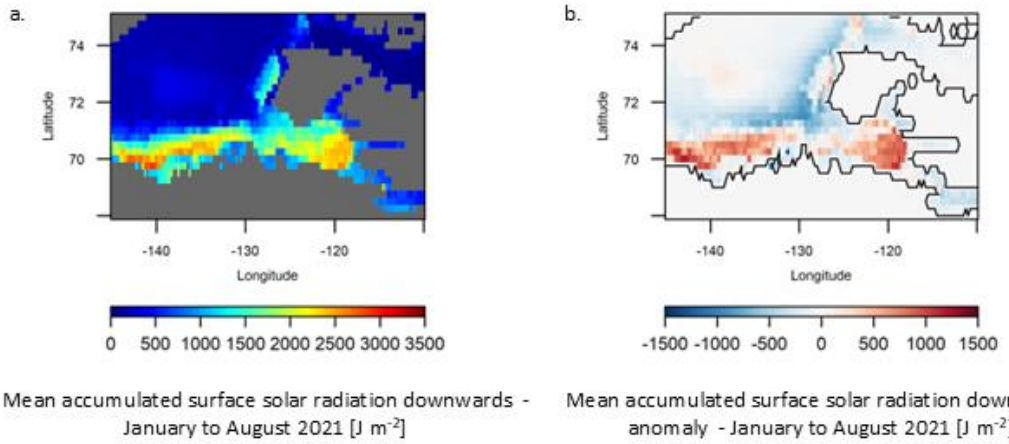

Figure 19. (a) Mean accumulated sea ice-adjusted surface solar radiation downwards (J m^{-2}) between January and August in 2021 (inclusive), and (b) accumulated surface solar radiation downwards anomaly (J m^{-2}) between January and August 2021 (inclusive) compared to the climatological average over the period 1983-2010.

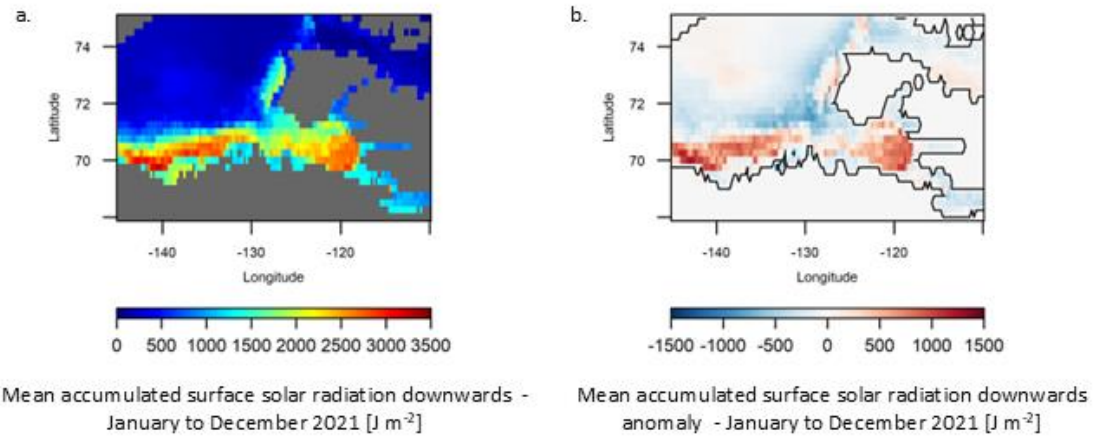

Figure 20. (a) Mean accumulated sea ice-adjusted surface solar radiation downwards (J m^{-2}) between January and December in 2021 (inclusive), and (b) accumulated surface solar radiation downwards anomaly (J m^{-2}) between January and December 2021 (inclusive) compared to the climatological average over the period 1983-2010.

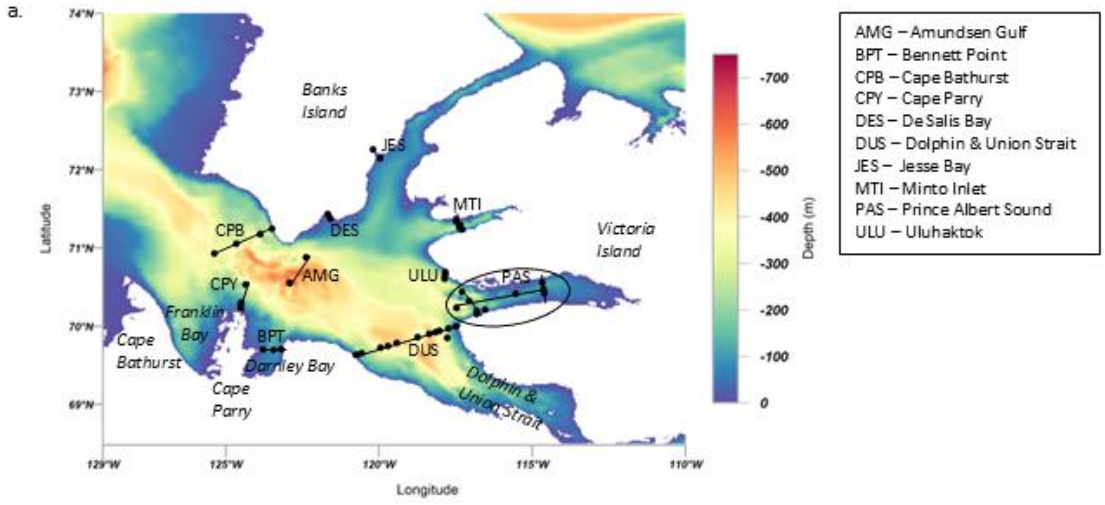

Figure 21. (a) CTD station and section locations in the Amundsen Gulf region in 2021, overlain on ETOPO1 bathymetry data, and (b) example profiles of temperature, salinity, potential density (σ, θ), and N^2 from Jesse Bay station 1.1 in 2021. The horizontal dotted line (grey) indicates the depth of maximum N^2.

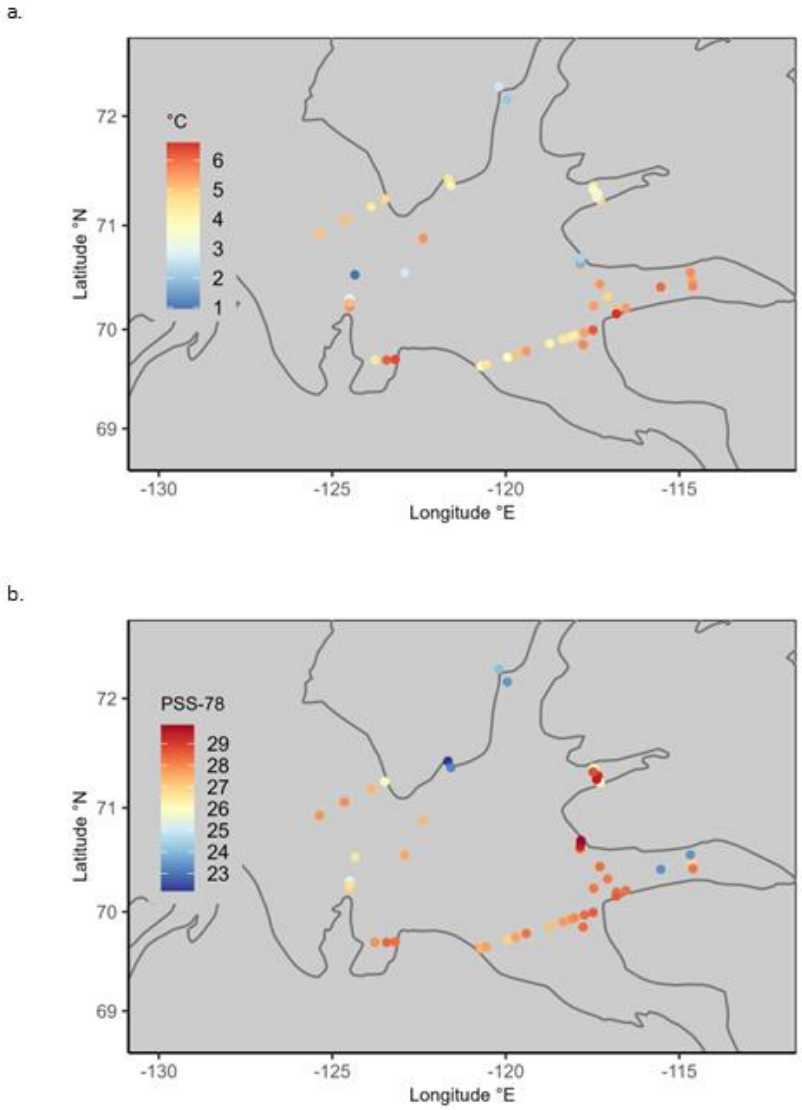

Figure 22. (a) Surface temperature (°C), and (b) surface salinity at each CBS-MEA station in 2021.

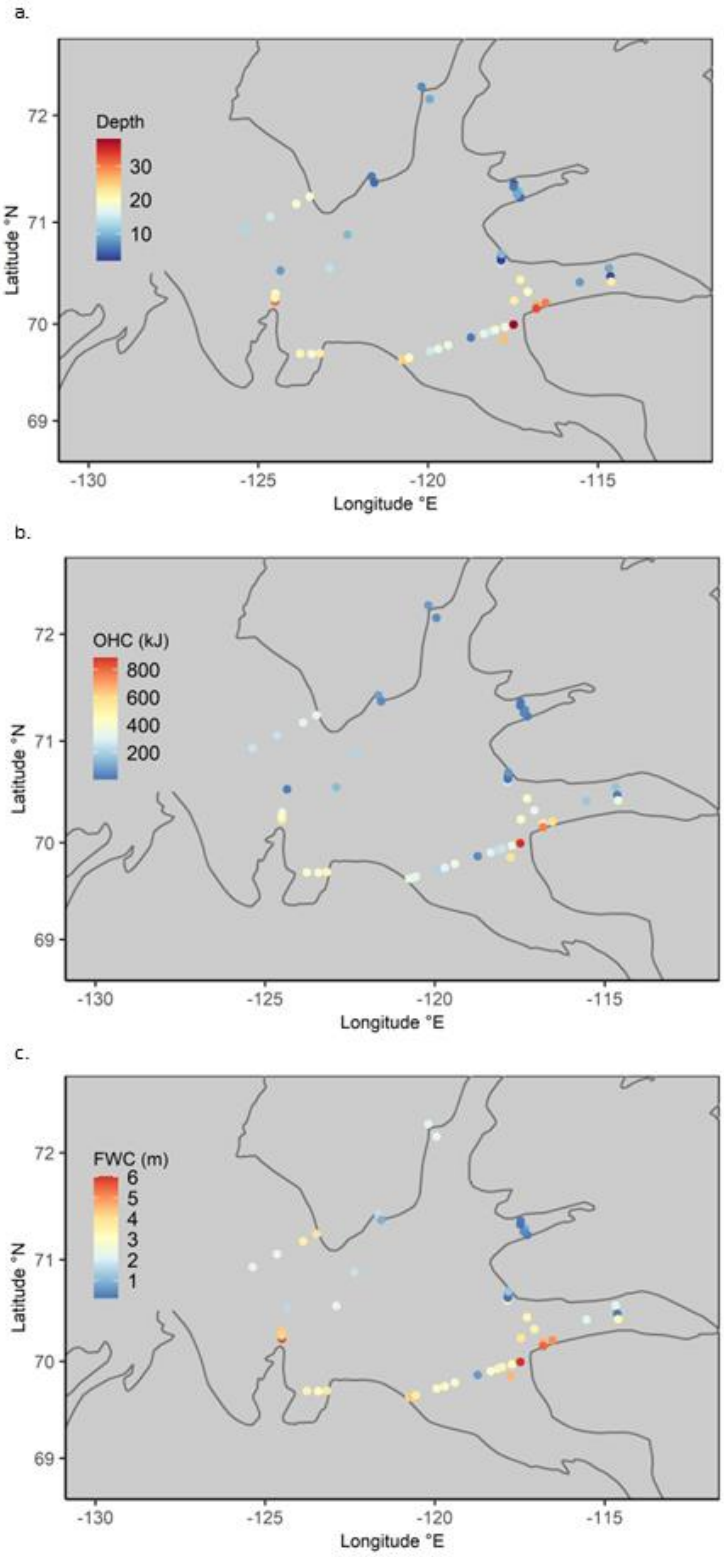

Figure 23. (a) Depth of the maximum N^2 (dbar), (b) ocean heat content (kJ in a 1 m^2 column to a depth of the N^2 max), and (c) Freshwater anomaly (m) relative to S = 34.8, to the depth of the N^2 max at each CBS-MEA station in 2021.

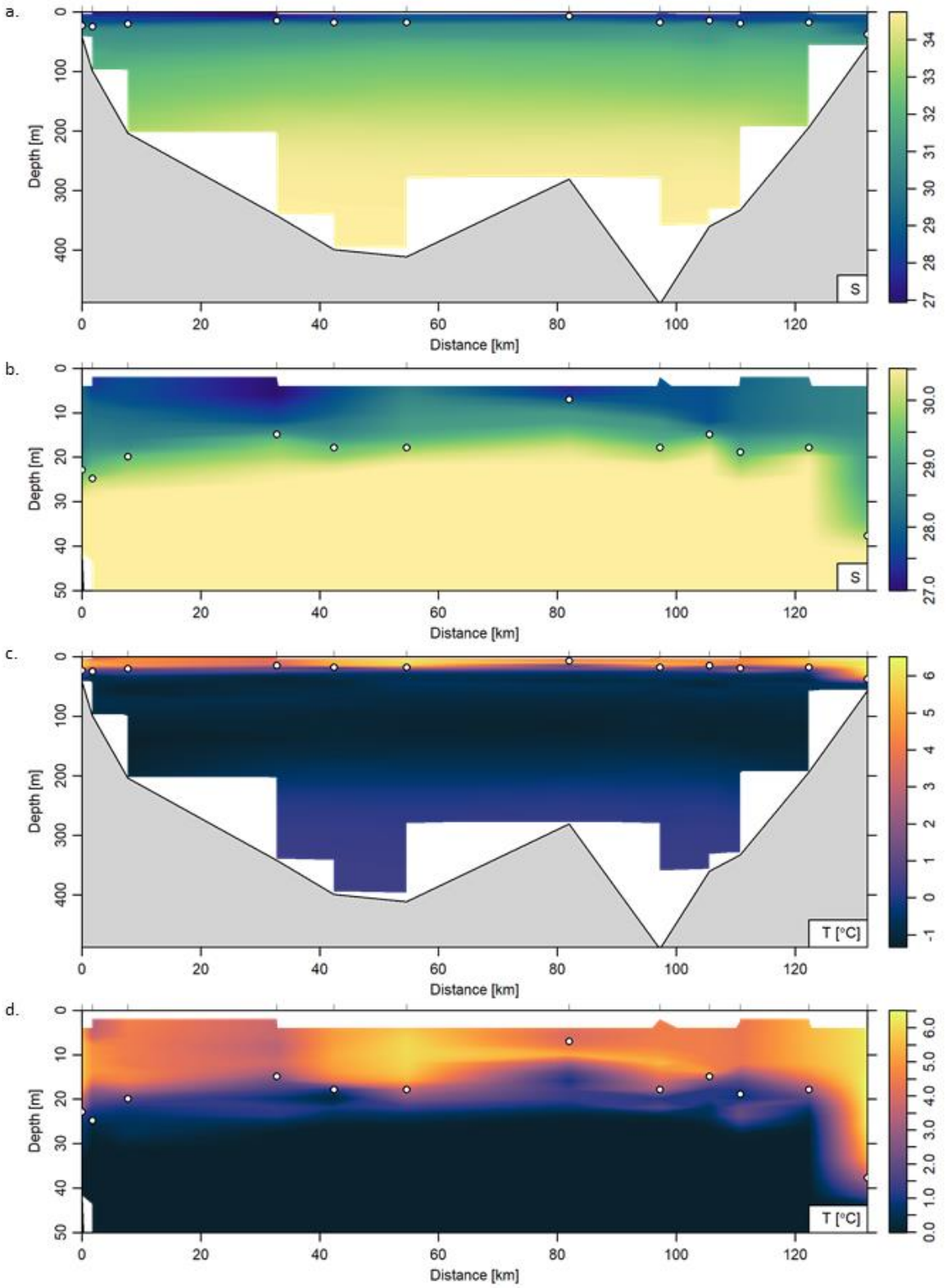

Figure 24. Sections from west to east across Dolphin and Union Strait in 2019: salinity (a, b) and temperature (c, d). Full depth is shown in (a, c) and enlarged to show only the top 50 m in (b, d). N^2-derived surface layer depths at each station are denoted by white dots.

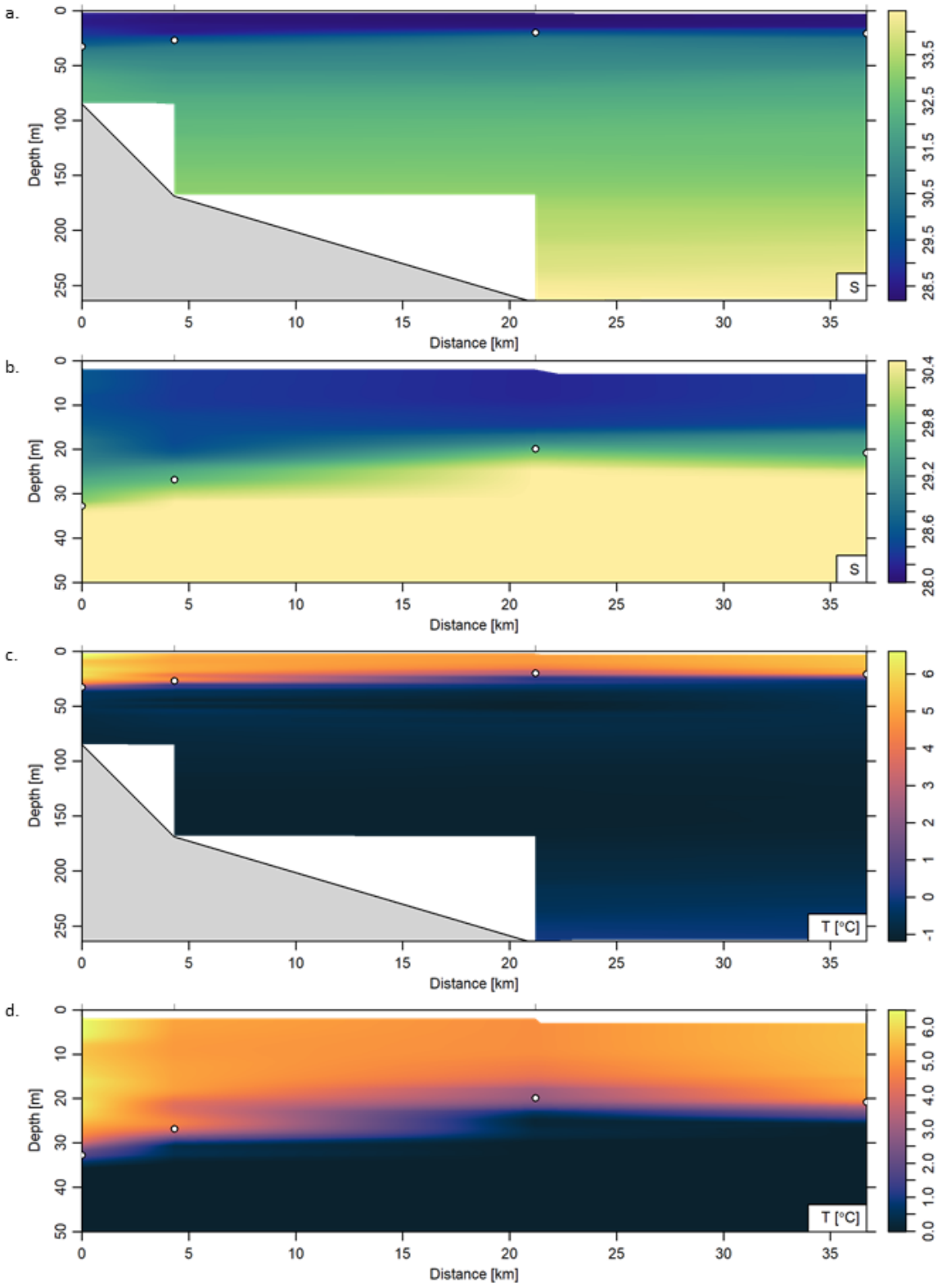

Figure 25. Sections from south to north across the west end of Prince Albert Sound in 2021: salinity (a, b) and temperature (c, d). Full depth is shown in (a, c) and enlarged to show only the top 50 m in (b, d). N^2-derived surface layer depths at each station are denoted by white dots.

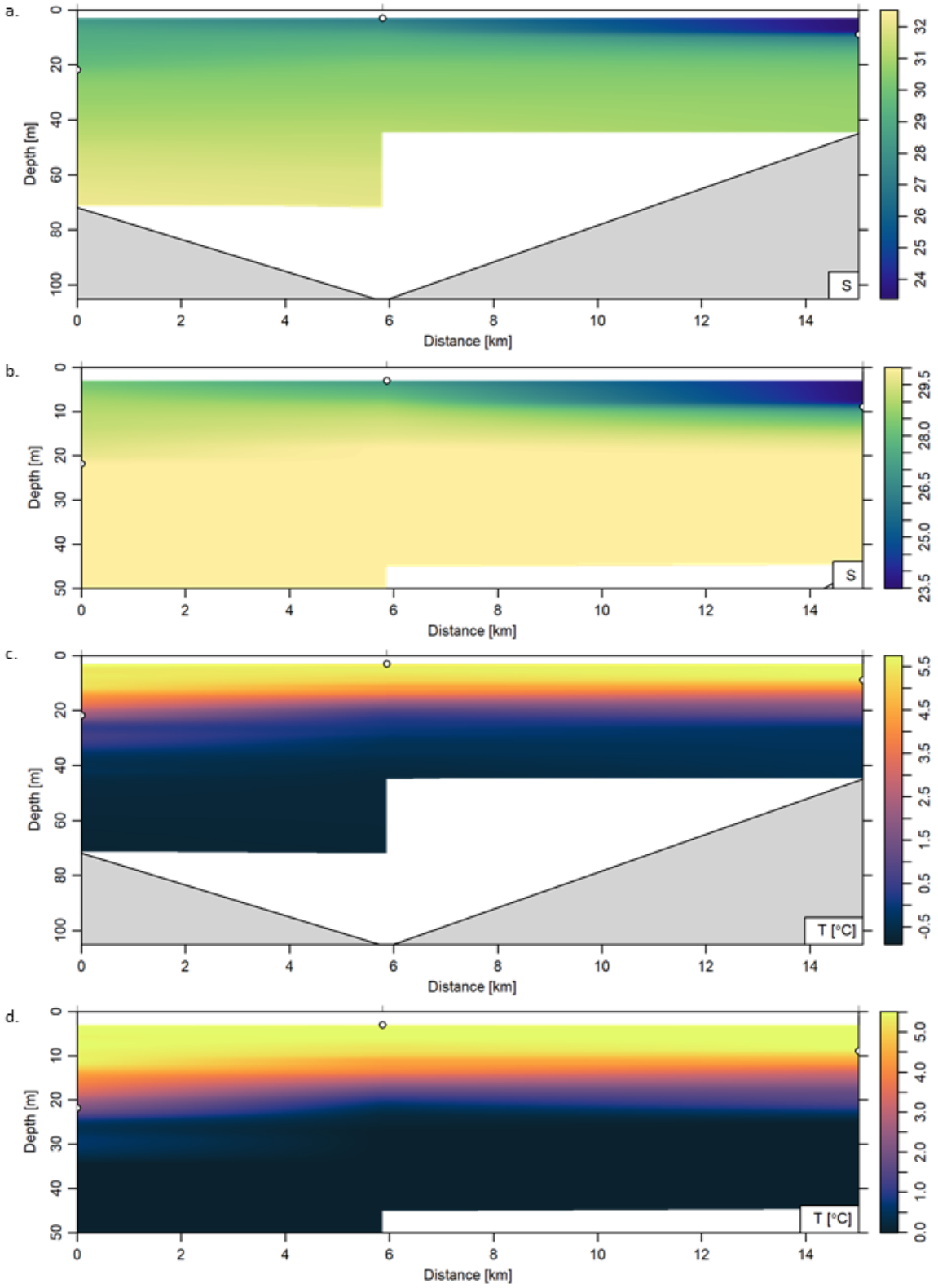

Figure 26. Sections from south to north across the east end of Prince Albert Sound in 2021: salinity (a, b) and temperature (c, d). Full depth is shown in (a, c) and enlarged to show only the top 50 m in (b, d). N^2-derived surface layer depths at each station are denoted by white dots.

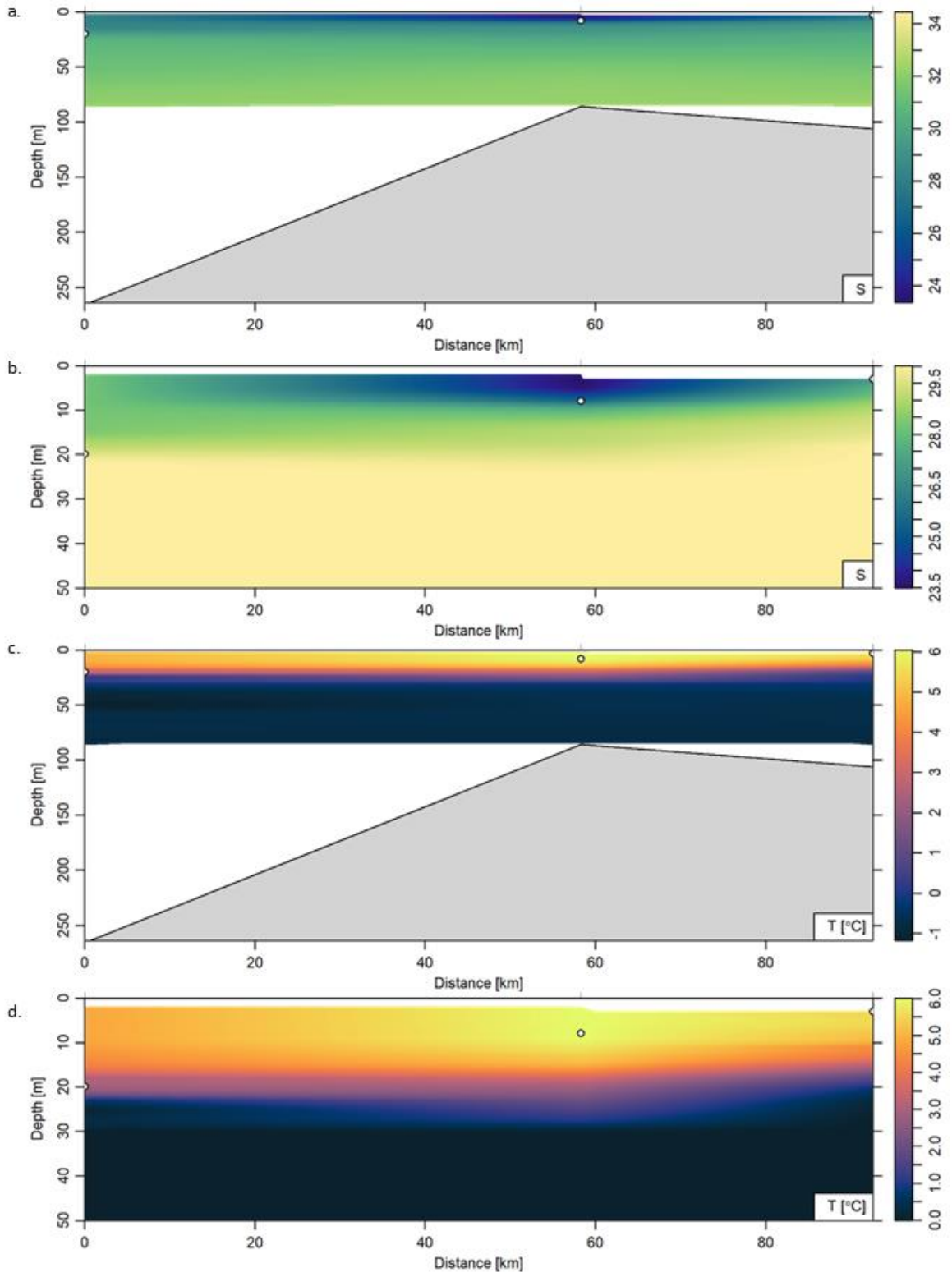

Figure 27. Sections from west to east in Prince Albert Sound in 2021: salinity (a, b) and temperature (c, d). Full depth is shown in (a, c) and enlarged to show only the top 50 m in (b, d). N^2-derived surface layer depths at each station are denoted by white dots.

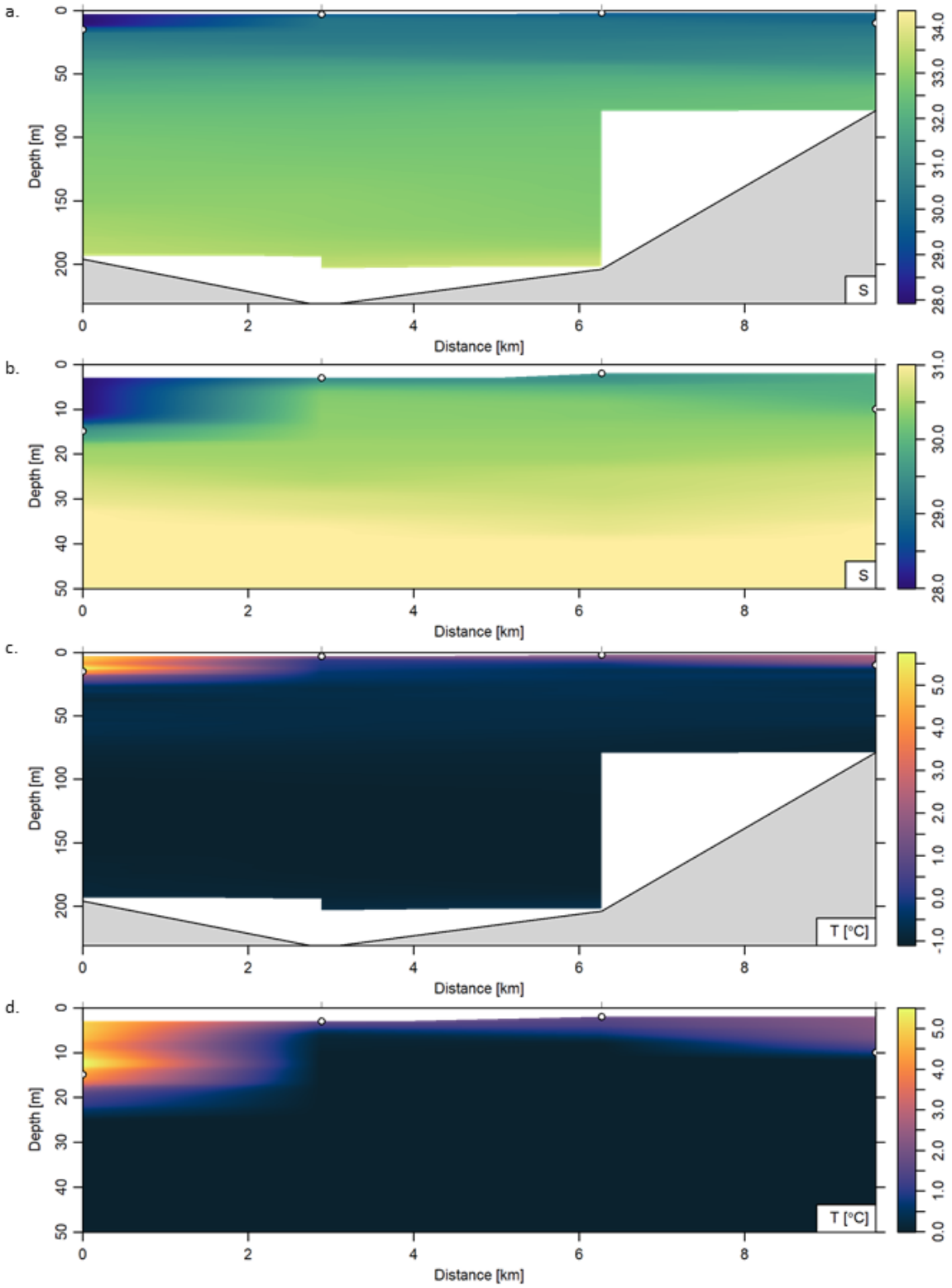

Figure 28. Sections from south to north on the Ulukhaktok transect in 2021: salinity (a, b) and temperature (c, d). Full depth is shown in (a, c) and enlarged to show only the top 50 m in (b, d). N^2-derived surface layer depths at each station are denoted by white dots.

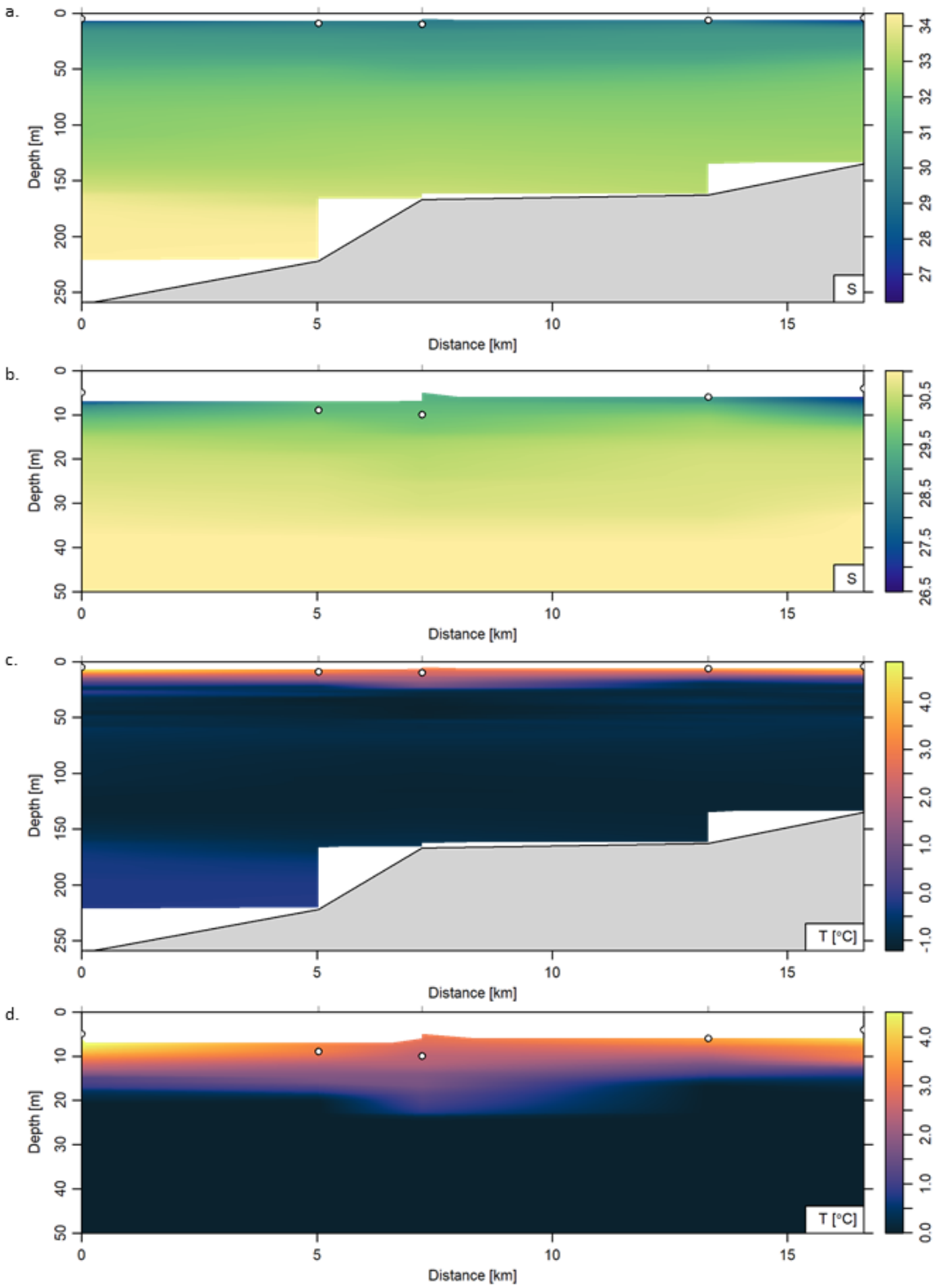

Figure 29. Sections from south to north in Minto Inlet in 2021: salinity (a, b) and temperature (c, d). Full depth is shown in (a, c) and enlarged to show only the top 50 m in (b, d). N^2-derived surface layer depths at each station are denoted by white dots.

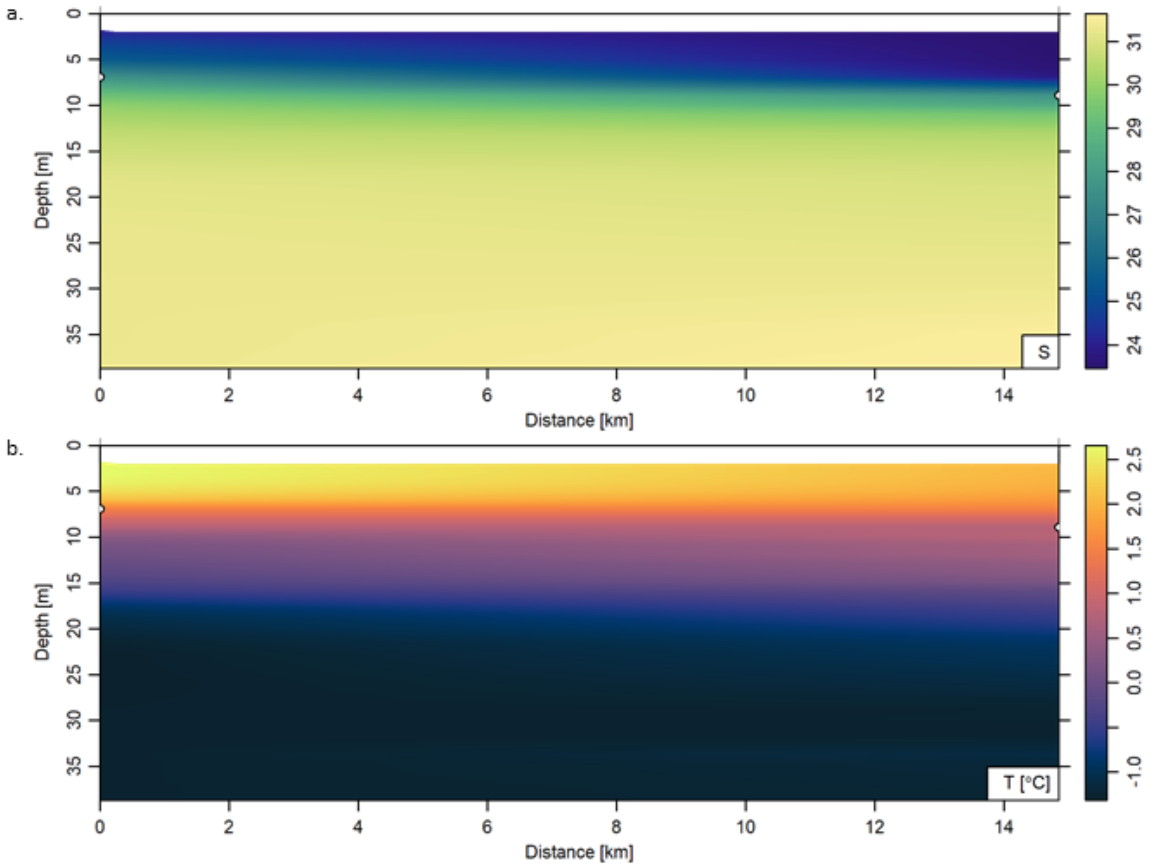

Figure 30. Sections from Northwest to Southeast in Jesse Bay in 2021: salinity (a) and temperature (b). N^2-derived surface layer depths at each station are connoted by white dots.

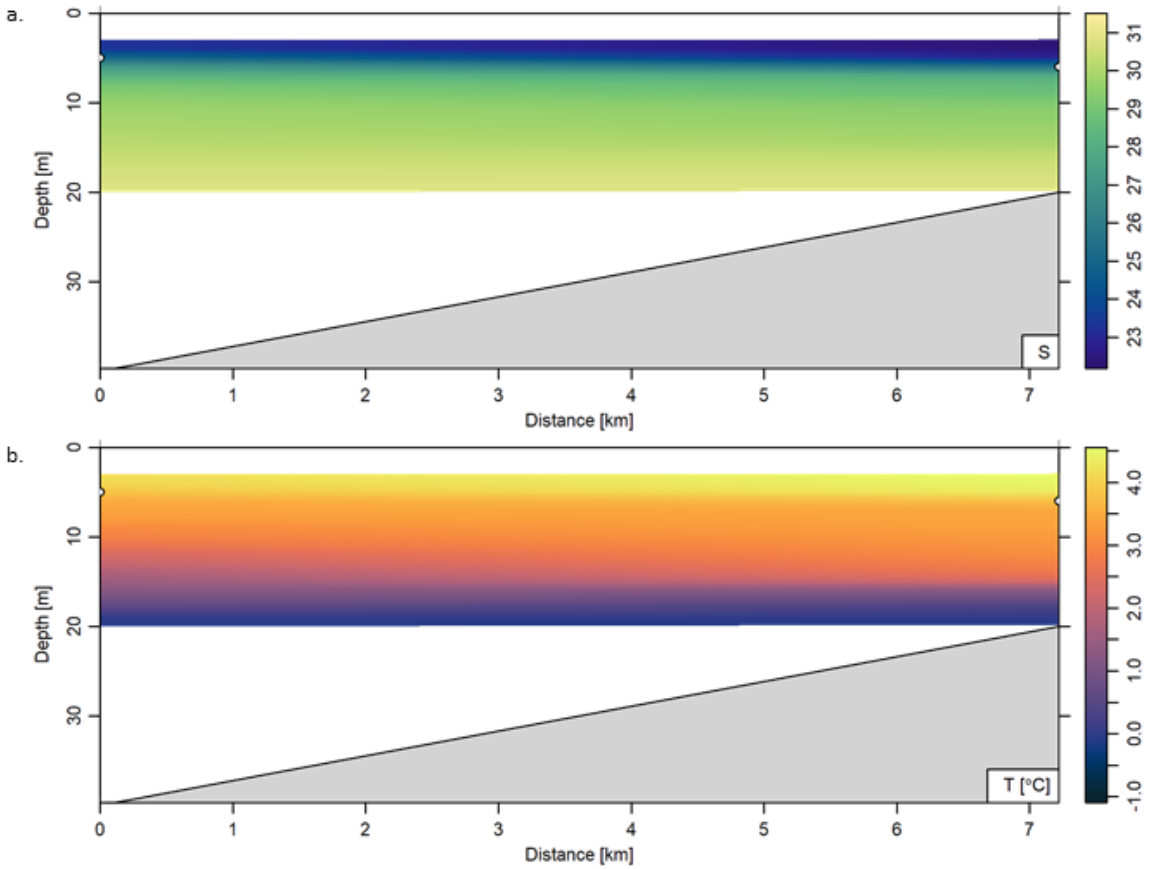

Figure 31. Sections from south to north in De Salis Bay in 2021: salinity (a) and temperature (b). N^2-derived surface layer depths at each station are connoted by white dots.

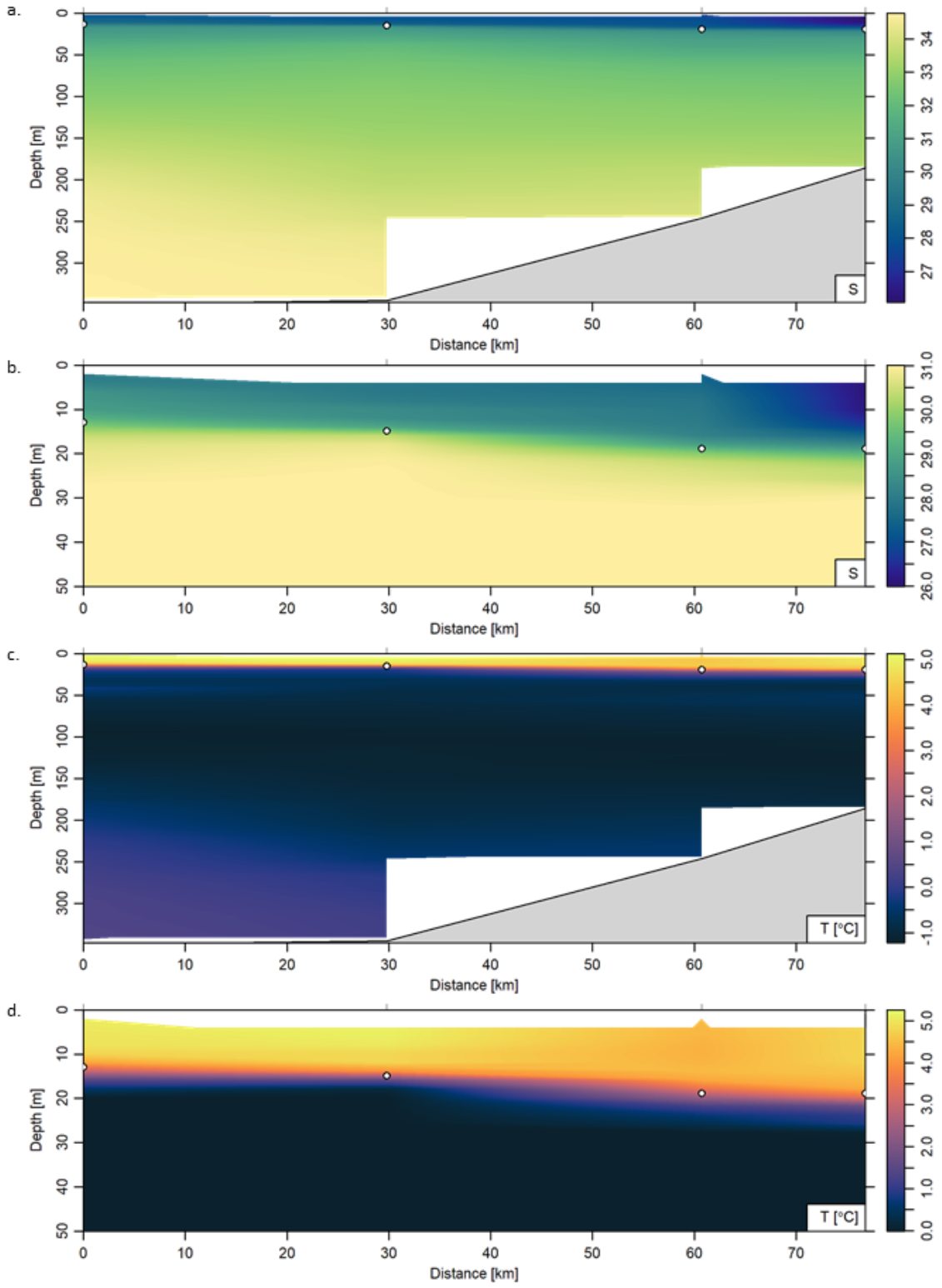

Figure 32. Sections from south to north along the Cape Bathurst transect in 2021: salinity (a, b) and temperature (c, d). Full depth is shown in (a, c) and enlarged to show only the top 50 m in (b, d). N^2-derived surface layer depths at each station are connoted by white dots.

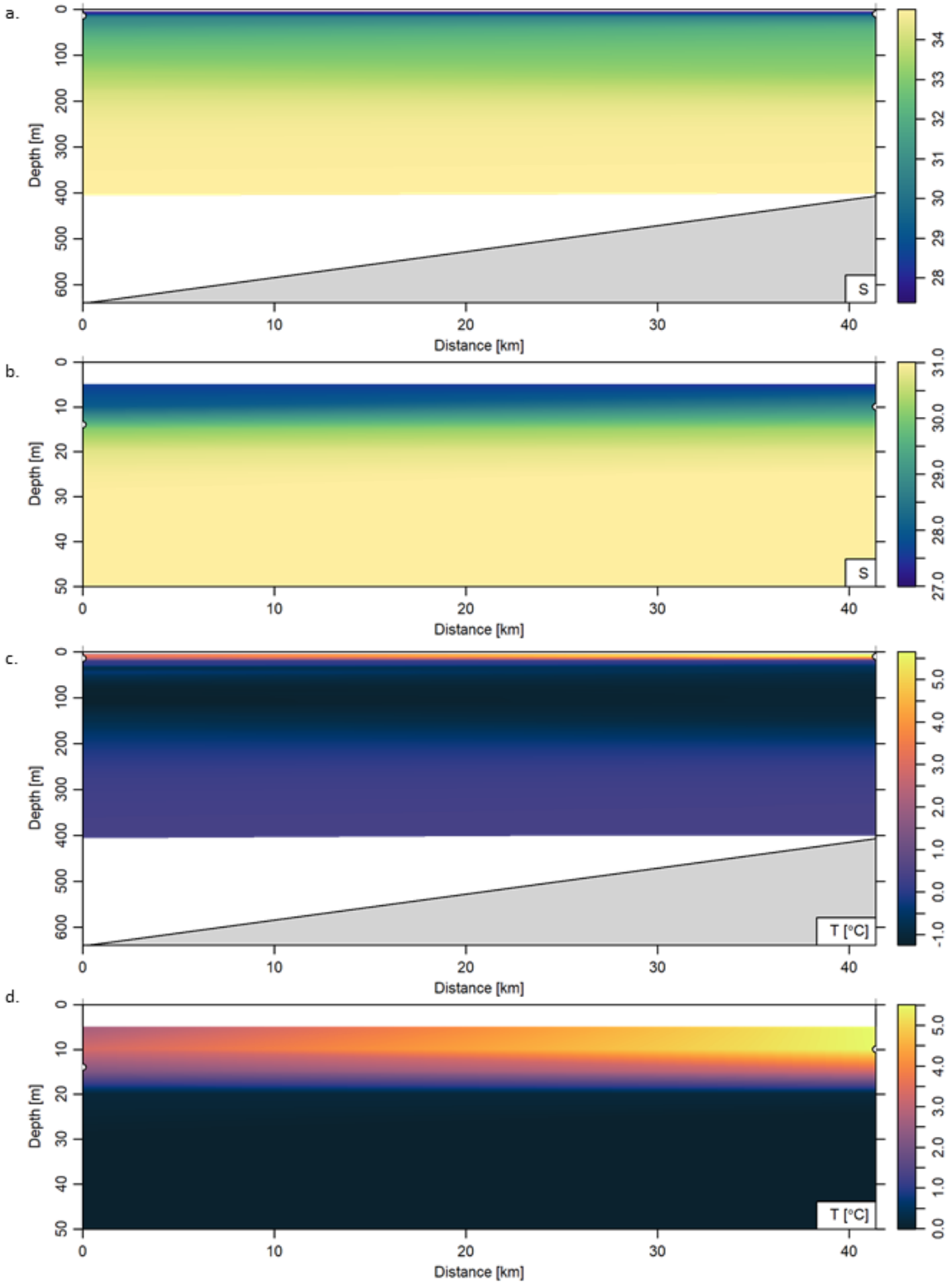

Figure 33. Sections from south to north in Amundsen Gulf for the two AMG stations in 2021: salinity (a, b) and temperature (c, d). Full depth is shown in (a, c) and enlarged to show only the top 50 m in (b, d). N^2-derived surface layer depths at each station are connoted by white dots.

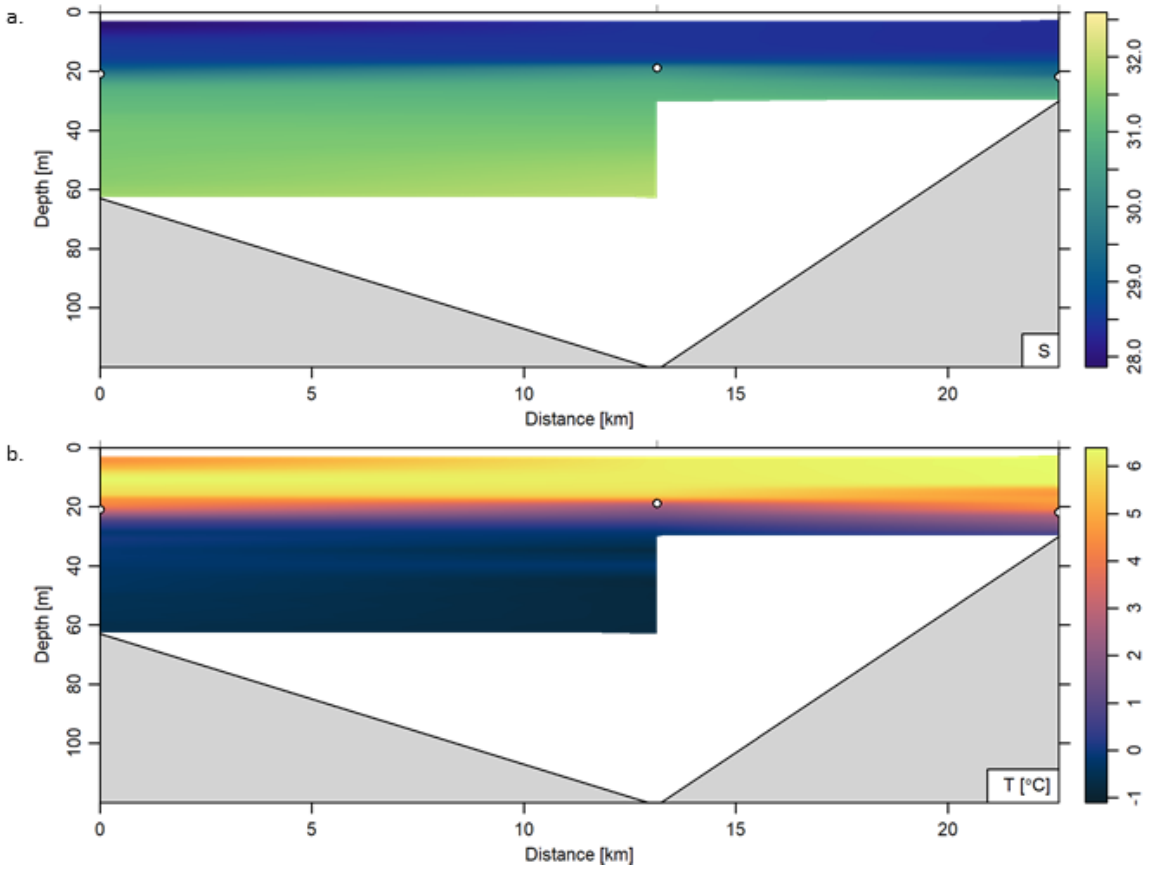

Figure 34. Salinity (a) and temperature (b) sections from west to east across Darnley Bay on the Bennett Point transect in 2021. N^2-derived surface layer depths at each station are connoted by white dots.

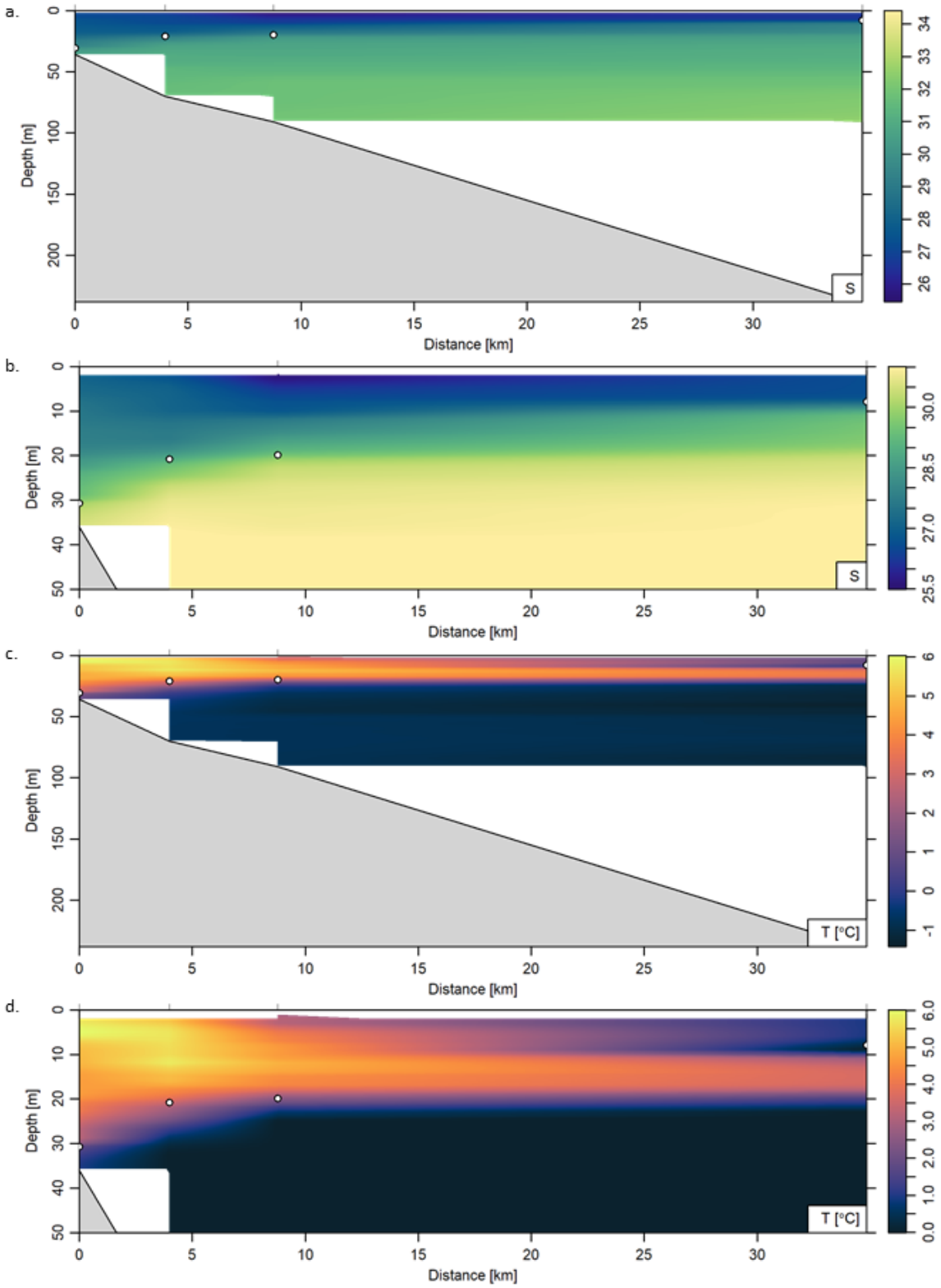

Figure 35. Sections from south to north across Amundsen Gulf using the Cape Parry stations in 2021: salinity (a, b) and temperature (c, d). Full depth is shown in (a, c) and enlarged to show only the top 50 m in (b, d). N^2-derived surface layer depths at each station are connoted by white dots.

8. Tables

Table 1. Surface and surface layer oceanographic parameters at each CBS-MEA station, August-September 2021. Freshwater content (FWC) and ocean heat content (OHC) is integrated over the surface layer (dbar) depth.

Station	Lat (°N)	Lon (°N)	Surface Temp (°C)	Surface Salinity	Surface depth (dbar)	Surface Layer (dbar)	OHC (kJ)	FWC (m)	Station Depth
DUS_01	69.63	-120.75	5.38	28.03	3	23	436.60	3.87	50
DUS_02	69.64	-120.71	3.42	27.37	2	25	338.30	4.38	108
DUS-03	69.65	-120.56	4.57	27.70	2	20	329.10	3.61	222
DUS_04	69.72	-119.95	3.75	26.96	2	15	207.45	2.93	355
DUS_HC3	69.75	-119.71	5.06	27.66	3	18	308.00	3.03	403
DUS_05	69.79	-119.41	5.53	28.28	3	18	371.71	2.73	418
DUS_06	69.86	-118.74	4.18	27.25	4	6	50.91	0.64	277
DUS_07	69.90	-118.36	4.46	27.77	2	17	303.31	2.98	499
DUS_HC1	69.92	-118.15	4.49	27.71	3	15	243.37	2.58	363
DUS_08	69.94	-118.02	4.28	28.02	2	19	257.52	3.34	346
DUS_09	69.97	-117.73	5.46	28.42	2	18	353.80	3.02	205
DUS_11	69.99	-117.49	6.22	28.55	3	38	885.58	6.03	60
DUS_HC4	69.85	-117.77	5.73	28.41	1	26	570.98	4.57	280
DUS_HC5	70.23	-117.47	5.51	28.20	2	22	427.35	3.80	214
PAS_02	70.32	-117.06	4.82	28.20	2	20	342.29	3.46	270
PAS_05	70.19	-116.81	5.16	28.33	2	27	523.93	4.62	181
PAS_05A	70.15	-116.81	6.60	28.58	1	33	759.97	5.51	83.8
PAS_01	70.44	-117.29	5.58	28.34	3	21	425.32	3.35	277
PAS_HC2	70.21	-116.54	5.50	28.30	3	30	581.45	5.01	165
PAS_HC4	70.41	-115.53	6.04	23.38	2	8	175.00	2.16	98
PAS_10	70.47	-114.63	5.41	26.97	3	3	22.46	0.23	114
PAS_11	70.42	-114.61	5.74	28.26	3	22	373.10	3.25	83
PAS_09	70.56	-114.68	5.68	23.41	3	9	163.86	2.22	60
ULU-08	70.61	-117.86	4.97	27.97	2.2	15	283.74	2.64	207
ULU_8.3	70.63	-117.85	1.79	29.32	3	3	7.47	0.16	259
ULU_8.2	70.66	-117.84	1.70	29.44	2	2	7.09	0.15	217
ULU_8.1	70.69	-117.83	2.25	29.85	2	10	69.03	1.26	91
MTI_03	71.37	-117.48	4.57	26.23	4	4	19.01	0.25	147
MTI_04	71.30	-117.34	3.04	29.32	5	10	68.46	0.92	175
MTI_05	71.24	-117.28	4.83	26.25	5	5	20.09	0.25	281
MTI_4.5	71.27	-117.38	3.24	29.48	7	9	39.80	0.46	238
MTI_3.5	71.33	-117.48	3.52	28.77	6	6	14.62	0.17	177
DES_01	71.43	-121.67	4.55	22.20	2	6	90.62	1.69	31
DES_02	71.38	-121.58	4.16	23.21	3	5	50.51	0.94	53
BPT_01B	69.70	-123.77	4.48	27.87	3	21	412.55	3.42	76
BPT_03	69.70	-123.43	6.16	28.41	3	19	404.96	3.02	126
BPT_05	69.70	-123.19	6.38	28.33	2	22	482.63	3.72	37
AMG_HC01	70.88	-122.38	5.61	27.36	2	10	209.38	1.78	424
AMG_03	70.55	-122.91	2.64	27.59	3	14	146.53	2.33	643
CPB_10	71.18	-123.88	4.41	27.37	2	19	315.51	3.52	277
CPB_11	71.25	-123.49	4.80	26.08	3	19	327.59	3.94	198
CPB_09	71.06	-124.65	5.12	27.92	3	15	252.26	2.41	352
CPB_08	70.93	-125.37	5.09	27.87	1	13	258.83	2.33	357
CPY_ICE1	70.53	-124.35	0.96	26.59	2	8	24.75	1.63	249
CPY_01	70.22	-124.50	5.68	27.09	2	31	560.97	5.74	44
CPY_ICE2	70.30	-124.50	2.84	25.48	1	20	338.71	4.33	90.1
CPY_02	70.26	-124.51	5.14	26.68	2	21	428.87	4.20	81
JES_HC1.	72.15	-119.96	2.02	23.47	2	9	54.93	2.41	45
JES_01.1	72.26	-120.20	2.62	24.06	0	7	79.90	2.21	38.5

Appendix A – Profiles and Maps

Salinity, temperature, potential density anomaly, and N^2, and T-S plots for each of the stations sampled during CBS-MEA 2021. Station name is indicated with the map, showing the station location as described in Figure 21 and Table 1.

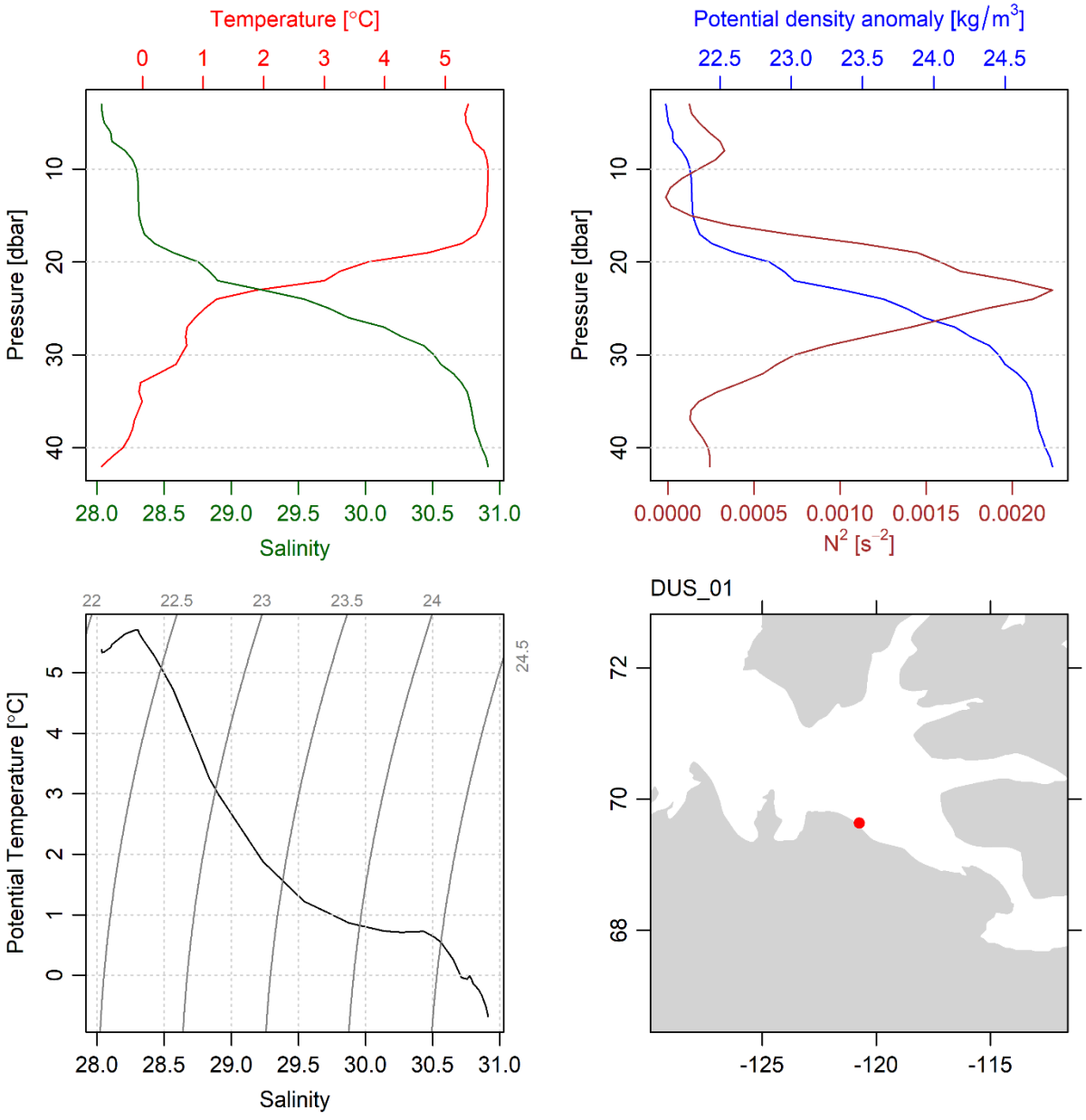

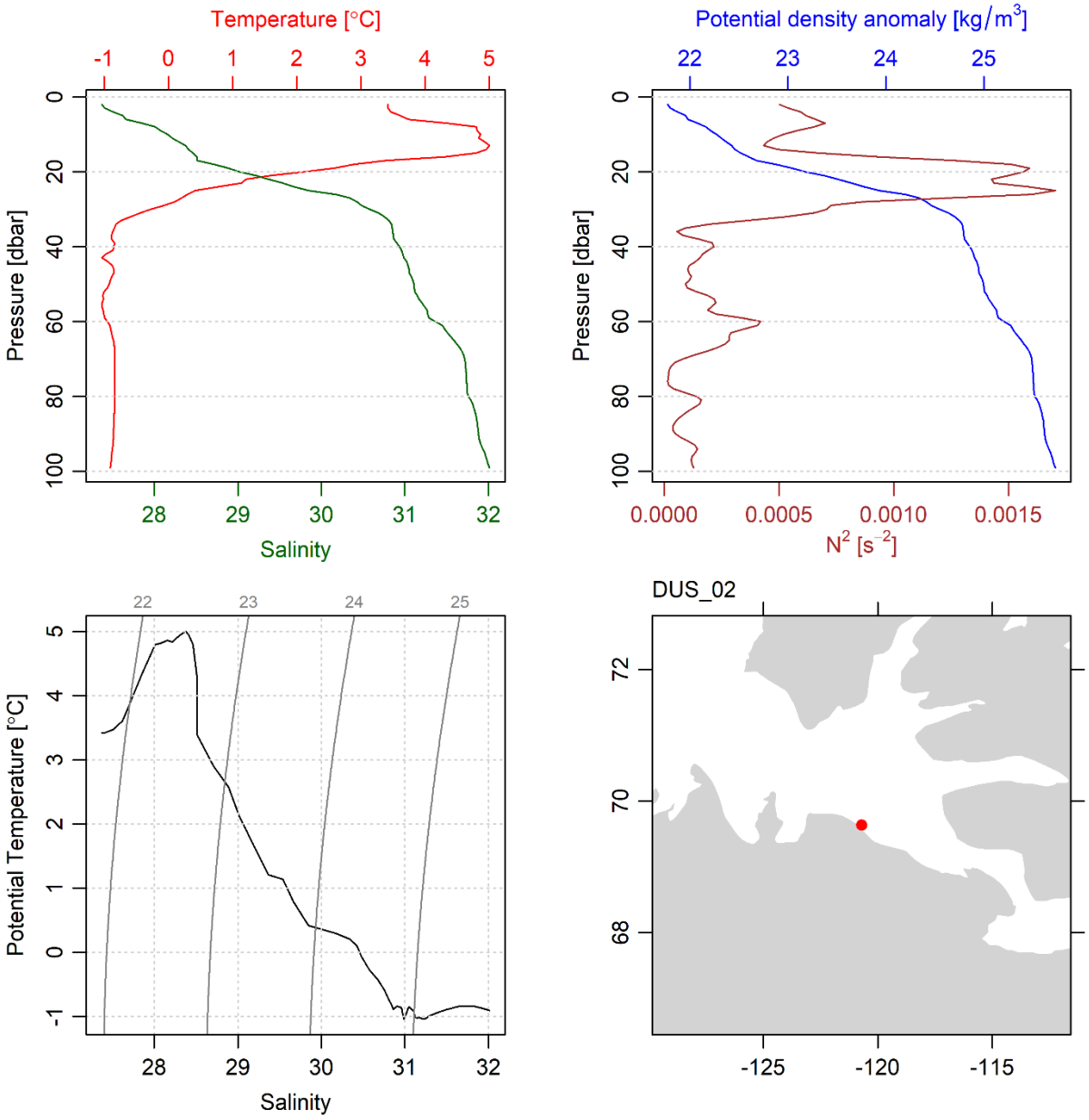
Temperature [°C]
-1 0 1 2 3 4 5
Pressure [dbar]
0 20 40 60 80 100
28 29 30 31 32
Salinity
Potential density anomaly [kg/m3]
22 23 24 25
0.0000 0.0005 0.0010 0.0015
N2 [s−2]
Potential Temperature [°C]
22 23 24 25
-1 0 1 2 3 4 5
DUS_02
72 70 68
-125 -120 -115

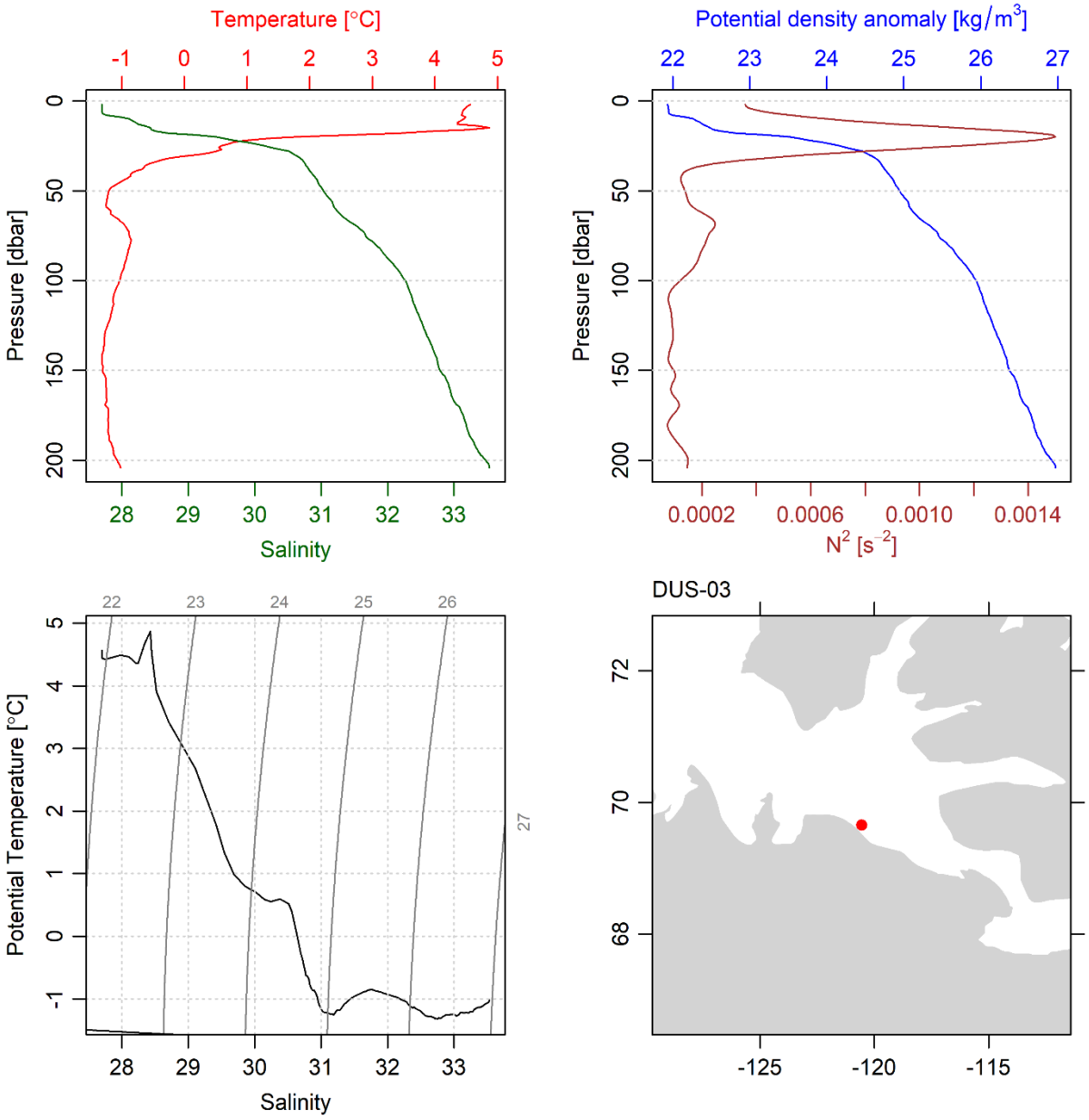
Temperature [°C]
-1 0 1 2 3 4 5
Pressure [dbar]
0 50 100 150 200
28 29 30 31 32 33
Salinity
Potential density anomaly [kg/m3]
22 23 24 25 26 27
0.0002 0.0006 0.0010 0.0014
N2 [s−2]
Potential Temperature [°C]
22 23 24 25 26
27
DUS-03
72 70 68
-125 -120 -115

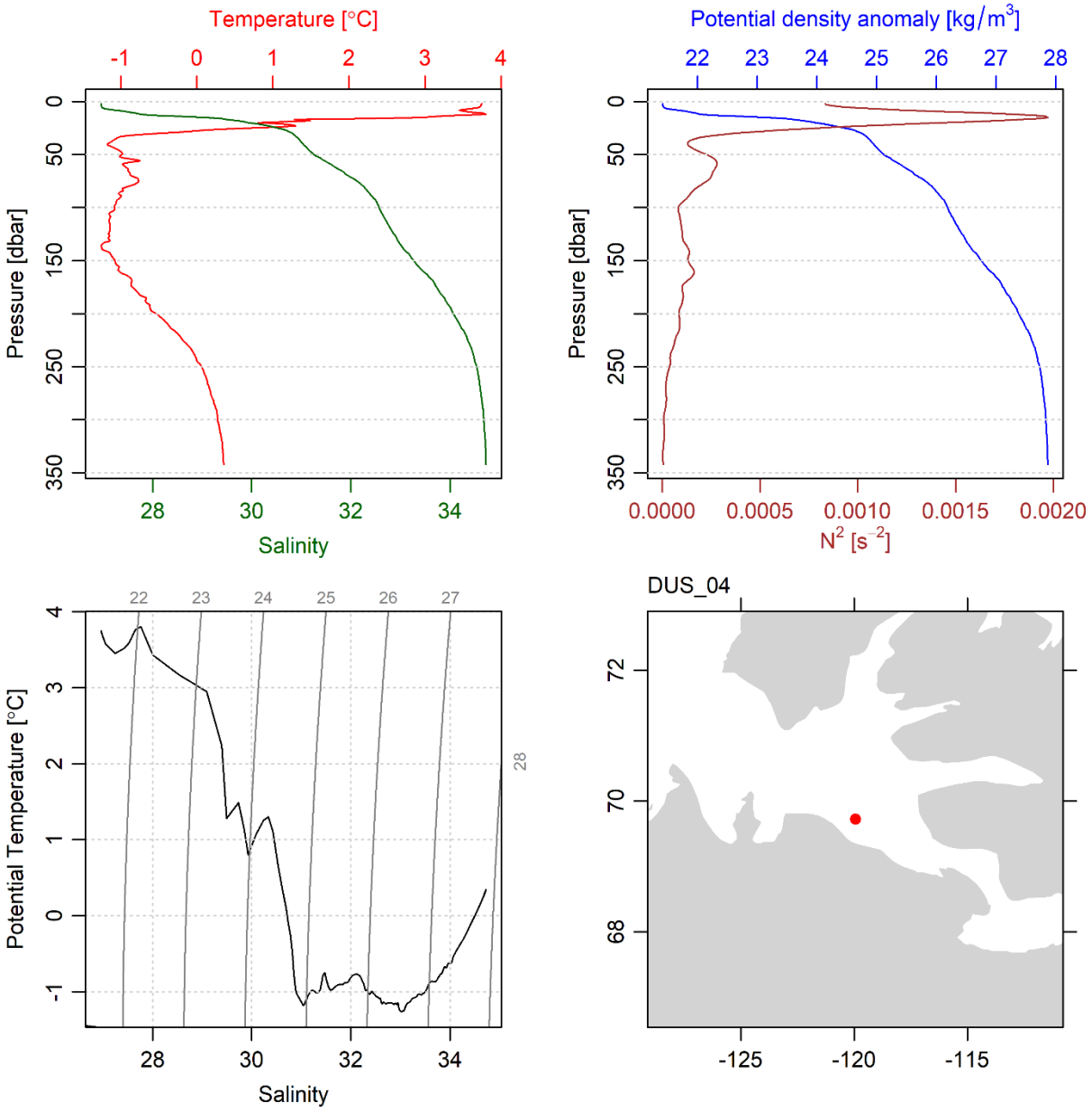
Temperature [°C]
-1
0
1
2
3
4
Pressure [dbar]
0
50
150
250
350
28
30
32
34
Salinity
Potential density anomaly [kg/m3]
22
23
24
25
26
27
28
0.0000
0.0005
0.0010
0.0015
0.0020
N2 [s−2]
Potential Temperature [°C]
22
23
24
25
26
27
28
DUS_04
72
70
68
-125
-120
-115

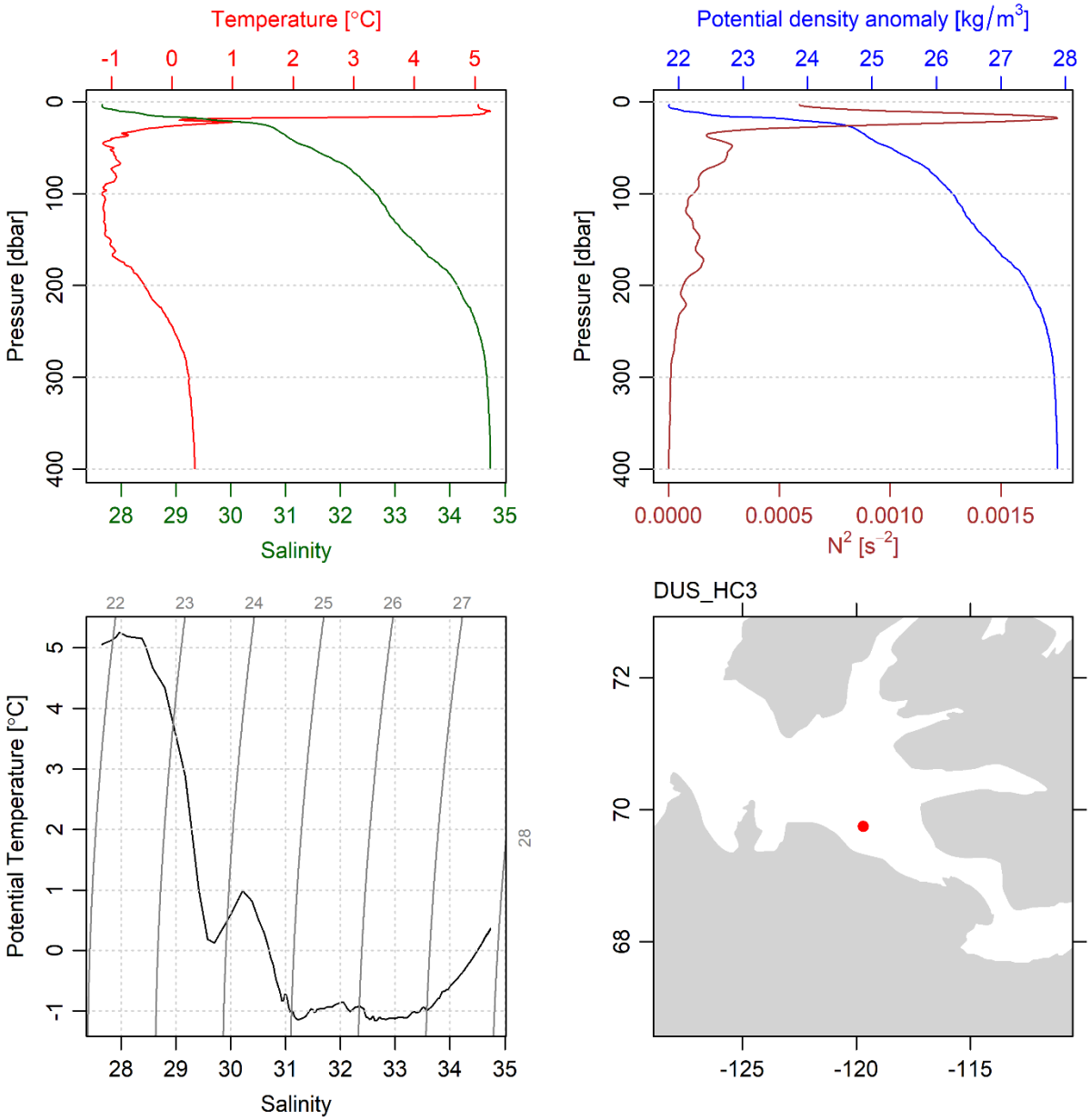
Temperature [°C]
-1 0 1 2 3 4 5
Pressure [dbar]
0 100 200 300 400
28 29 30 31 32 33 34 35
Salinity
Potential density anomaly [kg/m3]
22 23 24 25 26 27 28
0.0000 0.0005 0.0010 0.0015
N2 [s−2]
Potential Temperature [°C]
22 23 24 25 26 27
28
DUS_HC3
72 70 68
-125 -120 -115

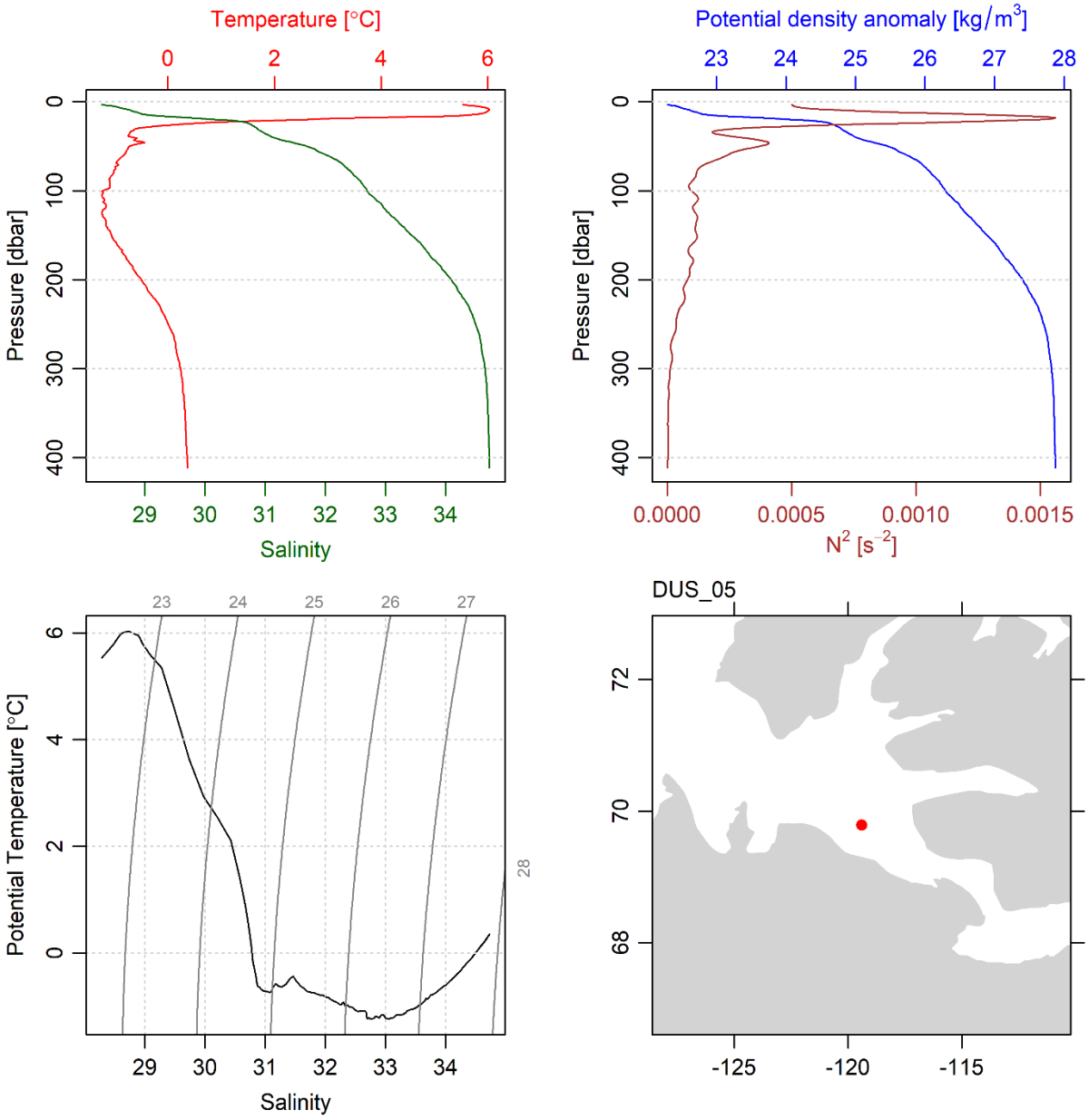
Temperature [°C]
0
2
4
6
Pressure [dbar]
0
100
200
300
400
29
30
31
32
33
34
Salinity
Potential density anomaly [kg/m3]
23
24
25
26
27
28
0.0000
0.0005
0.0010
0.0015
N2 [s−2]
Potential Temperature [°C]
23
24
25
26
27
28
DUS_05
72
70
68
-125
-120
-115

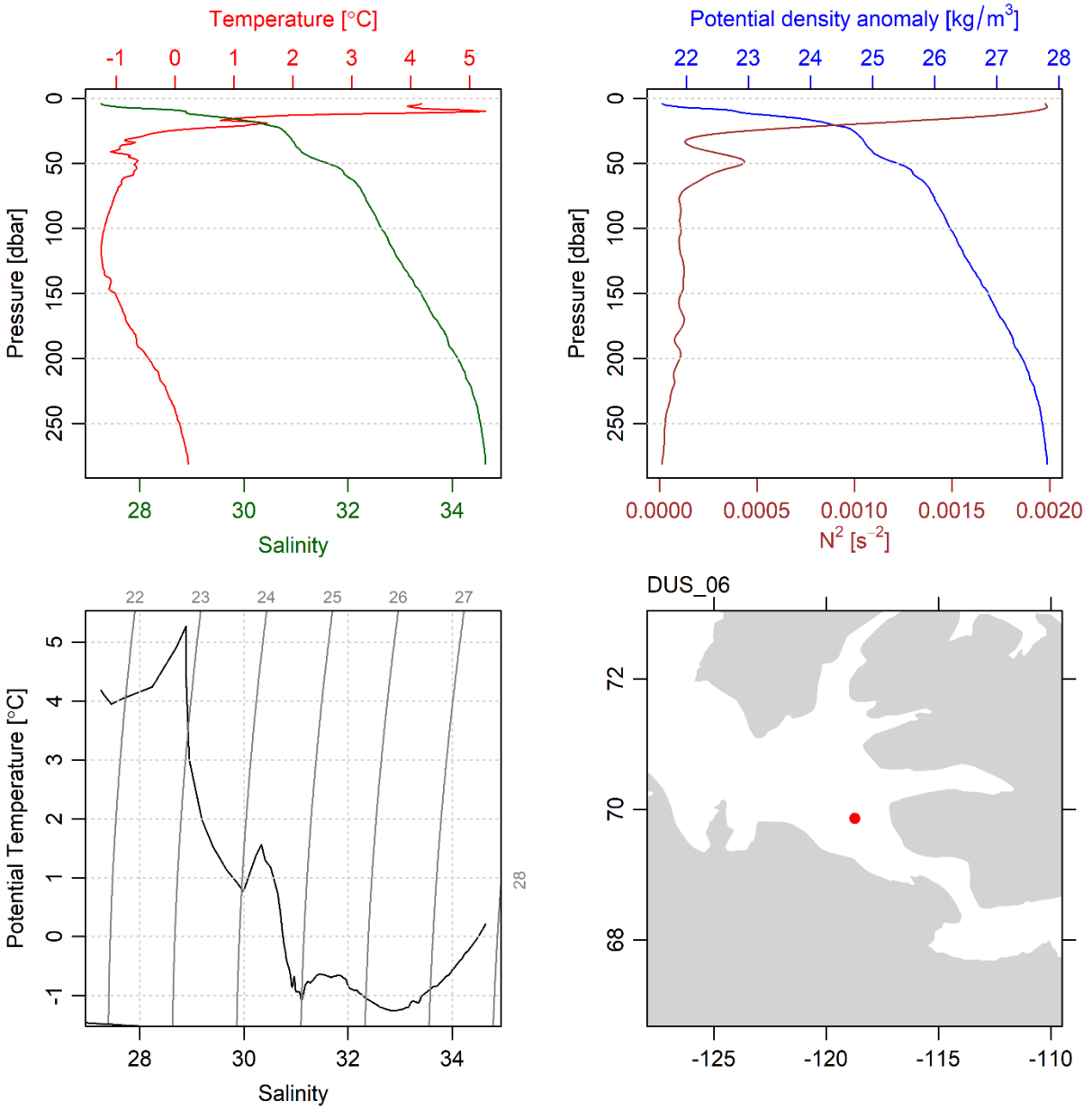
Temperature [°C]
-1 0 1 2 3 4 5
Pressure [dbar]
0 50 100 150 200 250
28 30 32 34
Salinity
Potential density anomaly [kg/m3]
22 23 24 25 26 27 28
0.0000 0.0005 0.0010 0.0015 0.0020
N2 [s−2]
Potential Temperature [°C]
22 23 24 25 26 27
-1 0 1 2 3 4 5
28
DUS_06
72 70 68
-125 -120 -115 -110

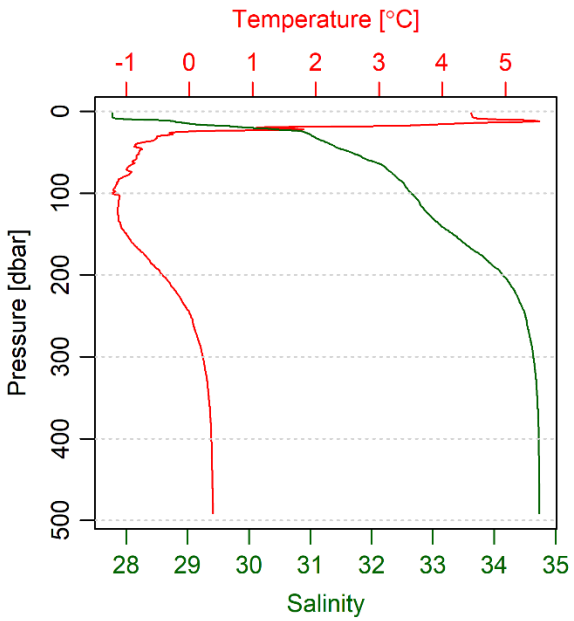
Temperature [°C]
-1
0
1
2
3
4
5
Pressure [dbar]
0
100
200
300
400
500
28
29
30
31
32
33
34
35
Salinity

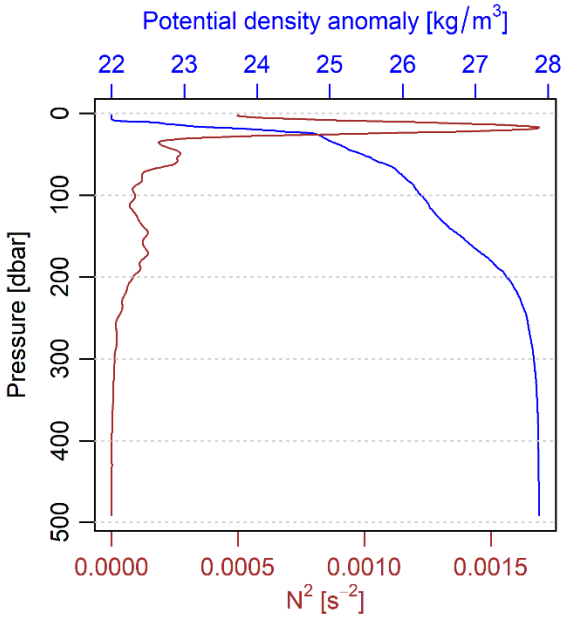
Potential density anomaly [kg/m3]
22
23
24
25
26
27
28
Pressure [dbar]
0
100
200
300
400
500
0.0000
0.0005
0.0010
0.0015
N2 [s−2]

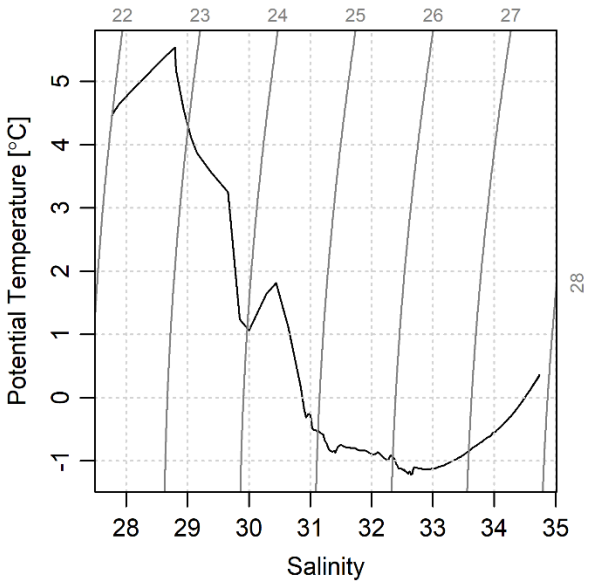
22
23
24
25
26
27
Potential Temperature [°C]
-1
0
1
2
3
4
5
28
29
30
31
32
33
34
35
Salinity
28

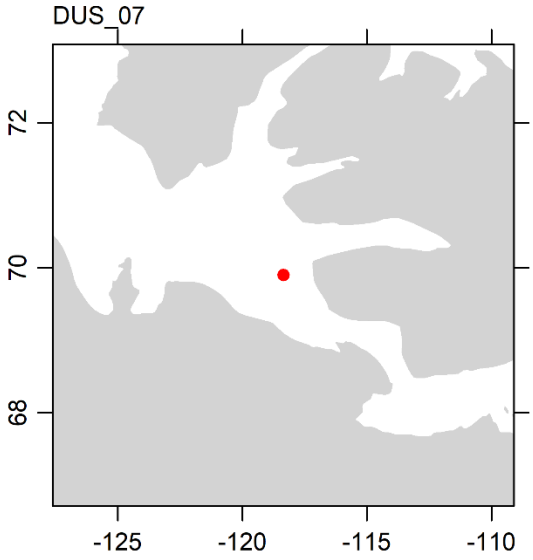
DUS_07
72
70
68
-125
-120
-115
-110

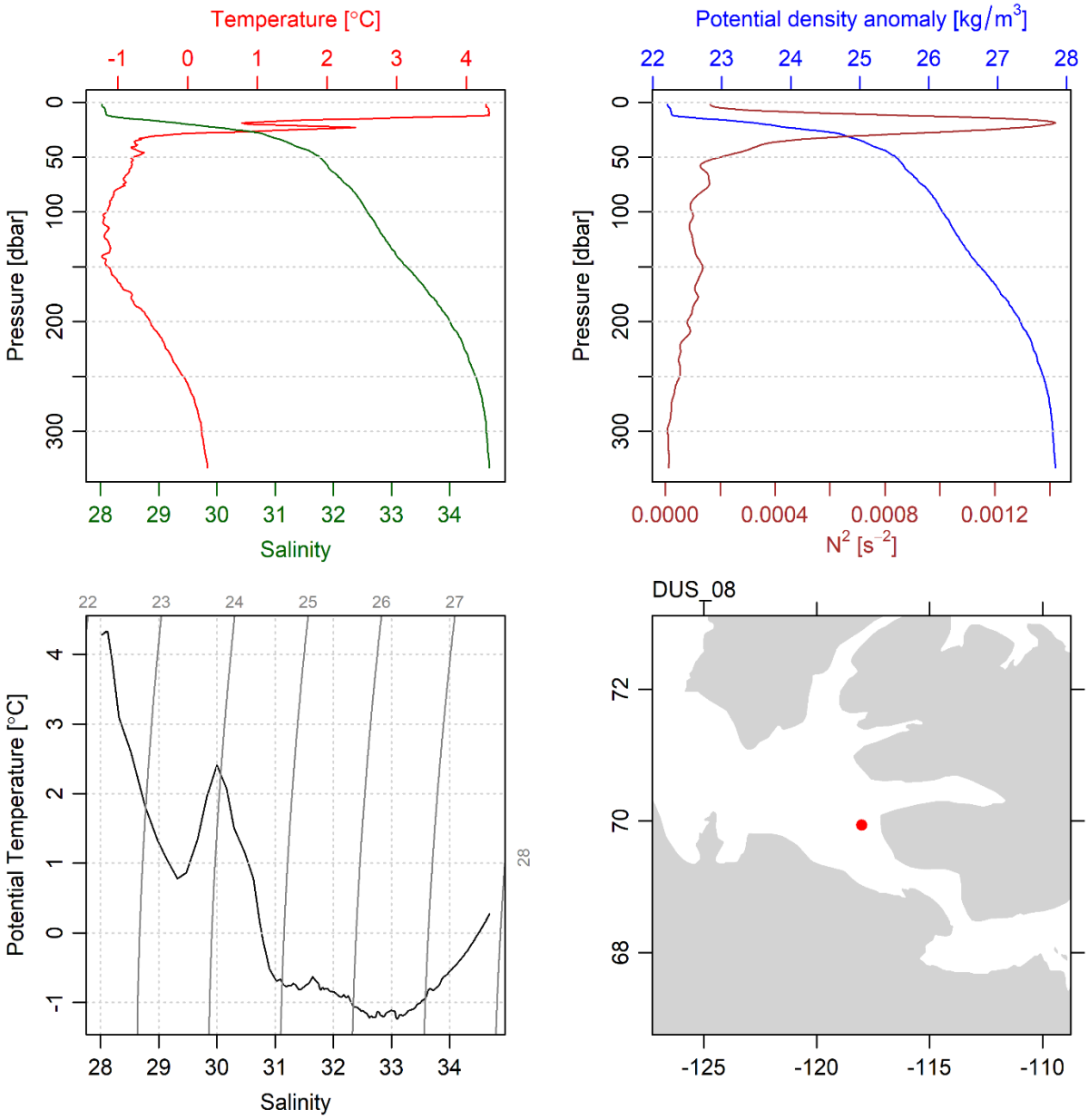
Temperature [°C]
-1 0 1 2 3 4
Pressure [dbar]
0 50 100 200 300
28 29 30 31 32 33 34
Salinity
Potential density anomaly [kg/m3]
22 23 24 25 26 27 28
0.0000 0.0004 0.0008 0.0012
N2 [s−2]
Potential Temperature [°C]
22 23 24 25 26 27
-1 0 1 2 3 4
28
DUS_08
72 70 68
-125 -120 -115 -110

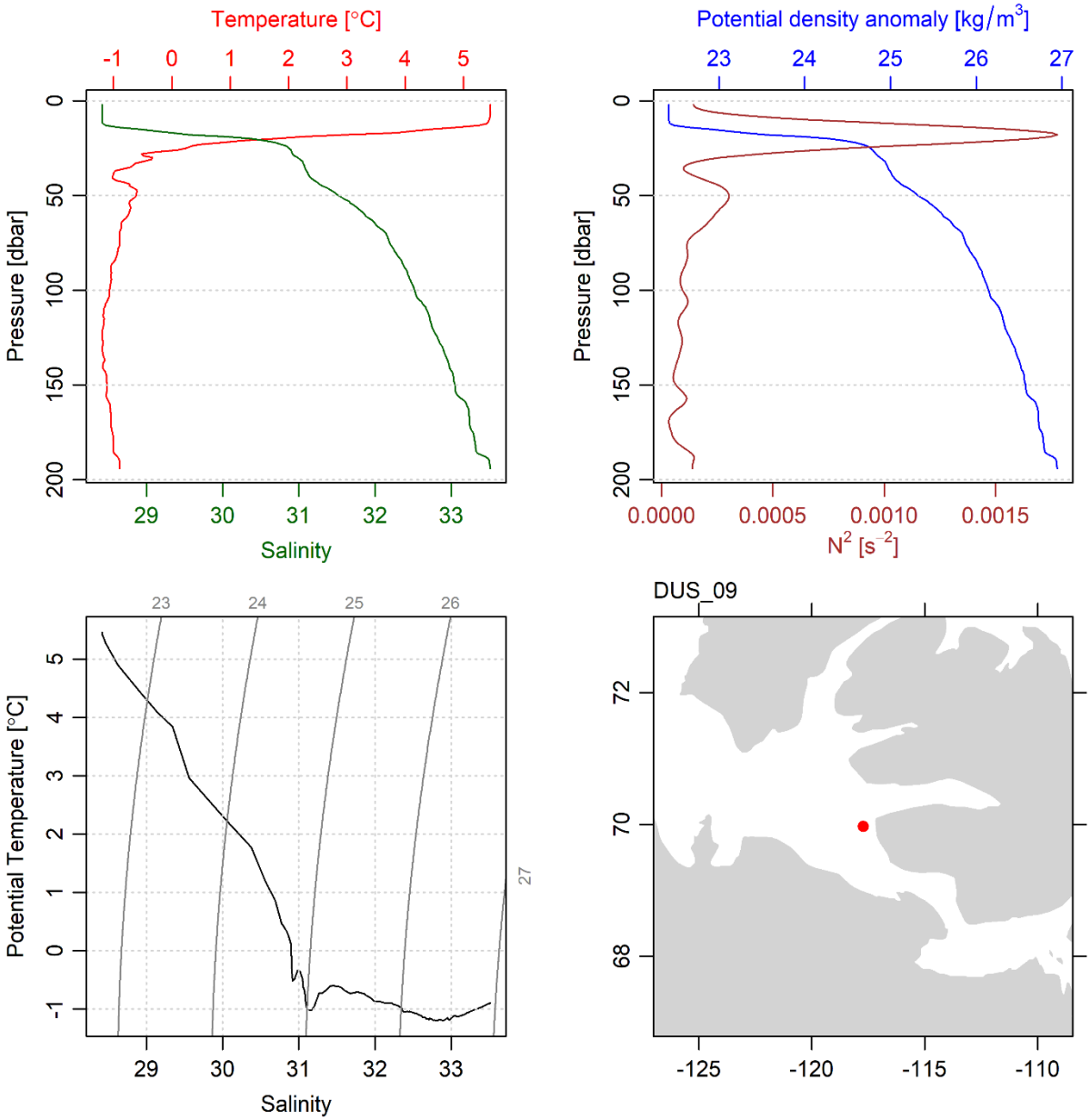
Temperature [°C]
-1 0 1 2 3 4 5
Pressure [dbar]
0 50 100 150 200
29 30 31 32 33
Salinity
Potential density anomaly [kg/m3]
23 24 25 26 27
0.0000 0.0005 0.0010 0.0015
N2 [s−2]
Potential Temperature [°C]
23 24 25 26
27
DUS_09
72 70 68
-125 -120 -115 -110

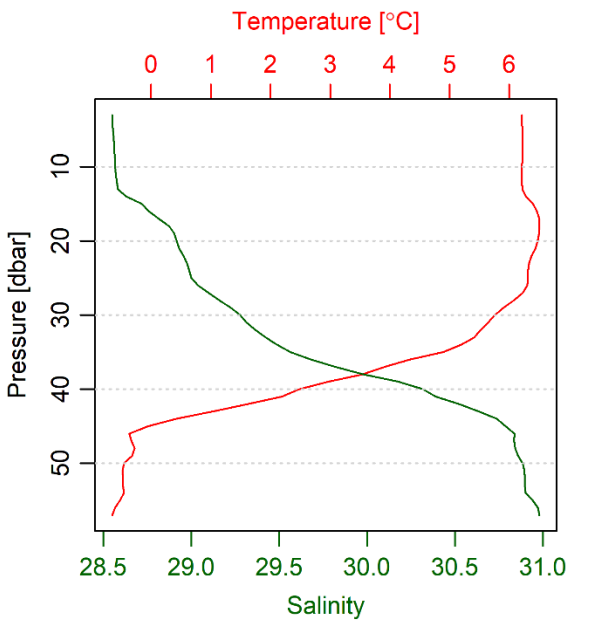
Temperature [°C]
0 1 2 3 4 5 6
Pressure [dbar]
10 20 30 40 50
28.5 29.0 29.5 30.0 30.5 31.0
Salinity

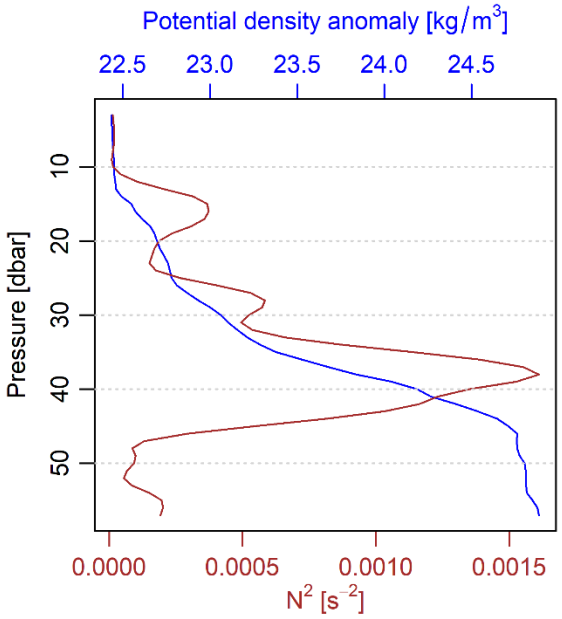
Potential density anomaly [kg/m3]
22.5 23.0 23.5 24.0 24.5
Pressure [dbar]
10 20 30 40 50
0.0000 0.0005 0.0010 0.0015
N2 [s−2]

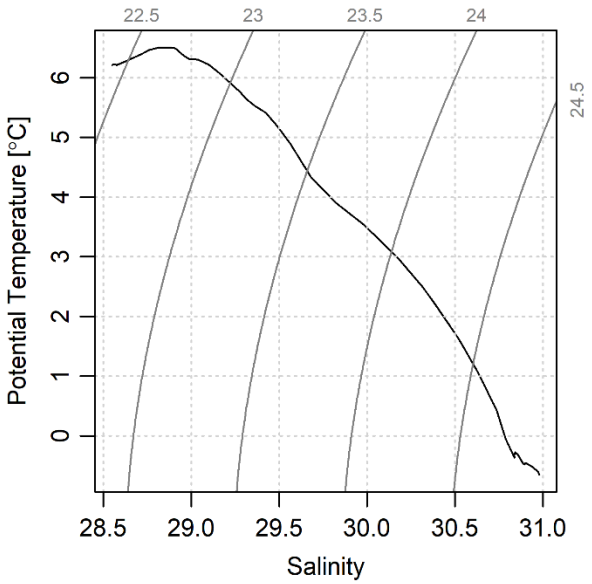
22.5 23 23.5 24 24.5
Potential Temperature [°C]
0 1 2 3 4 5 6
28.5 29.0 29.5 30.0 30.5 31.0
Salinity

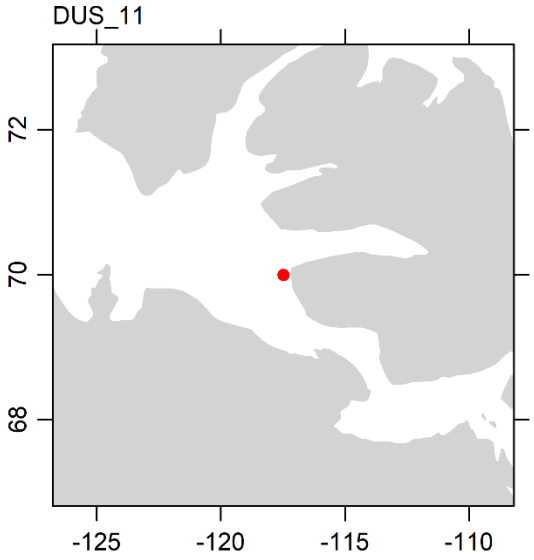
DUS_11
72
70
68
-125 -120 -115 -110

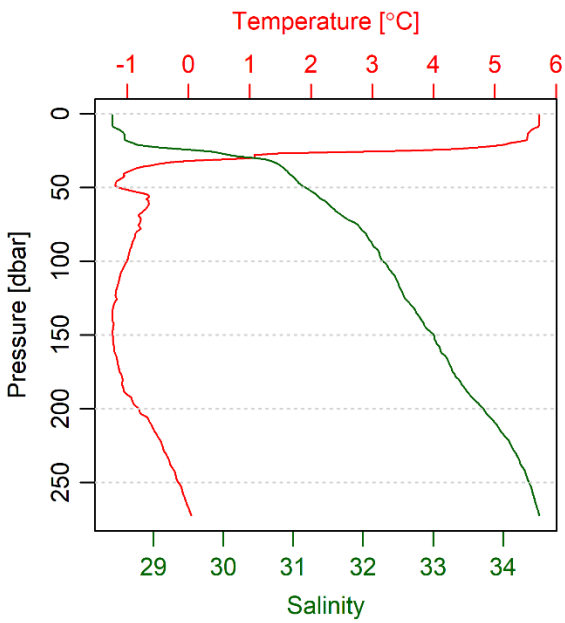
Temperature [°C]
-1
0
1
2
3
4
5
6
Pressure [dbar]
0
50
100
150
200
250
29
30
31
32
33
34
Salinity

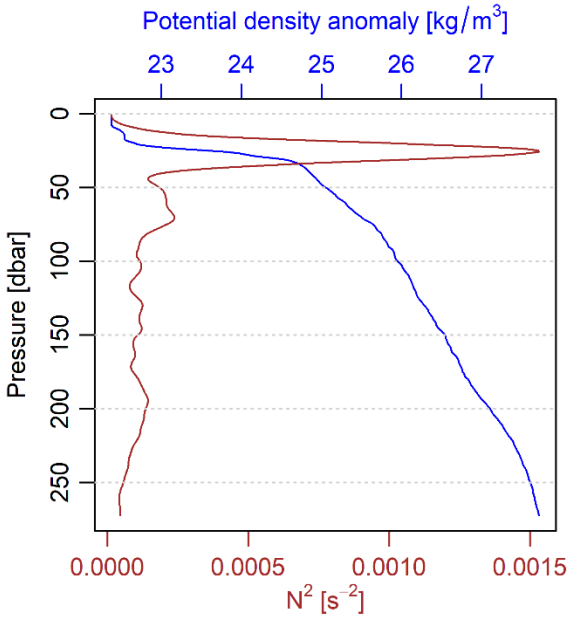
Potential density anomaly [kg/m3]
23
24
25
26
27
Pressure [dbar]
0
50
100
150
200
250
0.0000
0.0005
0.0010
0.0015
N2 [s−2]

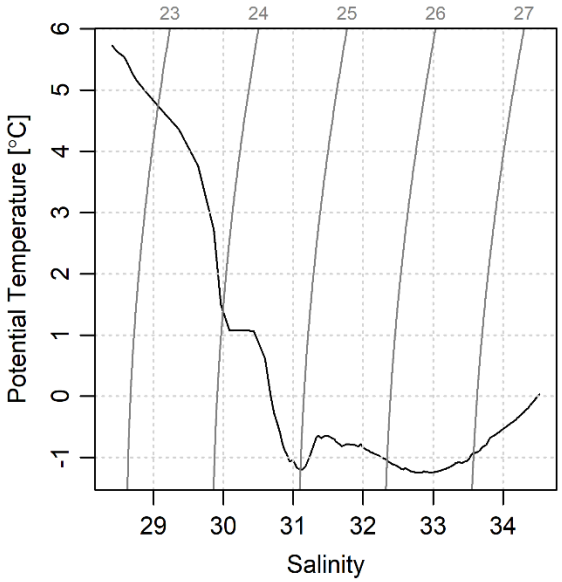
23
24
25
26
27
Potential Temperature [°C]
-1
0
1
2
3
4
5
6
29
30
31
32
33
34
Salinity

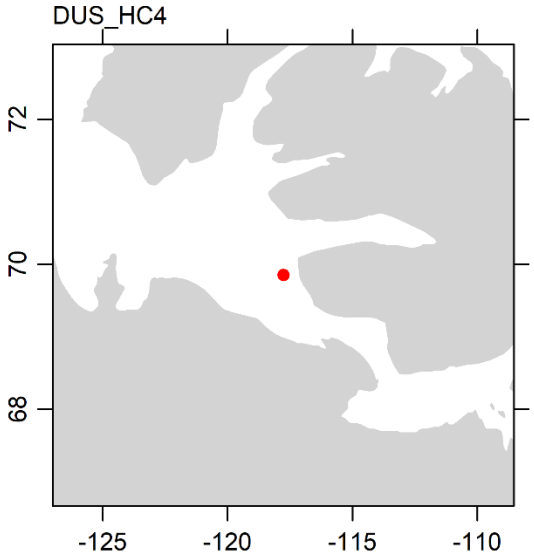
DUS_HC4
72
70
68
-125
-120
-115
-110

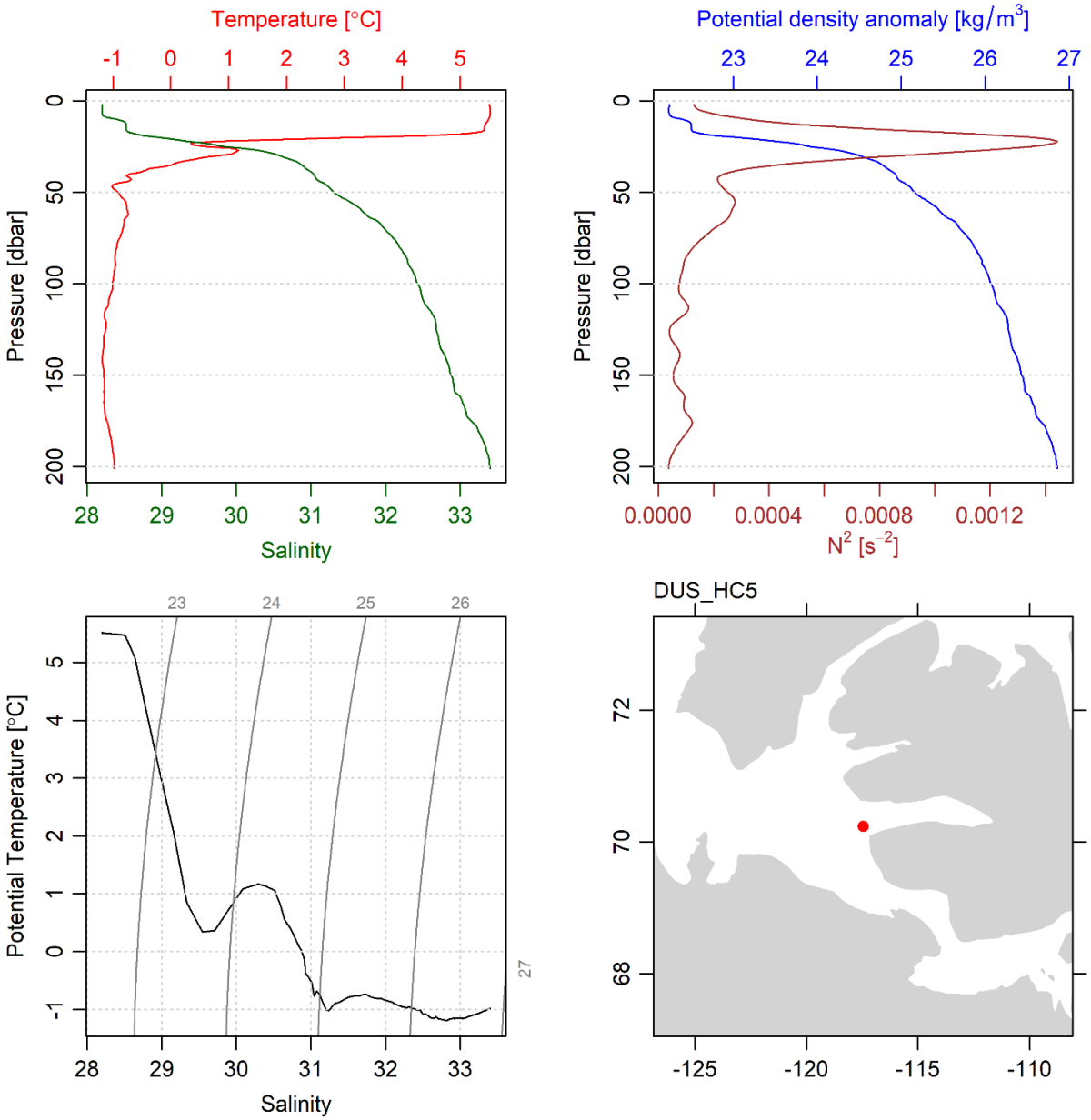
Temperature [°C]
-1 0 1 2 3 4 5
Pressure [dbar]
0 50 100 150 200
28 29 30 31 32 33
Salinity
Potential density anomaly [kg/m3]
23 24 25 26 27
0.0000 0.0004 0.0008 0.0012
N2 [s−2]
Potential Temperature [°C]
23 24 25 26
-1 0 1 2 3 4 5
27
DUS_HC5
68 70 72
-125 -120 -115 -110


Temperature [°C]
-1
0
1
2
3
4
5
Pressure [dbar]
0
50
100
150
200
250
28
29
30
31
32
33
34
Salinity

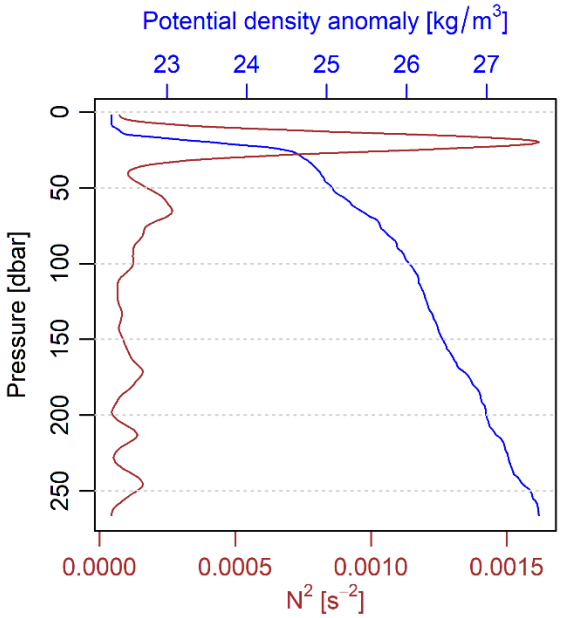
Potential density anomaly [kg/m3]
23
24
25
26
27
Pressure [dbar]
0
50
100
150
200
250
0.0000
0.0005
0.0010
0.0015
N2 [s−2]

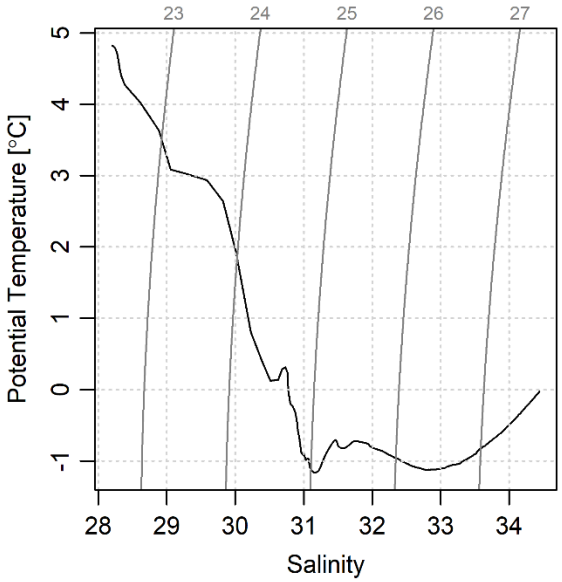
23
24
25
26
27
Potential Temperature [°C]
5
4
3
2
1
0
-1
28
29
30
31
32
33
34
Salinity

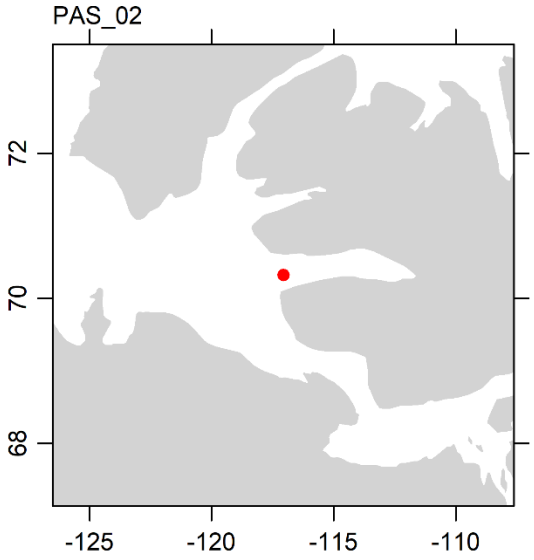
PAS_02
72
70
68
-125
-120
-115
-110

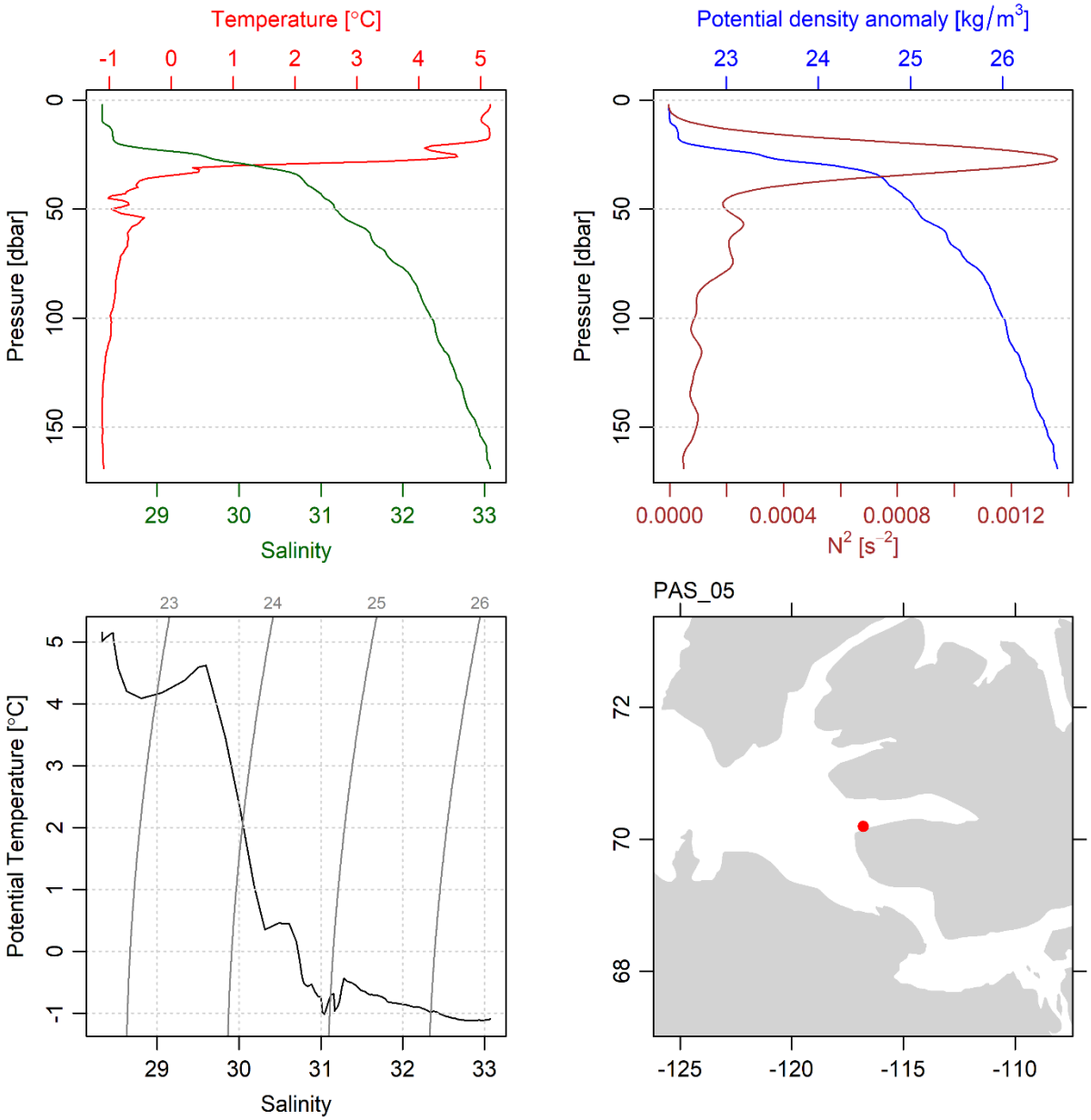
Temperature [°C]
-1
0
1
2
3
4
5
Pressure [dbar]
0
50
100
150
29
30
31
32
33
Salinity
Potential density anomaly [kg/m3]
23
24
25
26
0.0000
0.0004
0.0008
0.0012
N2 [s−2]
Potential Temperature [°C]
PAS_05
72
70
68
-125
-120
-115
-110

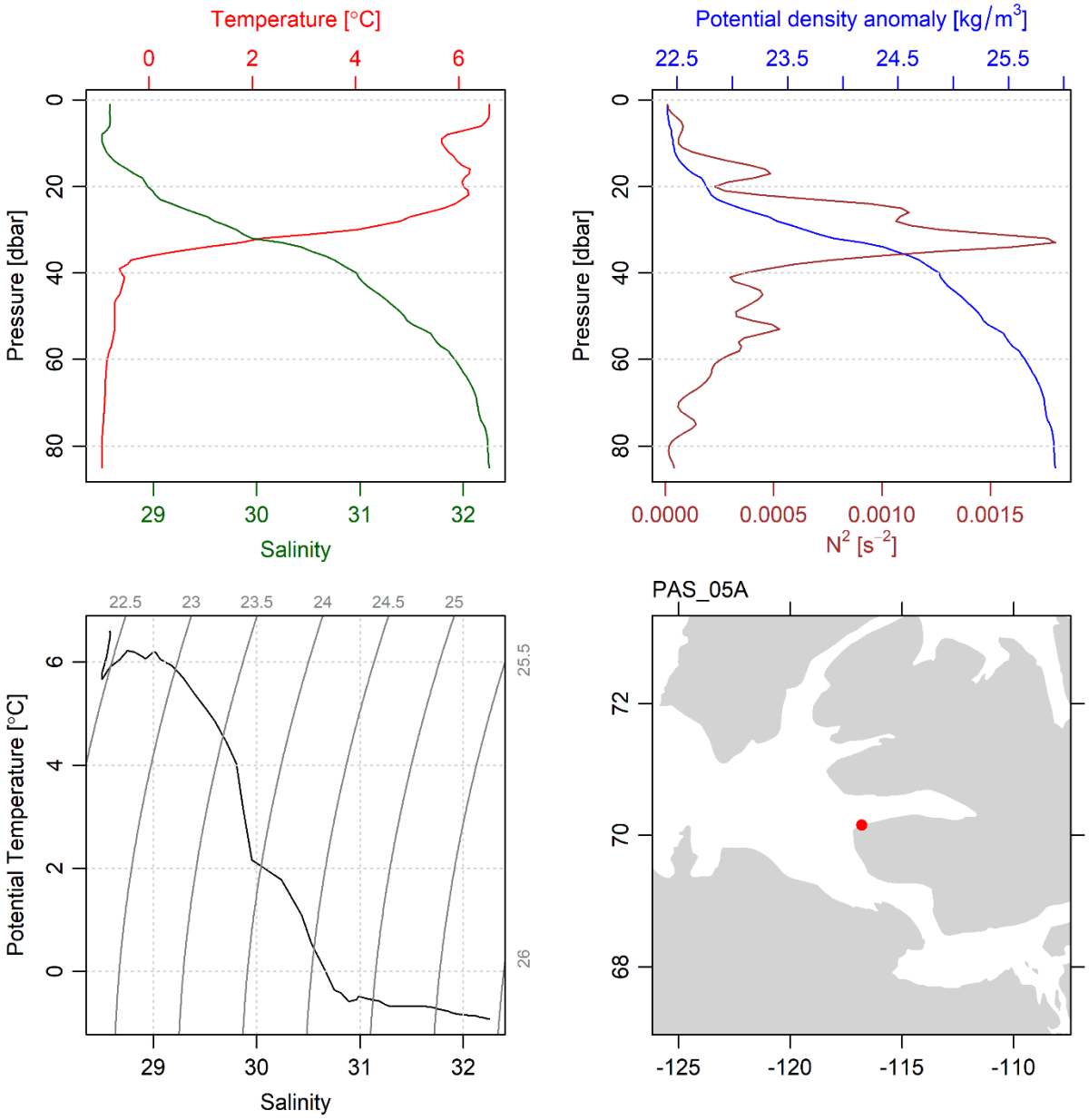
Temperature [°C]
0
2
4
6
Pressure [dbar]
0
20
40
60
80
29
30
31
32
Salinity
Potential density anomaly [kg/m3]
22.5
23.5
24.5
25.5
0.0000
0.0005
0.0010
0.0015
N2 [s−2]
22.5
23
23.5
24
24.5
25
25.5
26
Potential Temperature [°C]
PAS_05A
72
70
68
-125
-120
-115
-110

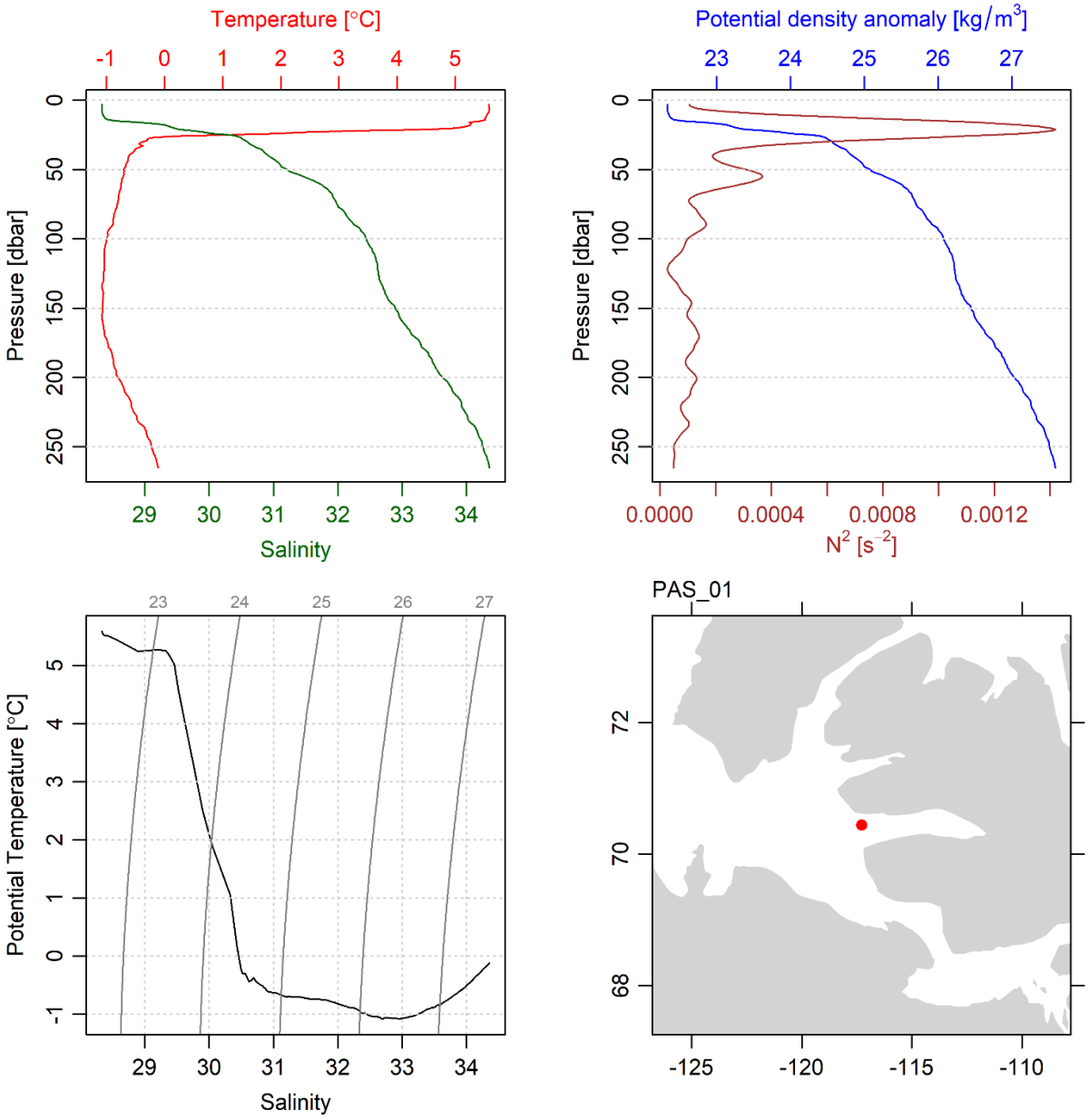
Temperature [°C]
-1 0 1 2 3 4 5
Pressure [dbar]
0 50 100 150 200 250
29 30 31 32 33 34
Salinity
Potential density anomaly [kg/m3]
23 24 25 26 27
Pressure [dbar]
0 50 100 150 200 250
0.0000 0.0004 0.0008 0.0012
N2 [s−2]
23 24 25 26 27
Potential Temperature [°C]
-1 0 1 2 3 4 5
29 30 31 32 33 34
Salinity
PAS_01
72 70 68
-125 -120 -115 -110

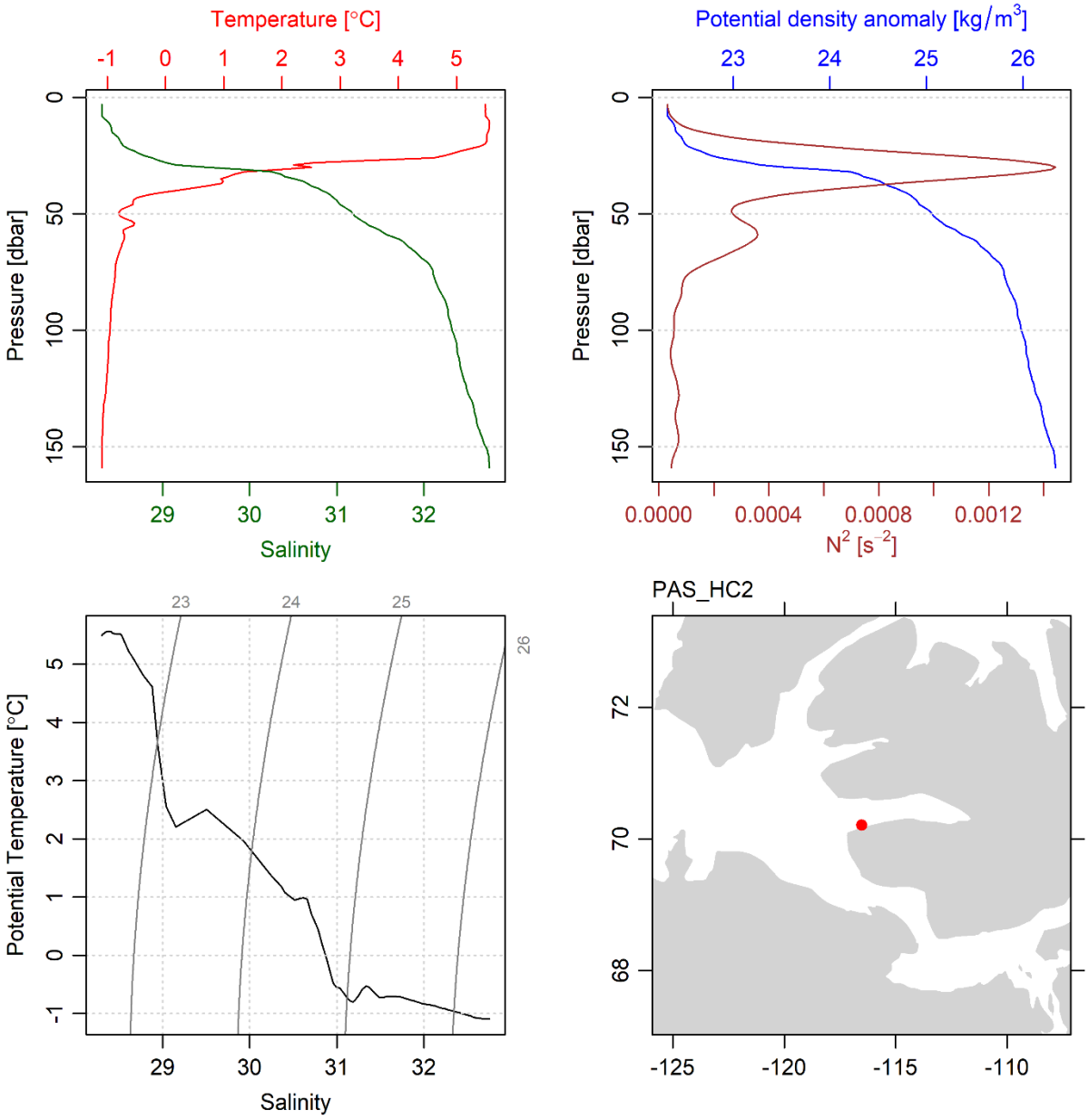
Temperature [°C]
-1
0
1
2
3
4
5
Pressure [dbar]
0
50
100
150
29
30
31
32
Salinity
Potential density anomaly [kg/m3]
23
24
25
26
0.0000
0.0004
0.0008
0.0012
N2 [s−2]
Potential Temperature [°C]
PAS_HC2
72
70
68
-125
-120
-115
-110

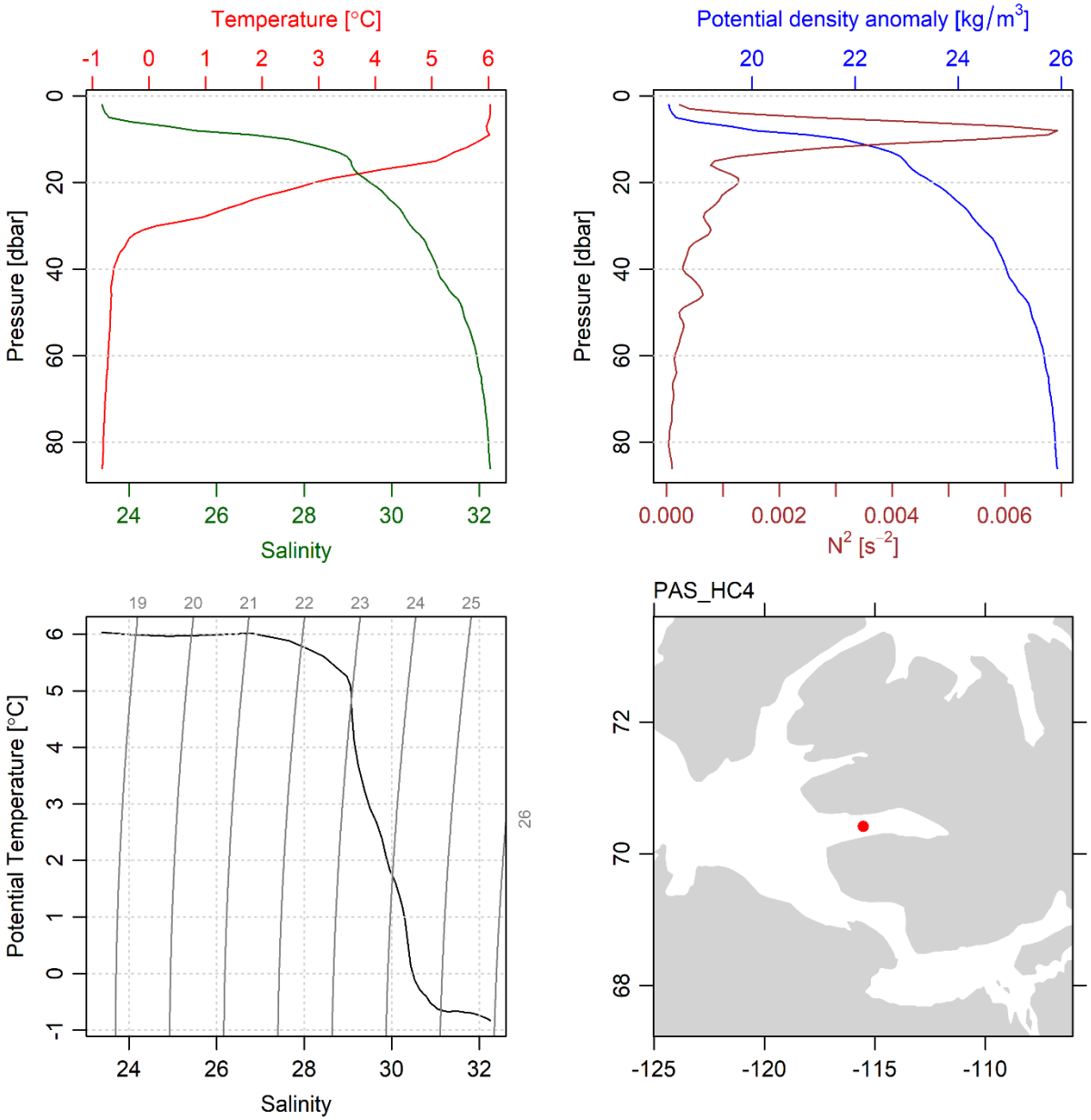
Temperature [°C]
-1 0 1 2 3 4 5 6
Pressure [dbar]
0 20 40 60 80
24 26 28 30 32
Salinity
Potential density anomaly [kg/m3]
20 22 24 26
0.000 0.002 0.004 0.006
N2 [s−2]
Potential Temperature [°C]
19 20 21 22 23 24 25
-1 0 1 2 3 4 5 6
26
PAS_HC4
68 70 72
-125 -120 -115 -110

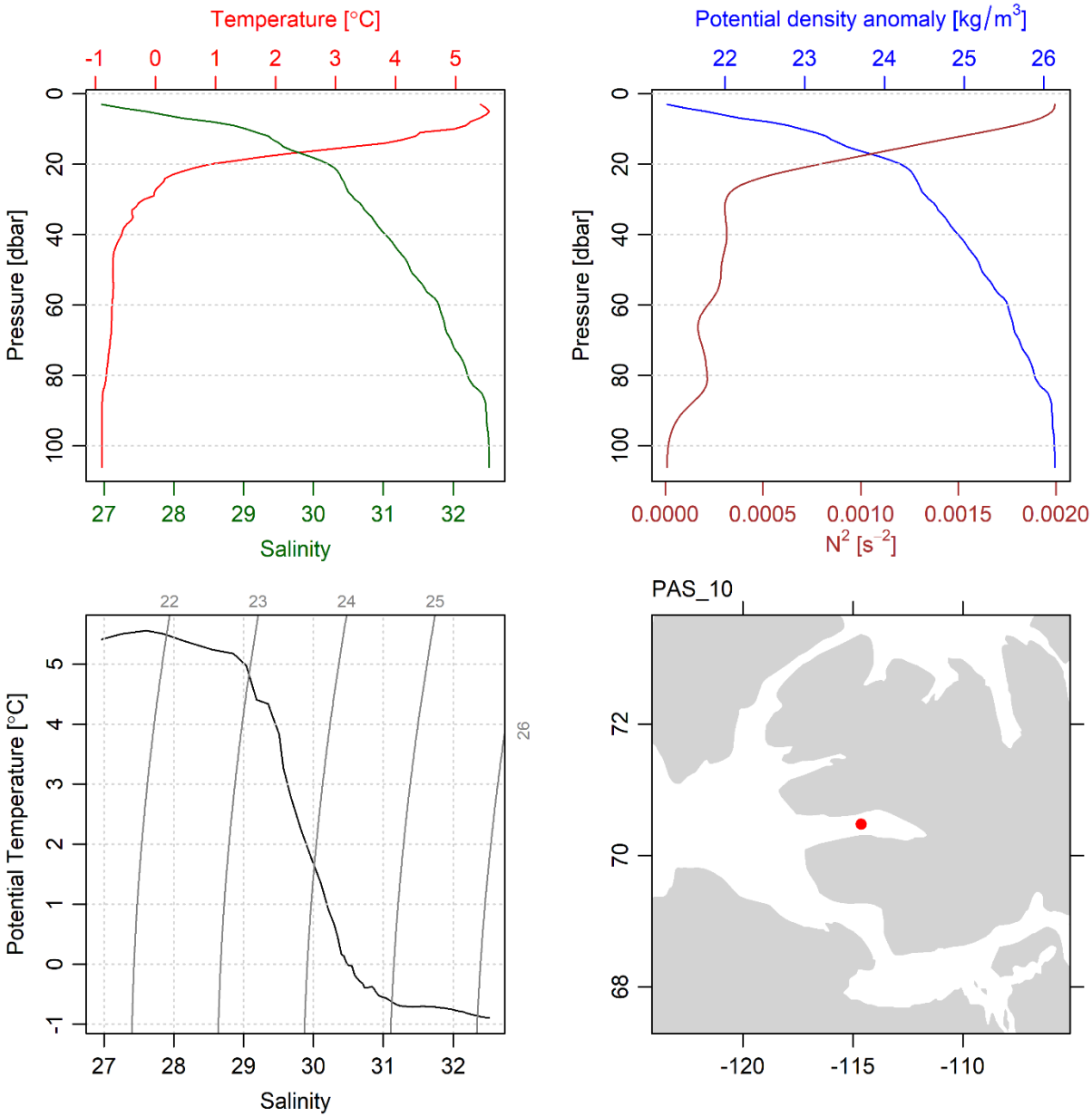
Temperature [°C]
-1 0 1 2 3 4 5
Pressure [dbar]
0 20 40 60 80 100
27 28 29 30 31 32
Salinity
Potential density anomaly [kg/m^3]
22 23 24 25 26
0.0000 0.0005 0.0010 0.0015 0.0020
N^2 [s^{-2}]
Potential Temperature [°C]
-1 0 1 2 3 4 5
22 23 24 25 26
PAS_10
68 70 72
-120 -115 -110

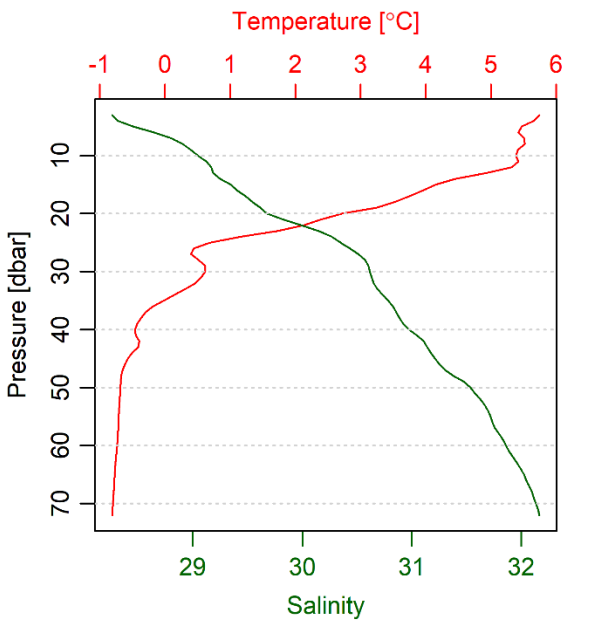
Temperature [°C]
-1
0
1
2
3
4
5
6
Pressure [dbar]
10
20
30
40
50
60
70
29
30
31
32
Salinity

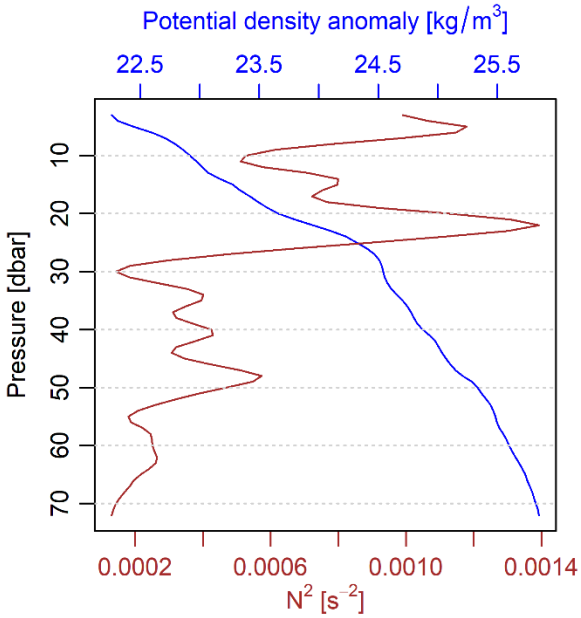
Potential density anomaly [kg/m3]
22.5
23.5
24.5
25.5
Pressure [dbar]
10
20
30
40
50
60
70
0.0002
0.0006
0.0010
0.0014
N2 [s−2]

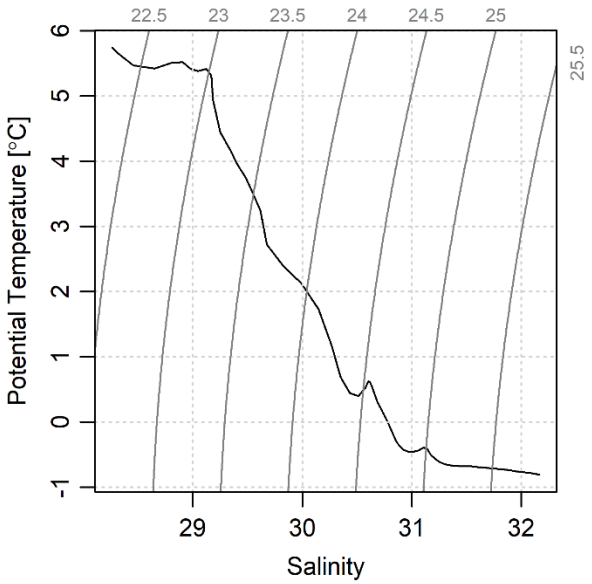
22.5
23
23.5
24
24.5
25
25.5
Potential Temperature [°C]
-1
0
1
2
3
4
5
6
29
30
31
32
Salinity

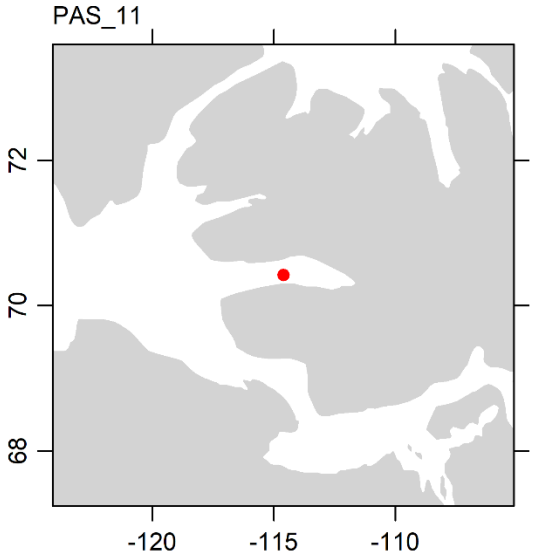
PAS_11
72
70
68
-120
-115
-110

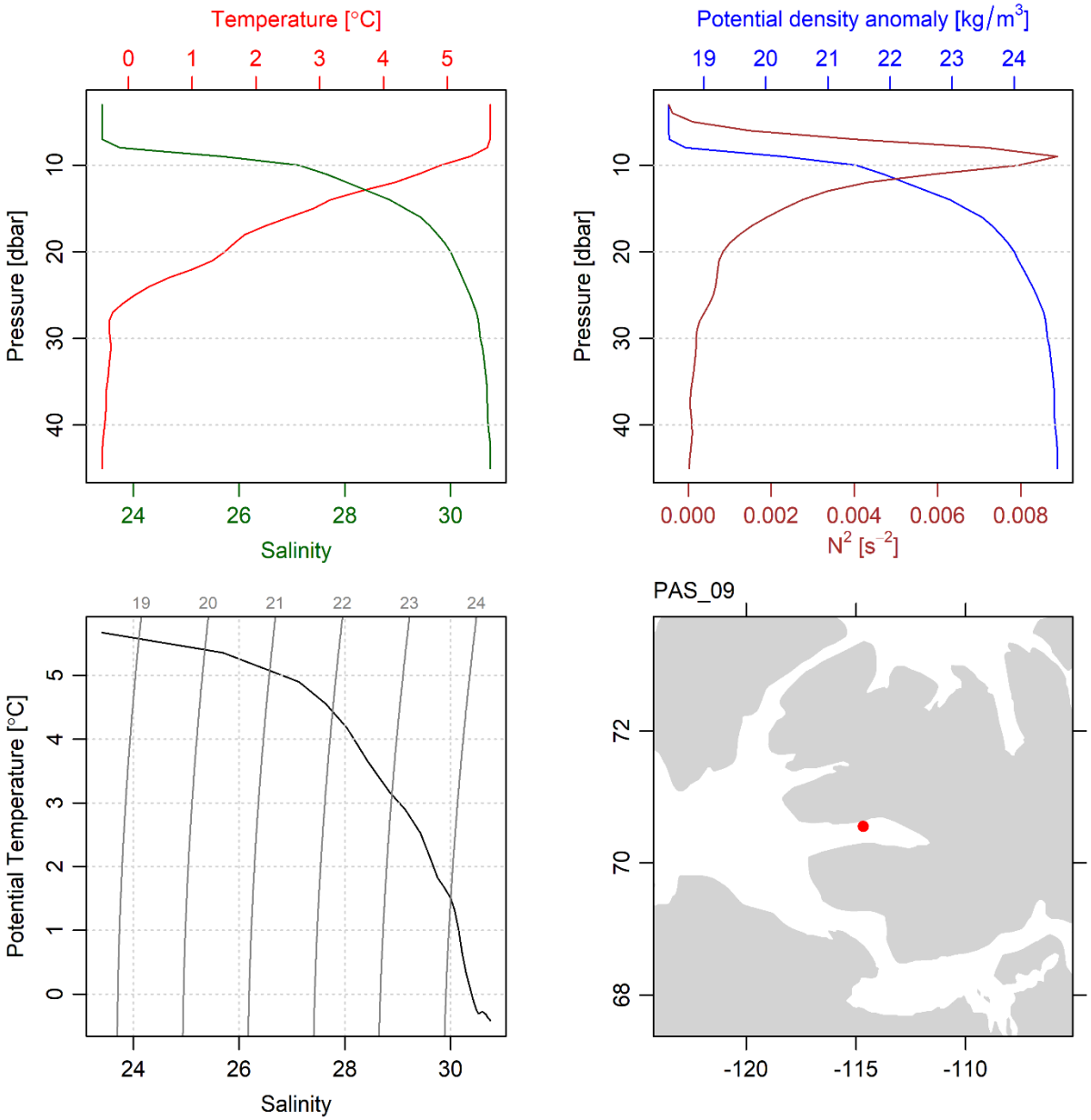
Temperature [°C]
0 1 2 3 4 5
Pressure [dbar]
10 20 30 40
24 26 28 30
Salinity
Potential density anomaly [kg/m3]
19 20 21 22 23 24
0.000 0.002 0.004 0.006 0.008
N2 [s−2]
Potential Temperature [°C]
0 1 2 3 4 5
19 20 21 22 23 24
PAS_09
72 70 68
-120 -115 -110

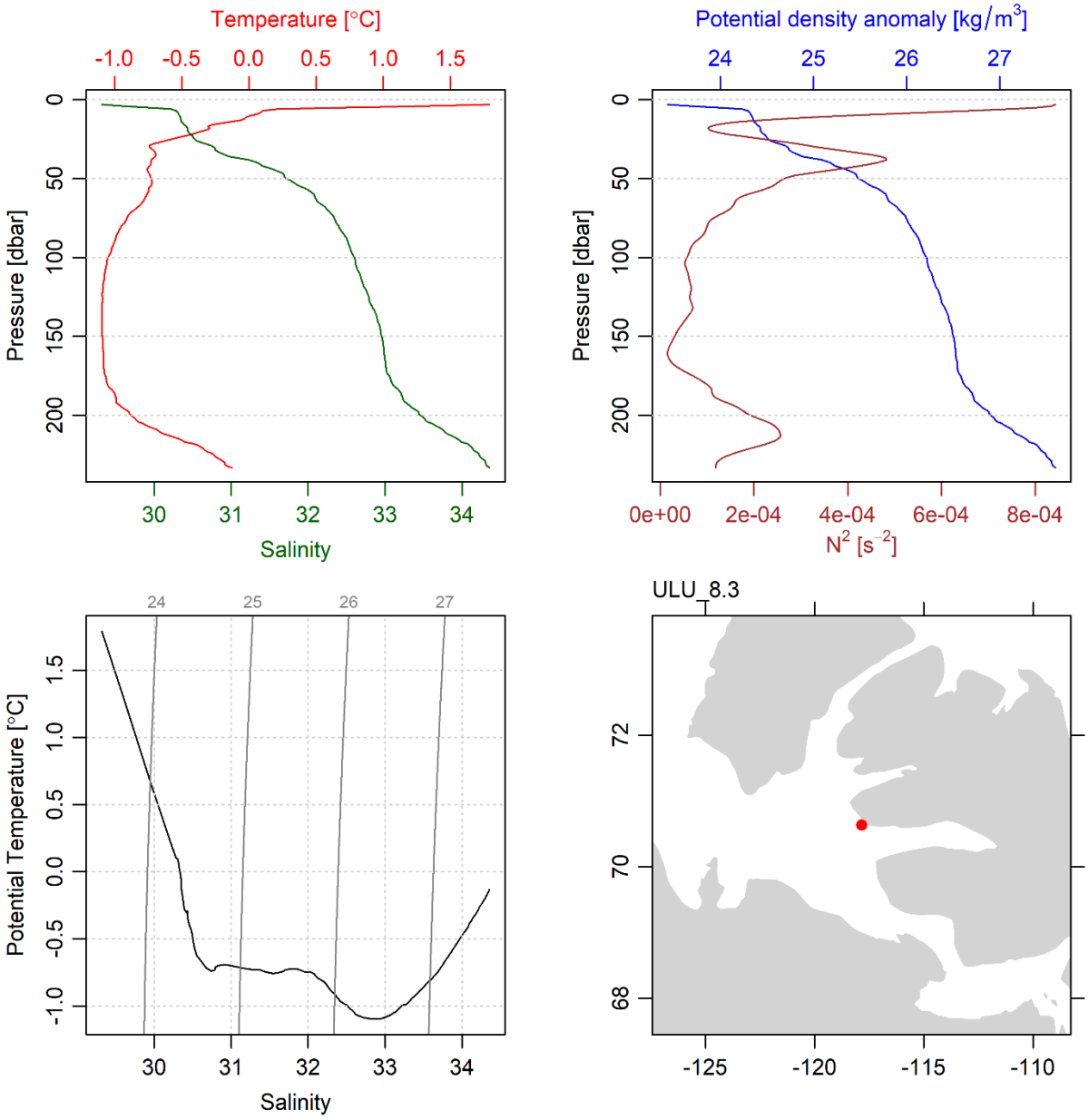
Temperature [°C]
-1.0
-0.5
0.0
0.5
1.0
1.5
Pressure [dbar]
0
50
100
150
200
30
31
32
33
34
Salinity
Potential density anomaly [kg/m3]
24
25
26
27
0e+00
2e-04
4e-04
6e-04
8e-04
N2 [s−2]
Potential Temperature [°C]
ULU_8.3
72
70
68
-125
-120
-115
-110

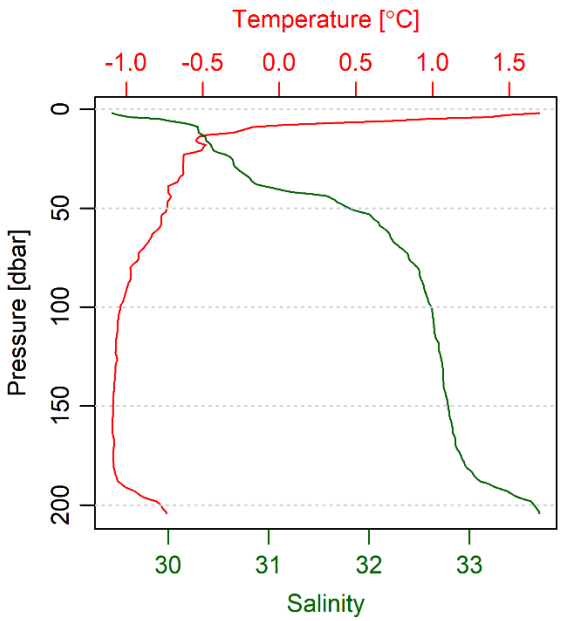
Temperature [°C]
-1.0
-0.5
0.0
0.5
1.0
1.5
Pressure [dbar]
0
50
100
150
200
30
31
32
33
Salinity

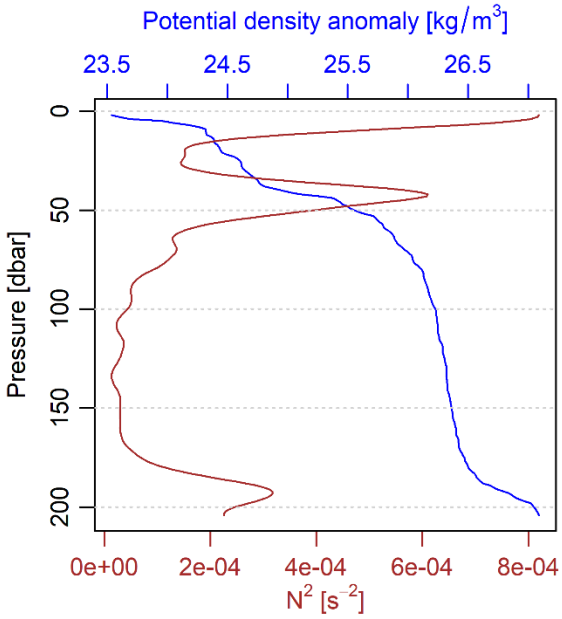
Potential density anomaly [kg/m3]
23.5
24.5
25.5
26.5
Pressure [dbar]
0
50
100
150
200
0e+00
2e-04
4e-04
6e-04
8e-04
N2 [s−2]

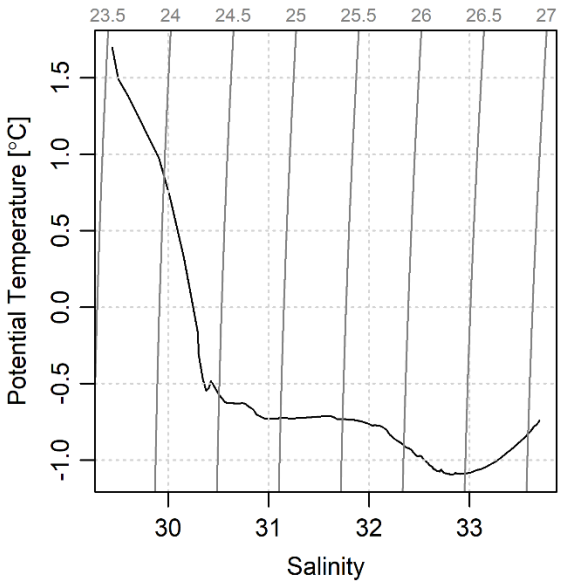
23.5
24
24.5
25
25.5
26
26.5
27
Potential Temperature [°C]
-1.0
-0.5
0.0
0.5
1.0
1.5
30
31
32
33
Salinity

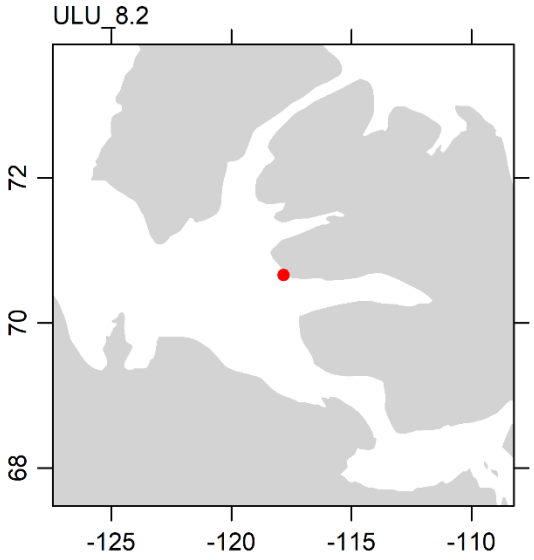
ULU_8.2
72
70
68
-125
-120
-115
-110

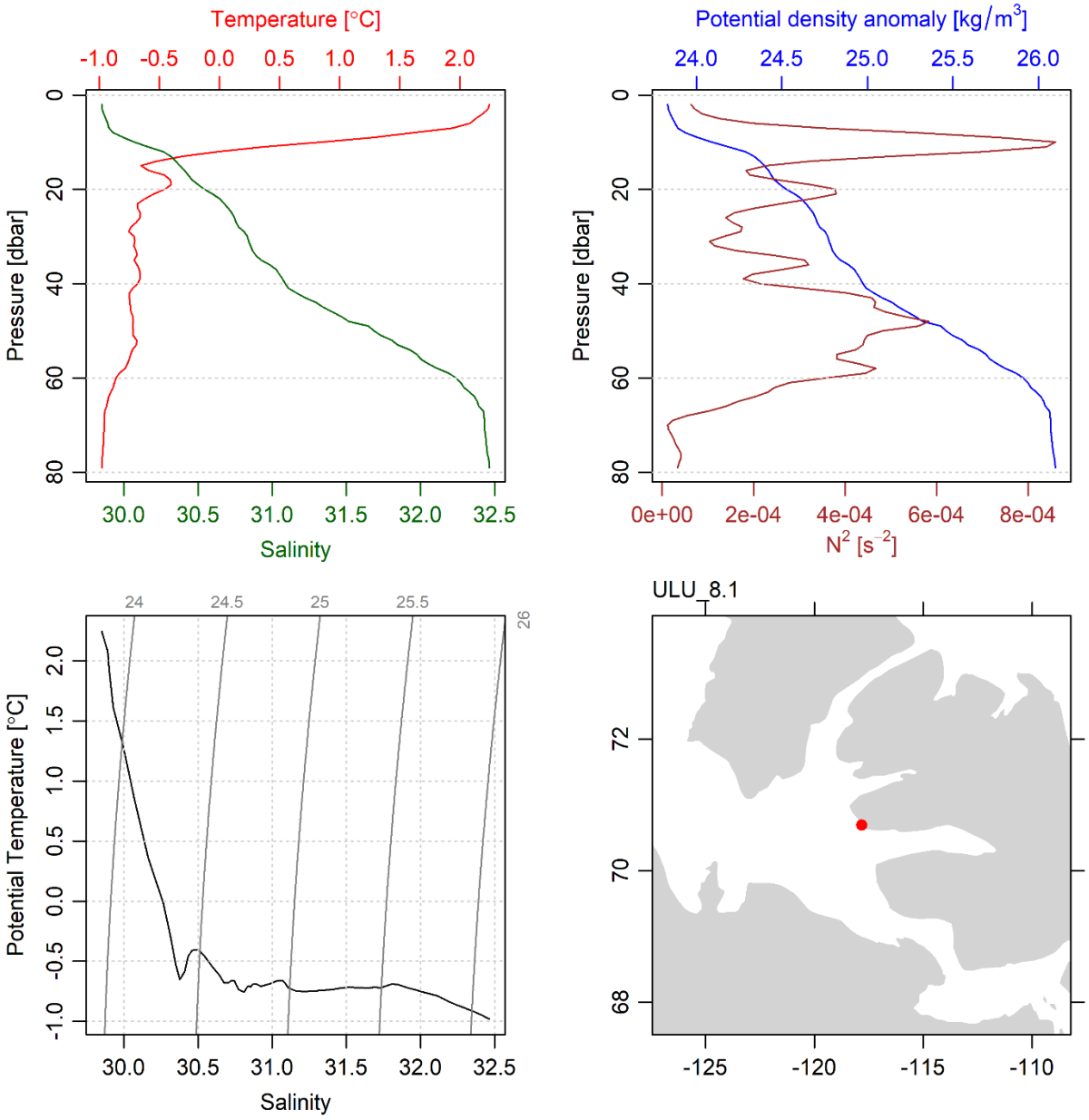
Temperature [°C]
-1.0 -0.5 0.0 0.5 1.0 1.5 2.0
Pressure [dbar]
0 20 40 60 80
30.0 30.5 31.0 31.5 32.0 32.5
Salinity
Potential density anomaly [kg/m3]
24.0 24.5 25.0 25.5 26.0
0e+00 2e-04 4e-04 6e-04 8e-04
N2 [s−2]
Potential Temperature [°C]
24 24.5 25 25.5 26
-1.0 -0.5 0.0 0.5 1.0 1.5 2.0
ULU_8.1
68 70 72
-125 -120 -115 -110

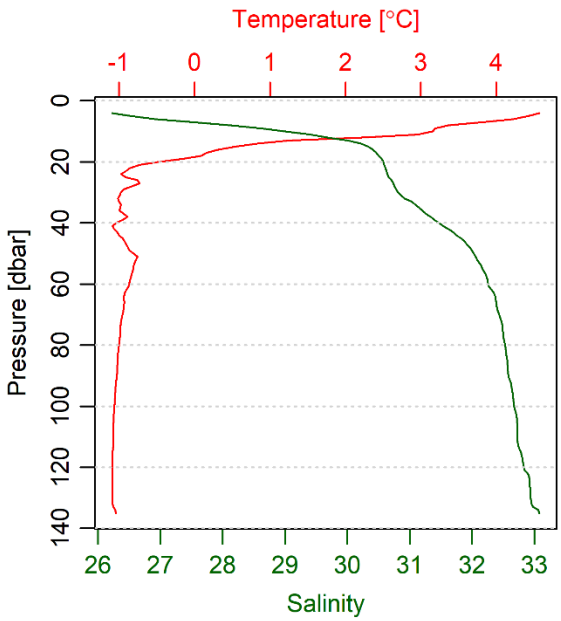
Temperature [°C]
-1
0
1
2
3
4
Pressure [dbar]
0
20
40
60
80
100
120
140
26
27
28
29
30
31
32
33
Salinity

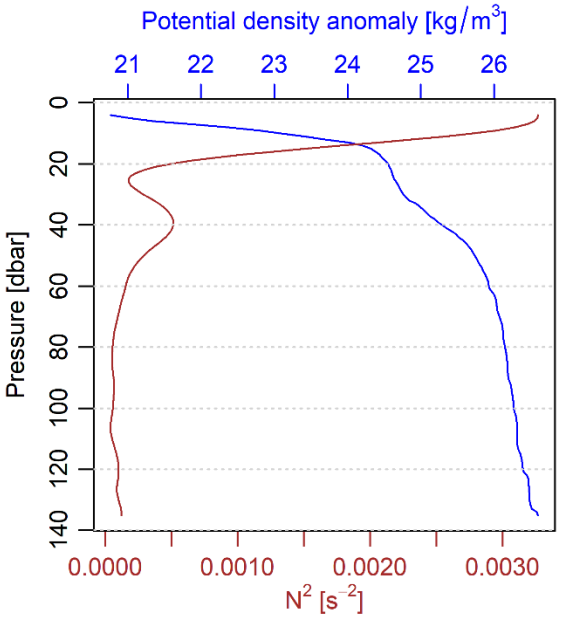
Potential density anomaly [kg/m3]
21
22
23
24
25
26
Pressure [dbar]
0
20
40
60
80
100
120
140
0.0000
0.0010
0.0020
0.0030
N2 [s−2]

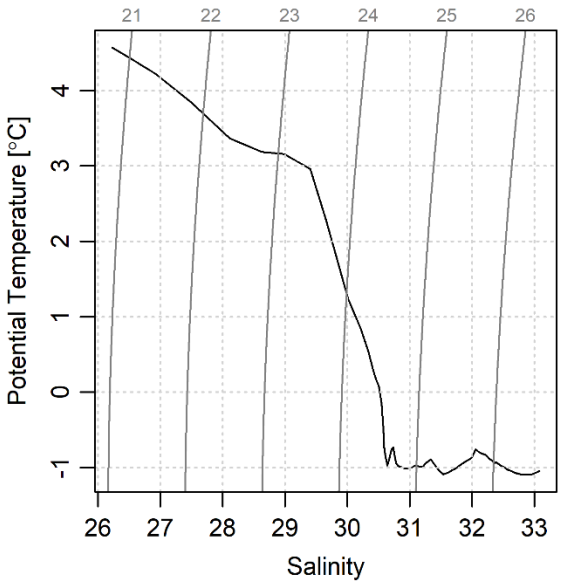
21
22
23
24
25
26
Potential Temperature [°C]
-1
0
1
2
3
4
26
27
28
29
30
31
32
33
Salinity

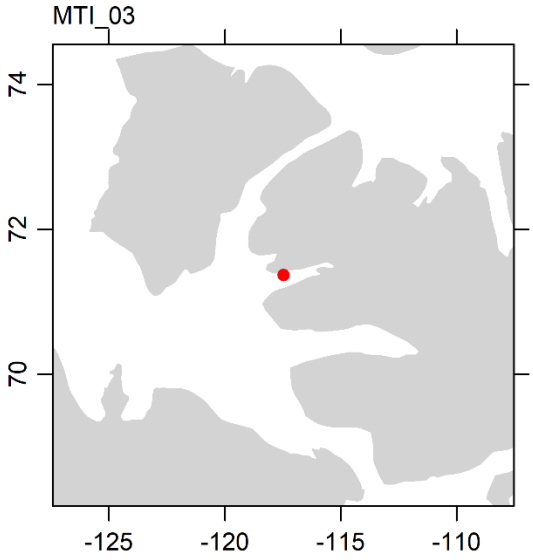
MTI_03
74
72
70
-125
-120
-115
-110

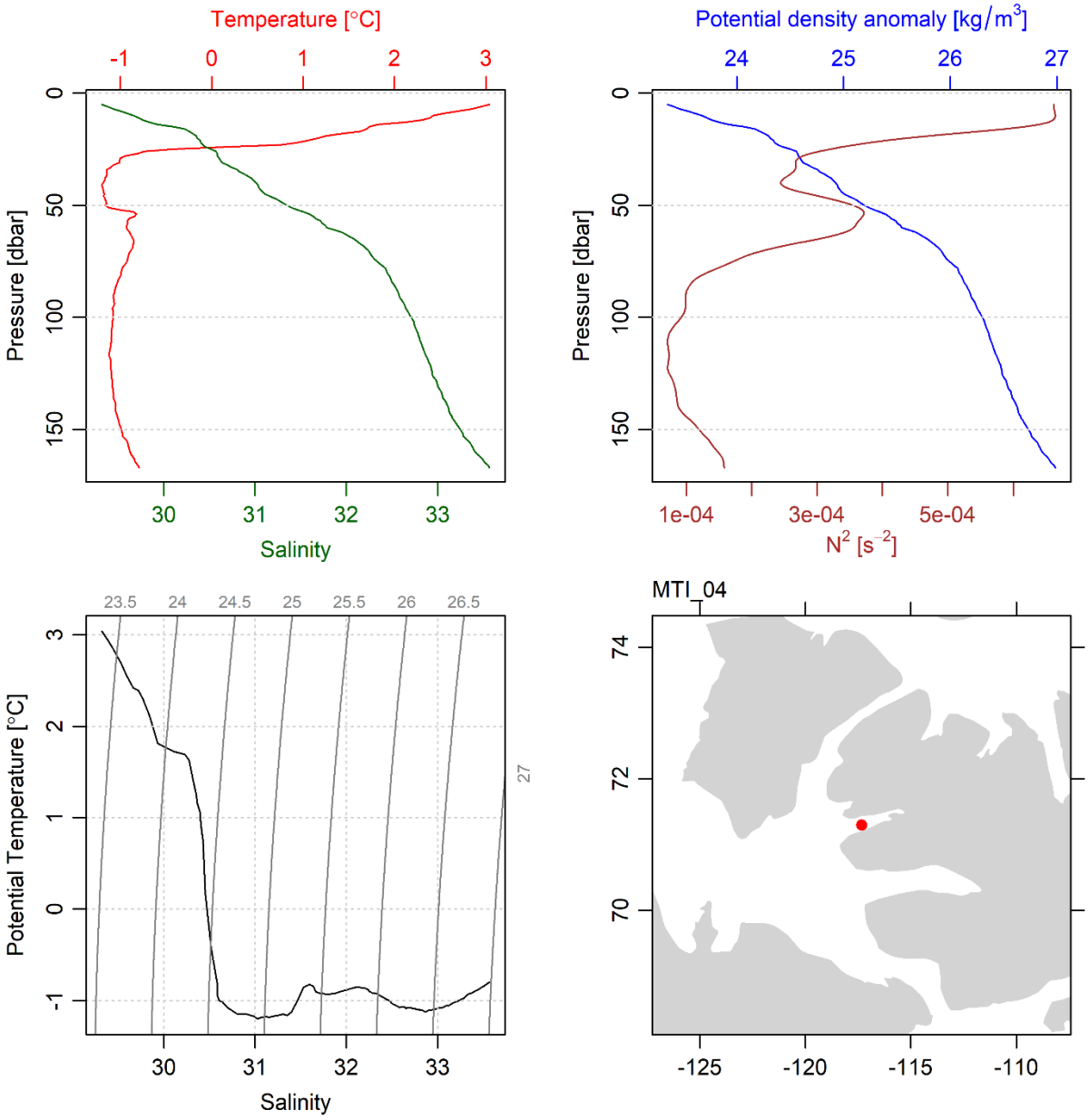
Temperature [°C]
-1
0
1
2
3
Pressure [dbar]
0
50
100
150
30
31
32
33
Salinity
Potential density anomaly [kg/m3]
24
25
26
27
1e-04
3e-04
5e-04
N2 [s−2]
23.5
24
24.5
25
25.5
26
26.5
Potential Temperature [°C]
27
MTI_04
74
72
70
-125
-120
-115
-110

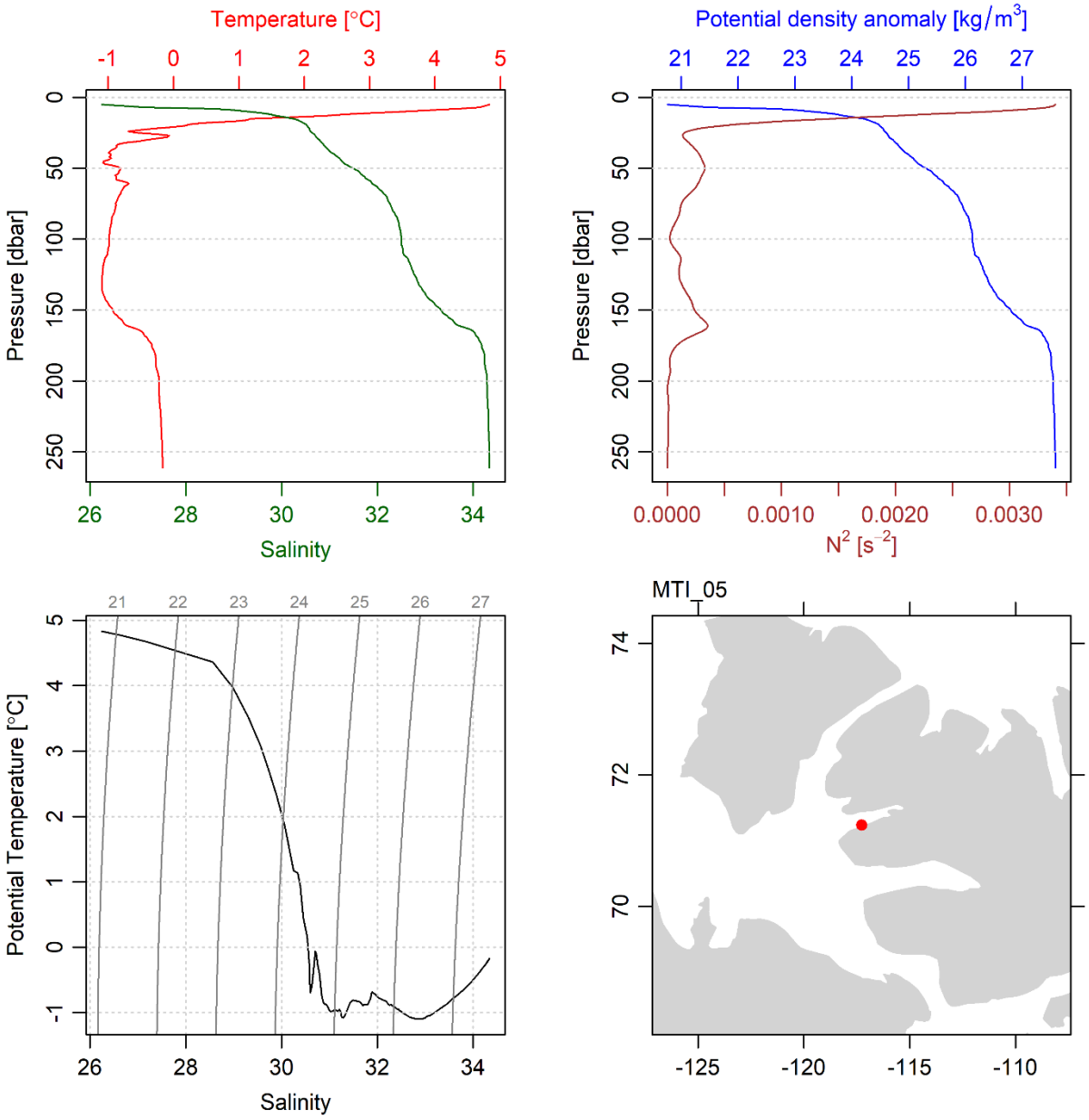
Temperature [°C]
-1
0
1
2
3
4
5
Pressure [dbar]
0
50
100
150
200
250
26
28
30
32
34
Salinity
Potential density anomaly [kg/m3]
21
22
23
24
25
26
27
0.0000
0.0010
0.0020
0.0030
N2 [s−2]
Potential Temperature [°C]
MTI_05
74
72
70
-125
-120
-115
-110

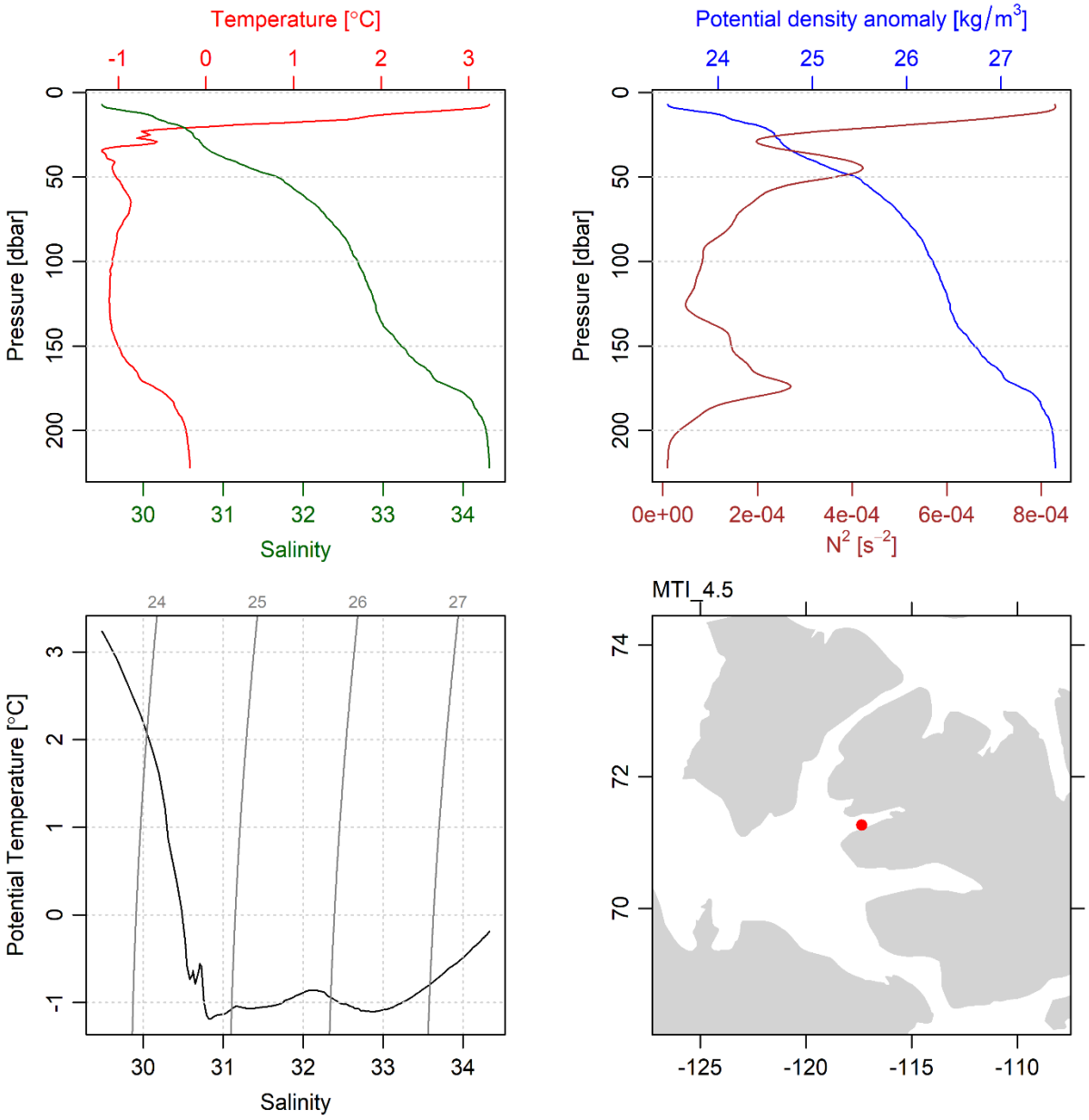
Temperature [°C]
-1
0
1
2
3
Pressure [dbar]
0
50
100
150
200
30
31
32
33
34
Salinity
Potential density anomaly [kg/m3]
24
25
26
27
0e+00
2e-04
4e-04
6e-04
8e-04
N2 [s−2]
Potential Temperature [°C]
MTI_4.5
74
72
70
-125
-120
-115
-110

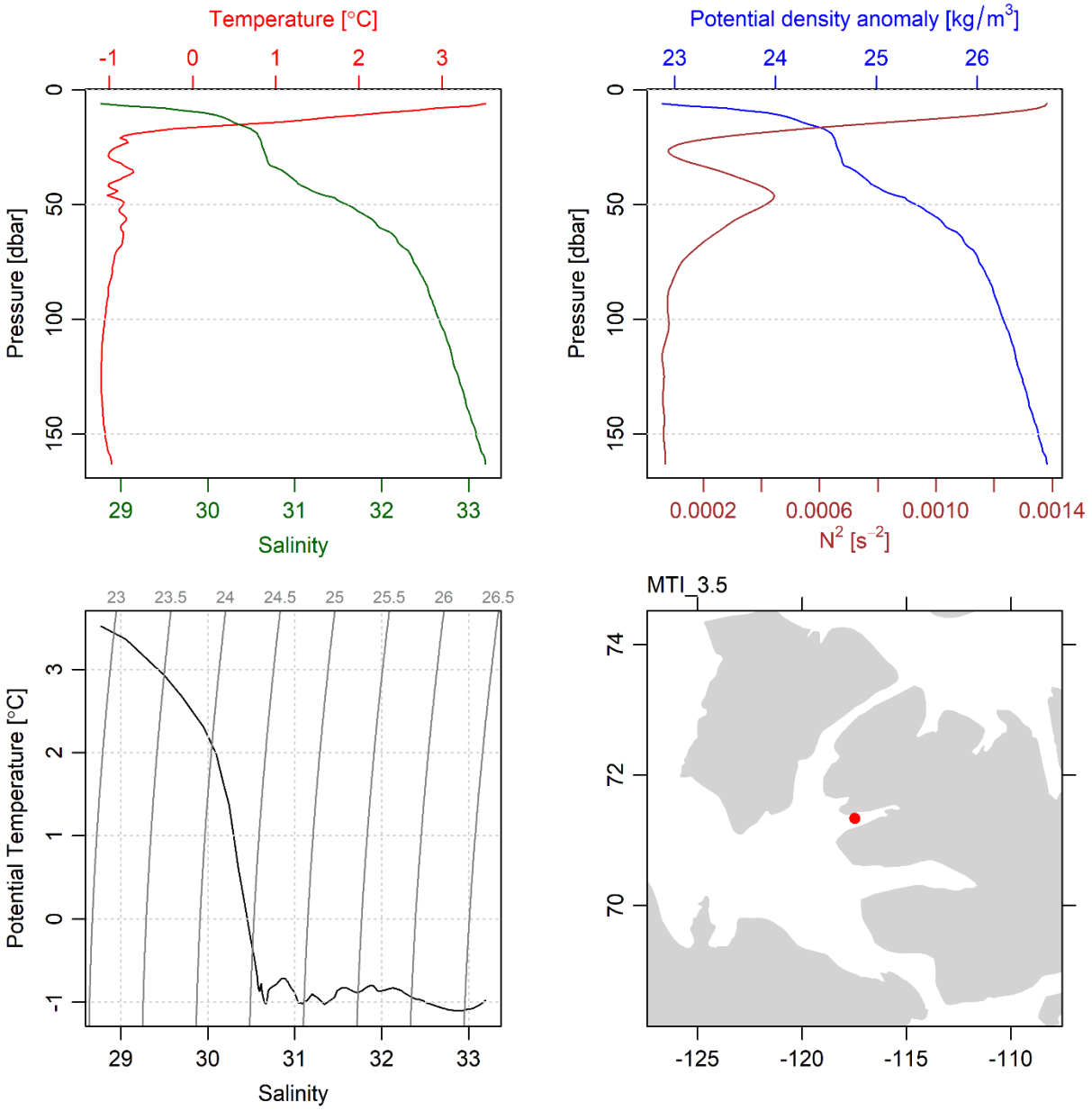
Temperature [°C]
-1
0
1
2
3
Pressure [dbar]
0
50
100
150
29
30
31
32
33
Salinity
Potential density anomaly [kg/m3]
23
24
25
26
0.0002
0.0006
0.0010
0.0014
N2 [s−2]
23
23.5
24
24.5
25
25.5
26
26.5
Potential Temperature [°C]
3
2
1
0
-1
MTI_3.5
74
72
70
-125
-120
-115
-110

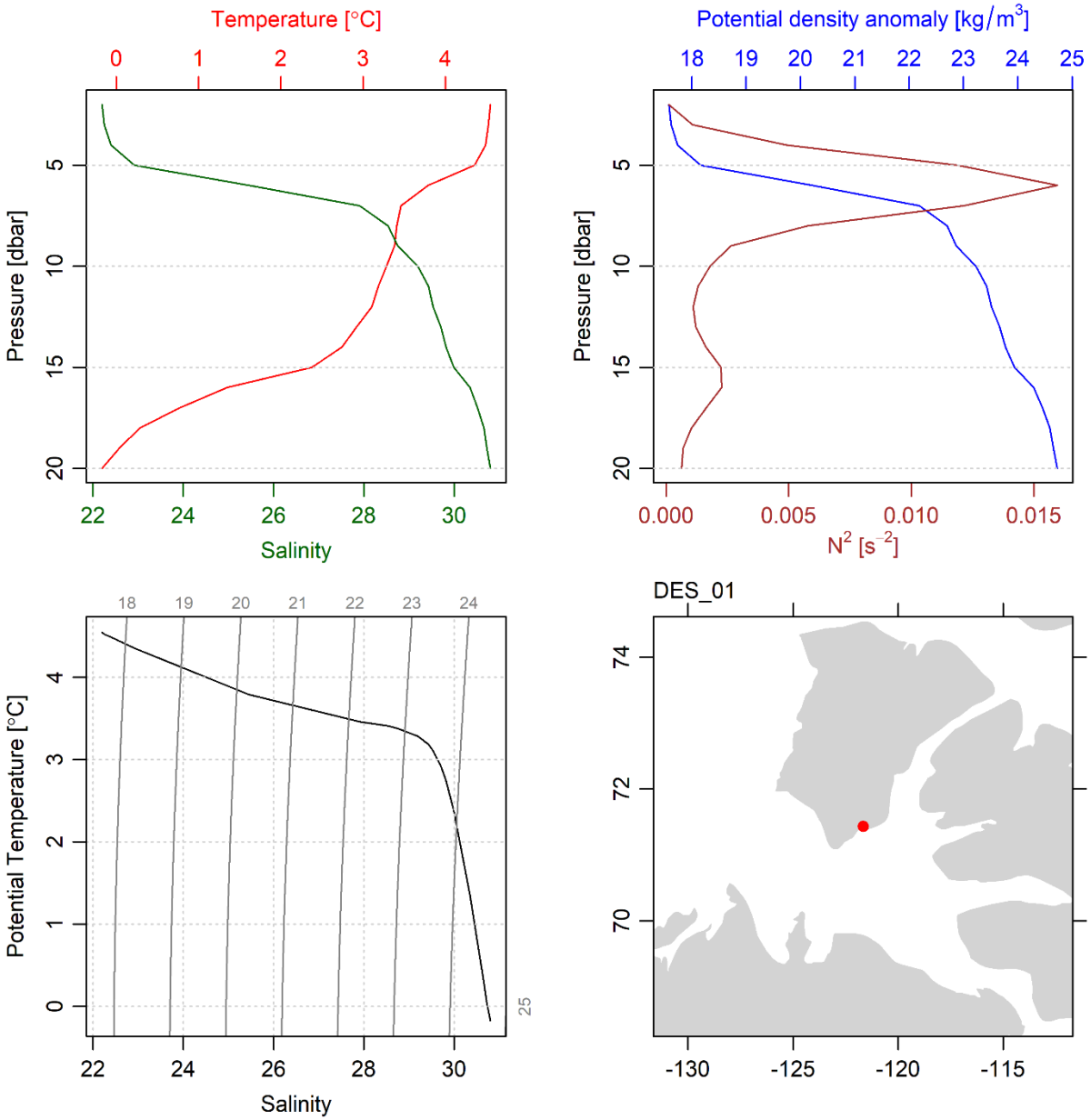
Temperature [°C]
0
1
2
3
4
Pressure [dbar]
5
10
15
20
22
24
26
28
30
Salinity
Potential density anomaly [kg/m3]
18
19
20
21
22
23
24
25
0.000
0.005
0.010
0.015
N2 [s−2]
Potential Temperature [°C]
DES_01
74
72
70
-130
-125
-120
-115

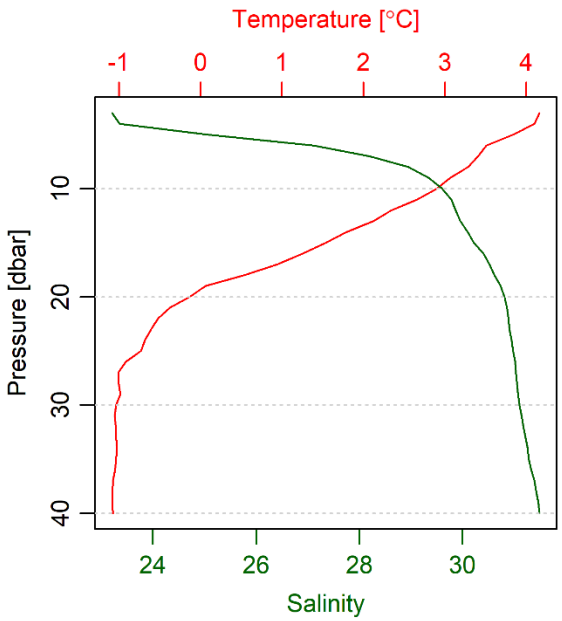
Temperature [°C]
-1
0
1
2
3
4
Pressure [dbar]
10
20
30
40
24
26
28
30
Salinity

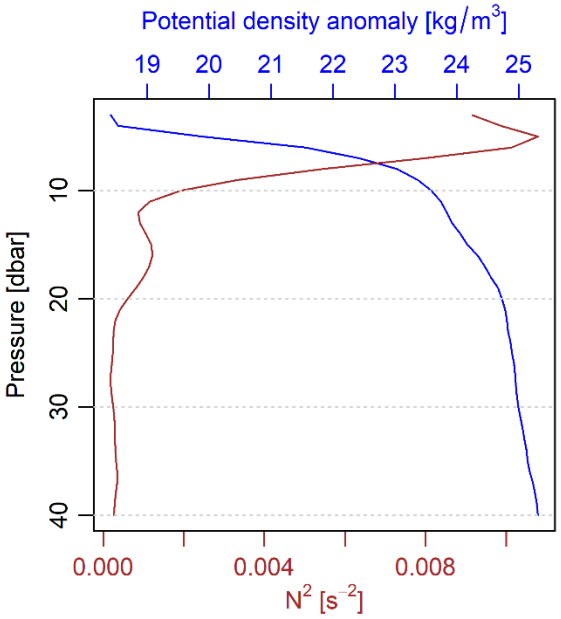
Potential density anomaly [kg/m3]
19
20
21
22
23
24
25
Pressure [dbar]
10
20
30
40
0.000
0.004
0.008
N2 [s−2]

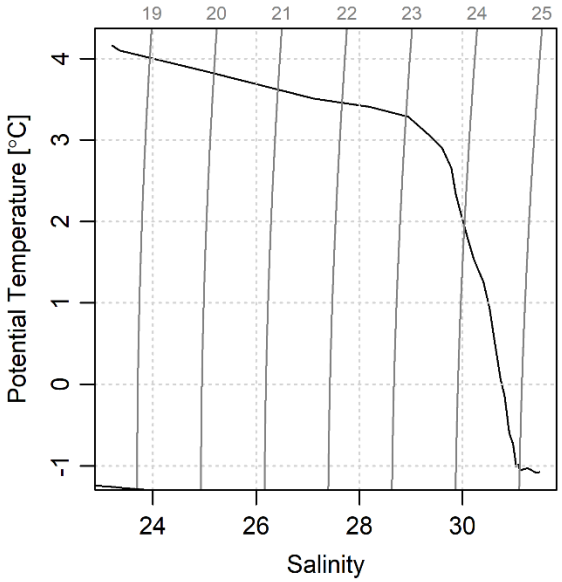
19
20
21
22
23
24
25
Potential Temperature [°C]
-1
0
1
2
3
4
24
26
28
30
Salinity

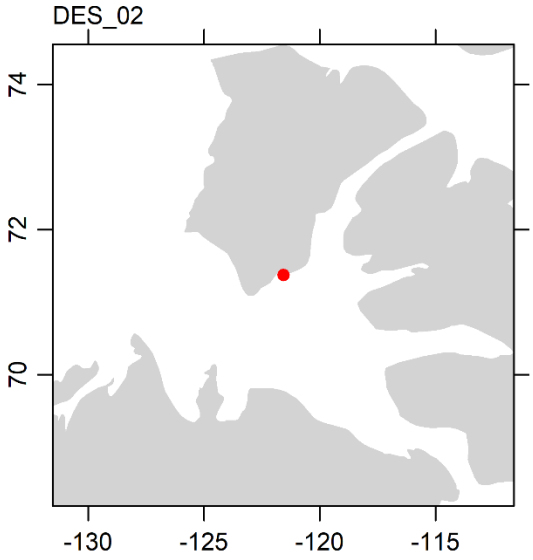
DES_02
74
72
70
-130
-125
-120
-115

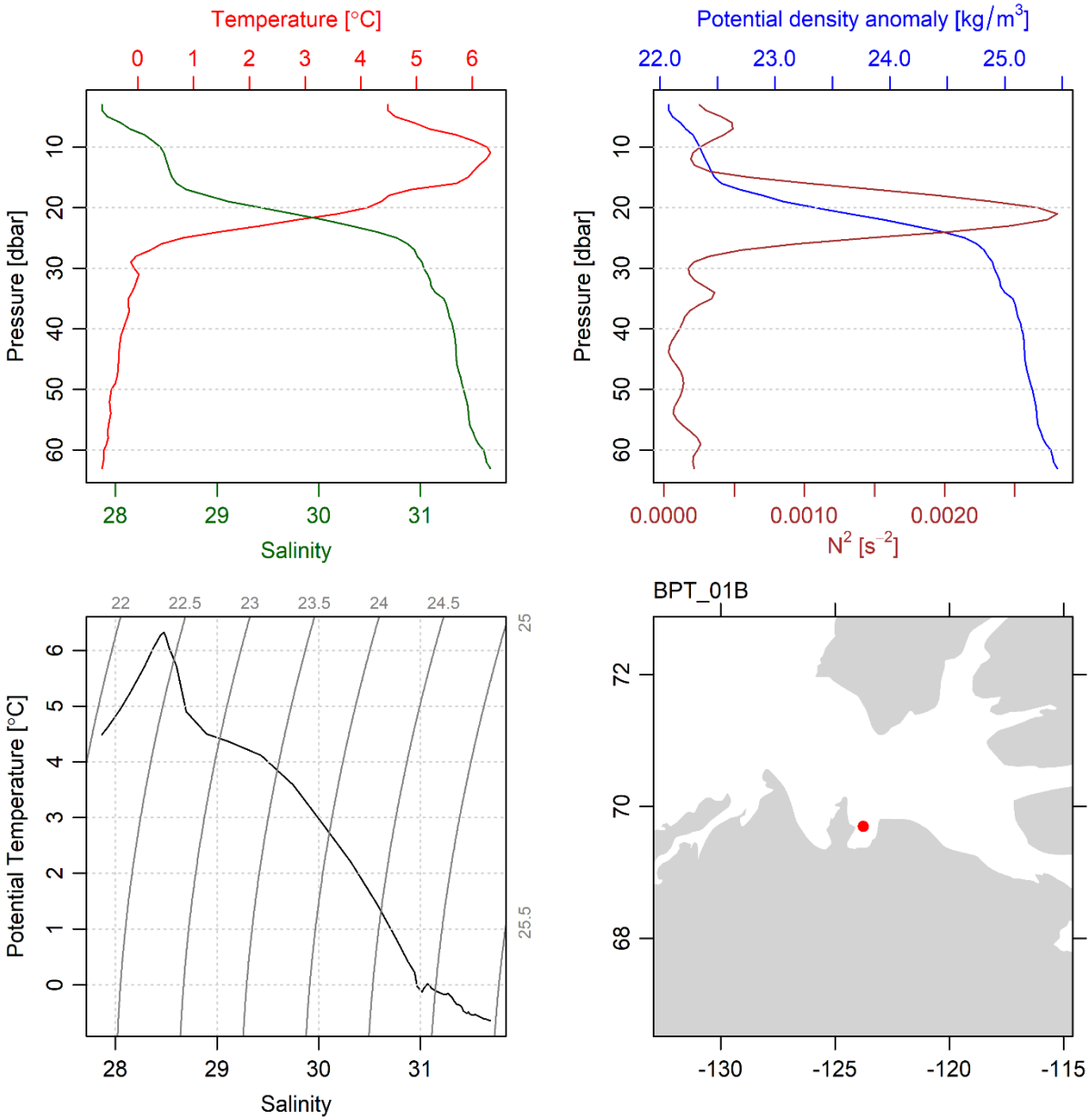
Temperature [°C]
0 1 2 3 4 5 6
Pressure [dbar]
10 20 30 40 50 60
28 29 30 31
Salinity
Potential density anomaly [kg/m3]
22.0 23.0 24.0 25.0
0.0000 0.0010 0.0020
N2 [s−2]
22 22.5 23 23.5 24 24.5
25
25.5
Potential Temperature [°C]
0 1 2 3 4 5 6
BPT_01B
72 70 68
-130 -125 -120 -115

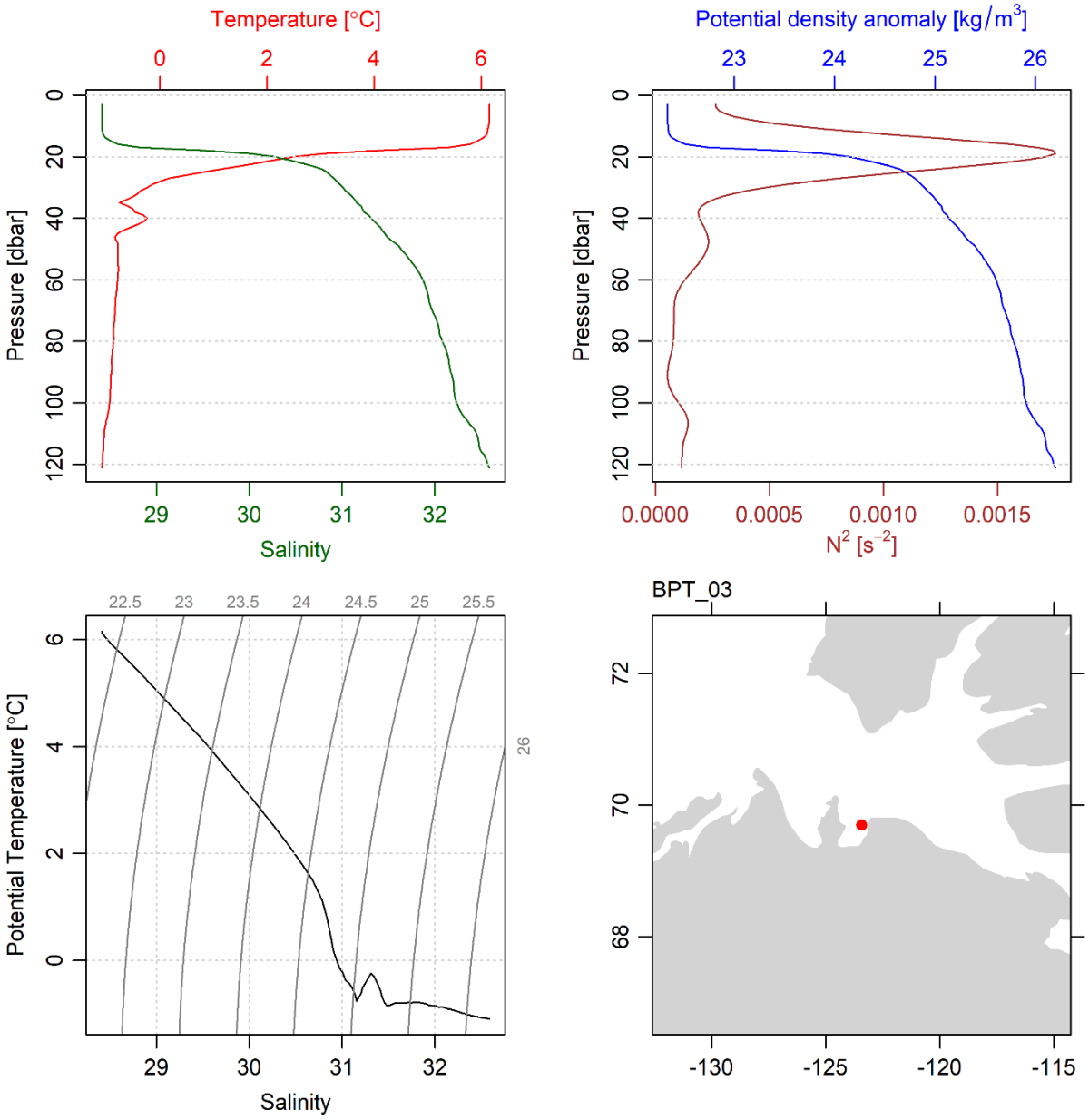
Temperature [°C]
0
2
4
6
Pressure [dbar]
0
20
40
60
80
100
120
29
30
31
32
Salinity
Potential density anomaly [kg/m3]
23
24
25
26
0.0000
0.0005
0.0010
0.0015
N2 [s−2]
22.5
23
23.5
24
24.5
25
25.5
26
Potential Temperature [°C]
BPT_03
72
70
68
-130
-125
-120
-115

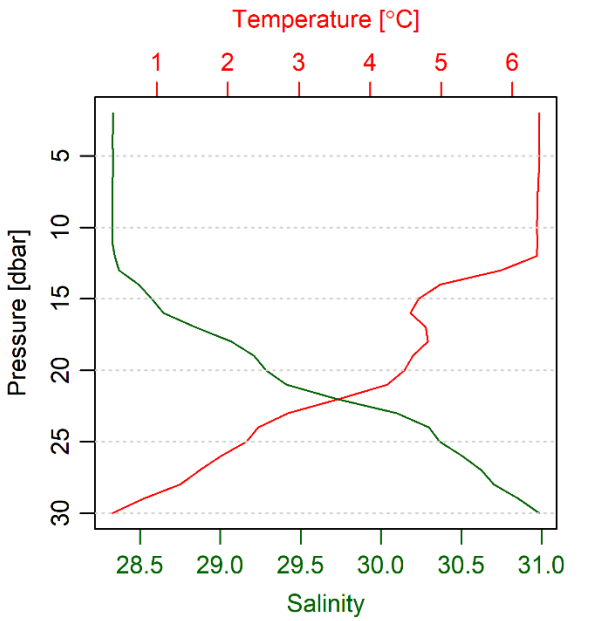
Temperature [°C]
1
2
3
4
5
6
Pressure [dbar]
5
10
15
20
25
30
28.5
29.0
29.5
30.0
30.5
31.0
Salinity

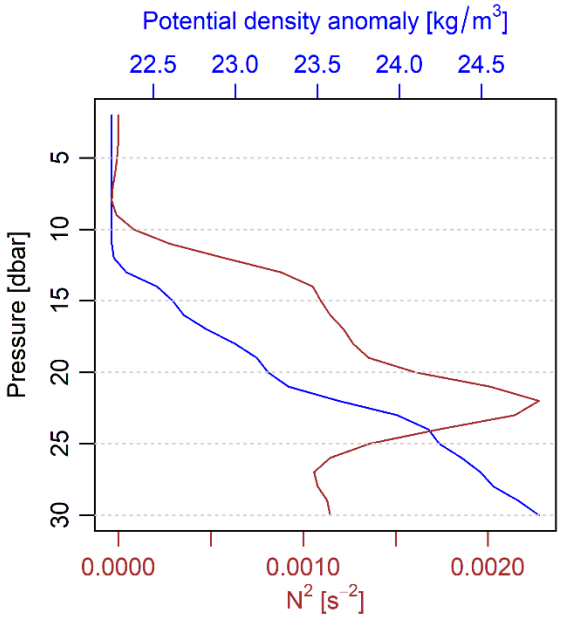
Potential density anomaly [kg/m3]
22.5
23.0
23.5
24.0
24.5
Pressure [dbar]
5
10
15
20
25
30
0.0000
0.0010
0.0020
N2 [s−2]

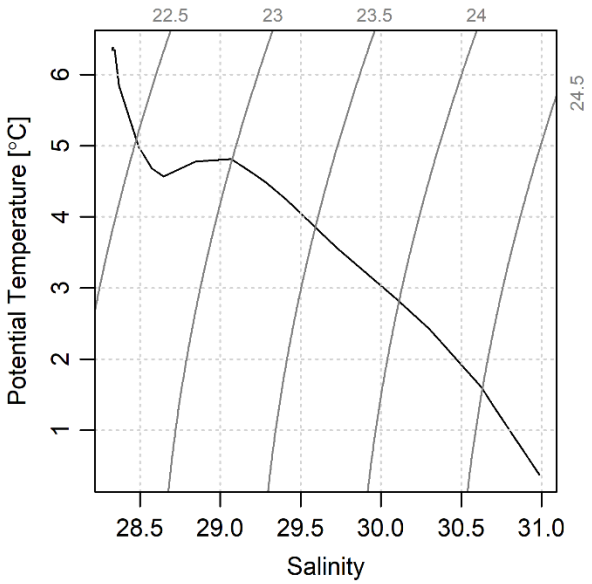
22.5
23
23.5
24
24.5
Potential Temperature [°C]
1
2
3
4
5
6
28.5
29.0
29.5
30.0
30.5
31.0
Salinity

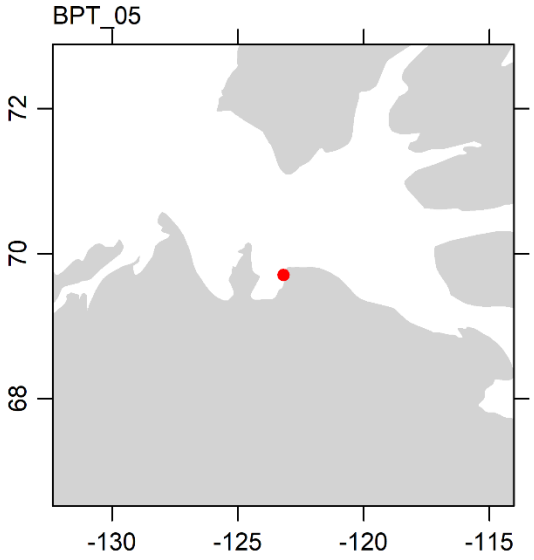
BPT_05
72
70
68
-130
-125
-120
-115

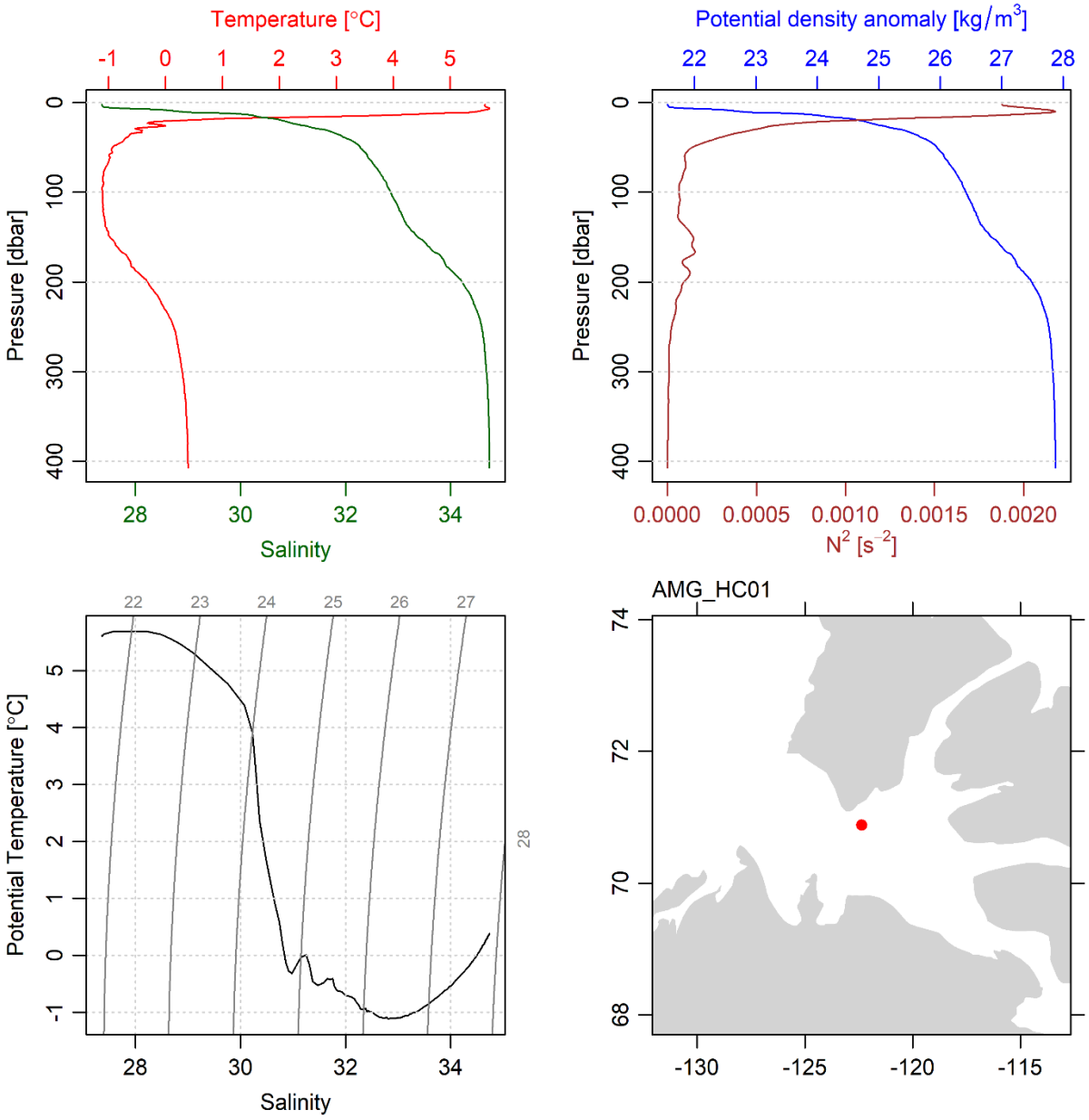
Temperature [°C]
-1 0 1 2 3 4 5
Pressure [dbar]
0 100 200 300 400
28 30 32 34
Salinity
Potential density anomaly [kg/m3]
22 23 24 25 26 27 28
0.0000 0.0005 0.0010 0.0015 0.0020
N2 [s−2]
Potential Temperature [°C]
22 23 24 25 26 27
28
AMG_HC01
74 72 70 68
-130 -125 -120 -115

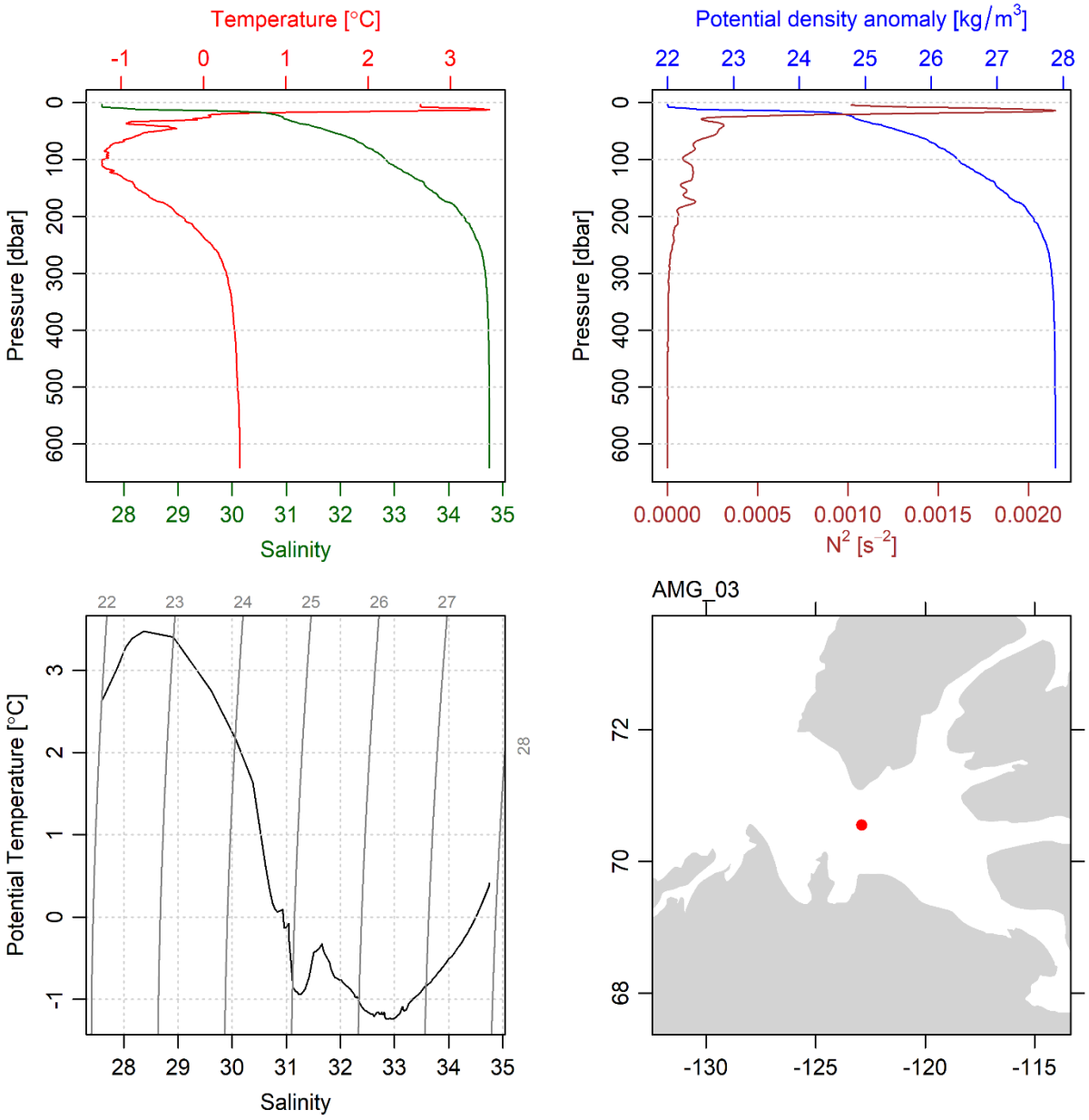
Temperature [°C]
-1
0
1
2
3
Pressure [dbar]
0
100
200
300
400
500
600
28
29
30
31
32
33
34
35
Salinity
Potential density anomaly [kg/m3]
22
23
24
25
26
27
28
0.0000
0.0005
0.0010
0.0015
0.0020
N2 [s−2]
Potential Temperature [°C]
-1
0
1
2
3
AMG_03
68
70
72
-130
-125
-120
-115

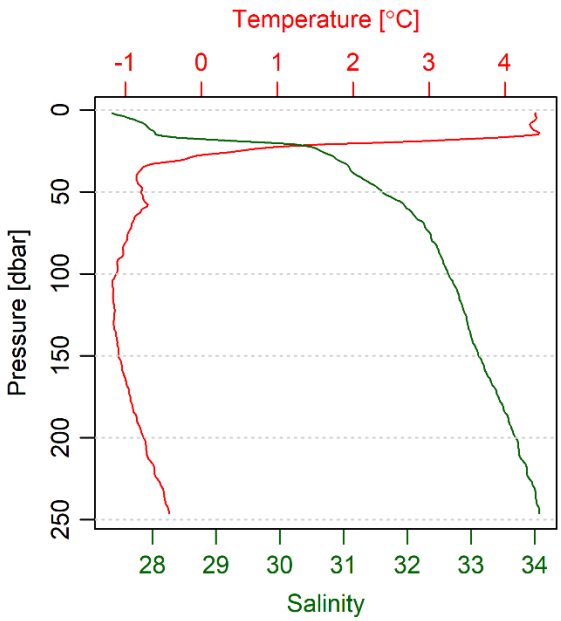
Temperature [°C]
-1
0
1
2
3
4
Pressure [dbar]
0
50
100
150
200
250
28
29
30
31
32
33
34
Salinity

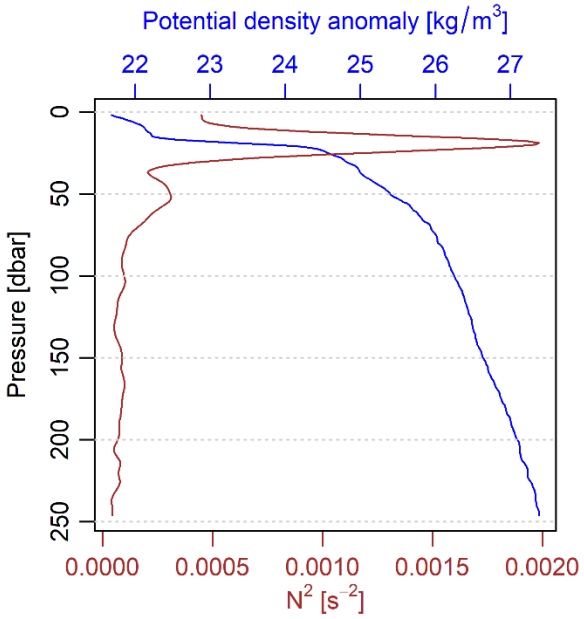
Potential density anomaly [kg/m3]
22
23
24
25
26
27
Pressure [dbar]
0
50
100
150
200
250
0.0000
0.0005
0.0010
0.0015
0.0020
N2 [s−2]

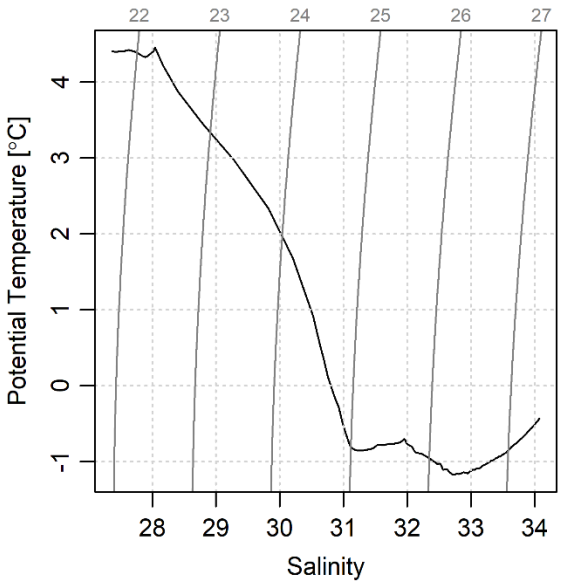
22
23
24
25
26
27
Potential Temperature [°C]
-1
0
1
2
3
4
28
29
30
31
32
33
34
Salinity

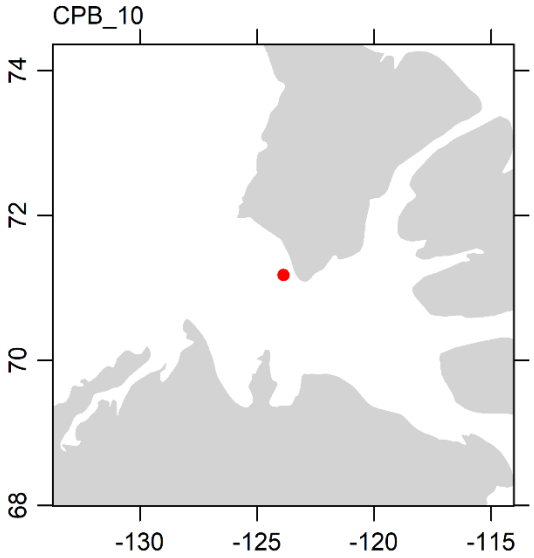
CPB_10
74
72
70
68
-130
-125
-120
-115

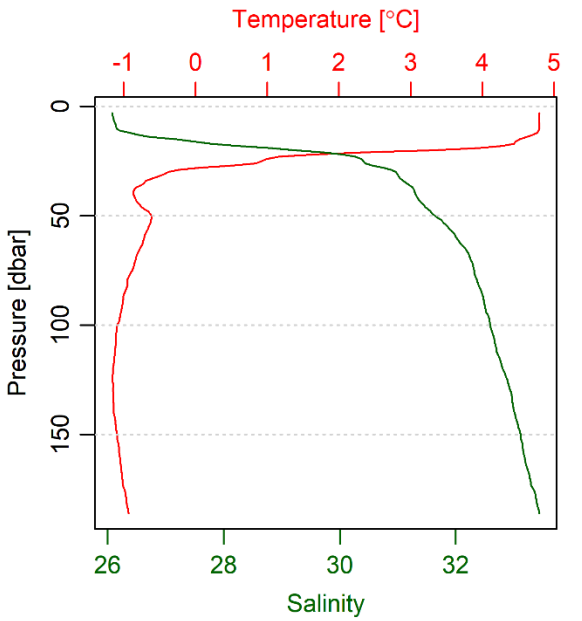
Temperature [°C]
-1
0
1
2
3
4
5
Pressure [dbar]
0
50
100
150
26
28
30
32
Salinity

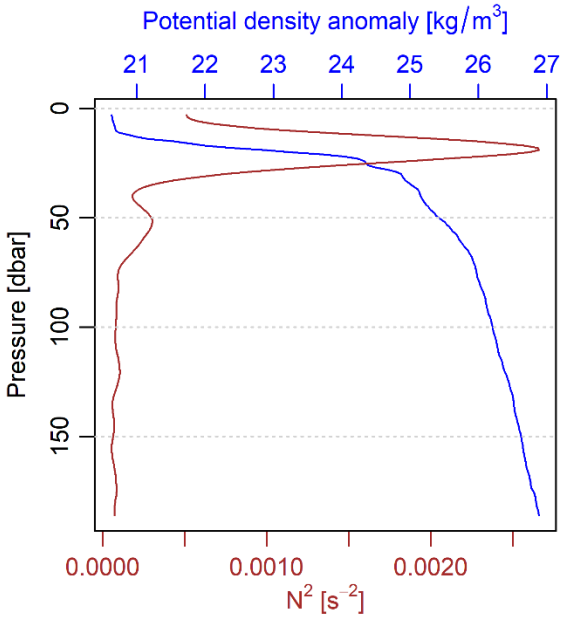
Potential density anomaly [kg/m3]
21
22
23
24
25
26
27
Pressure [dbar]
0
50
100
150
0.0000
0.0010
0.0020
N2 [s−2]

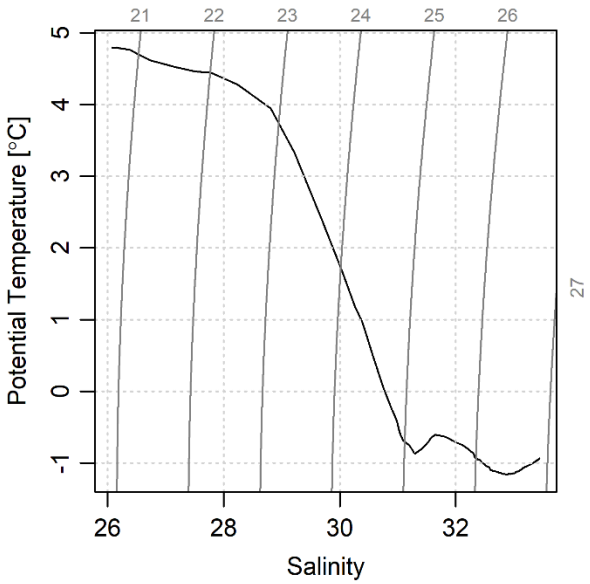
21
22
23
24
25
26
Potential Temperature [°C]
5
4
3
2
1
0
-1
27
26
28
30
32
Salinity

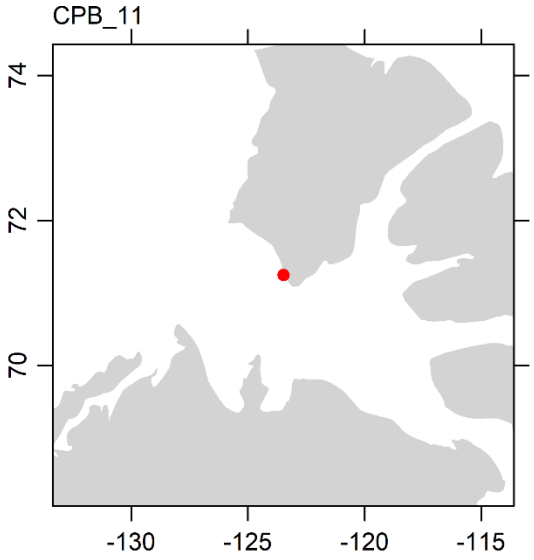
CPB_11
74
72
70
-130
-125
-120
-115

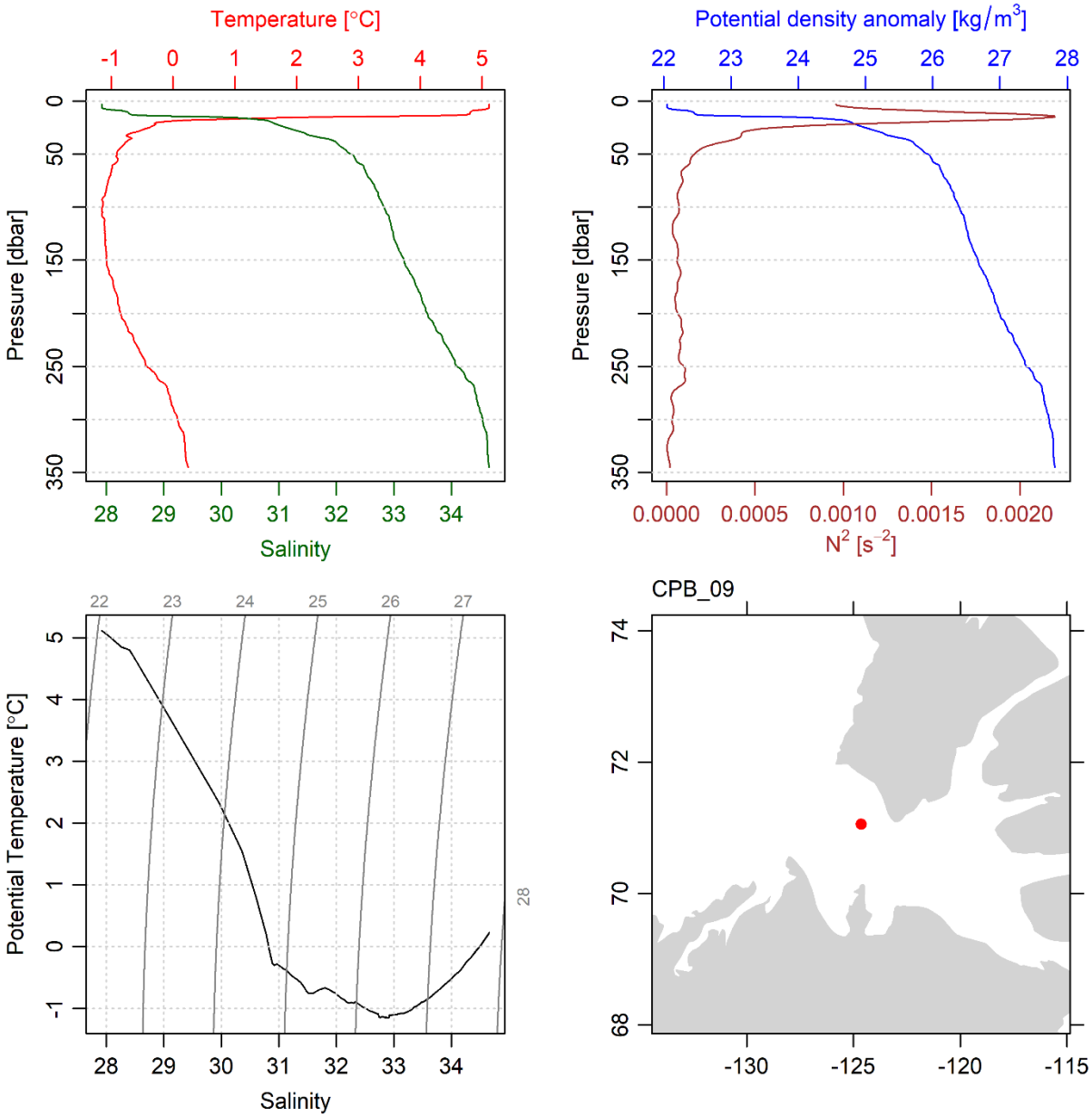
Temperature [°C]
-1 0 1 2 3 4 5
Pressure [dbar]
0 50 150 250 350
28 29 30 31 32 33 34
Salinity
Potential density anomaly [kg/m3]
22 23 24 25 26 27 28
0.0000 0.0005 0.0010 0.0015 0.0020
N2 [s−2]
22 23 24 25 26 27
Potential Temperature [°C]
-1 0 1 2 3 4 5
28
CPB_09
74 72 70 68
-130 -125 -120 -115

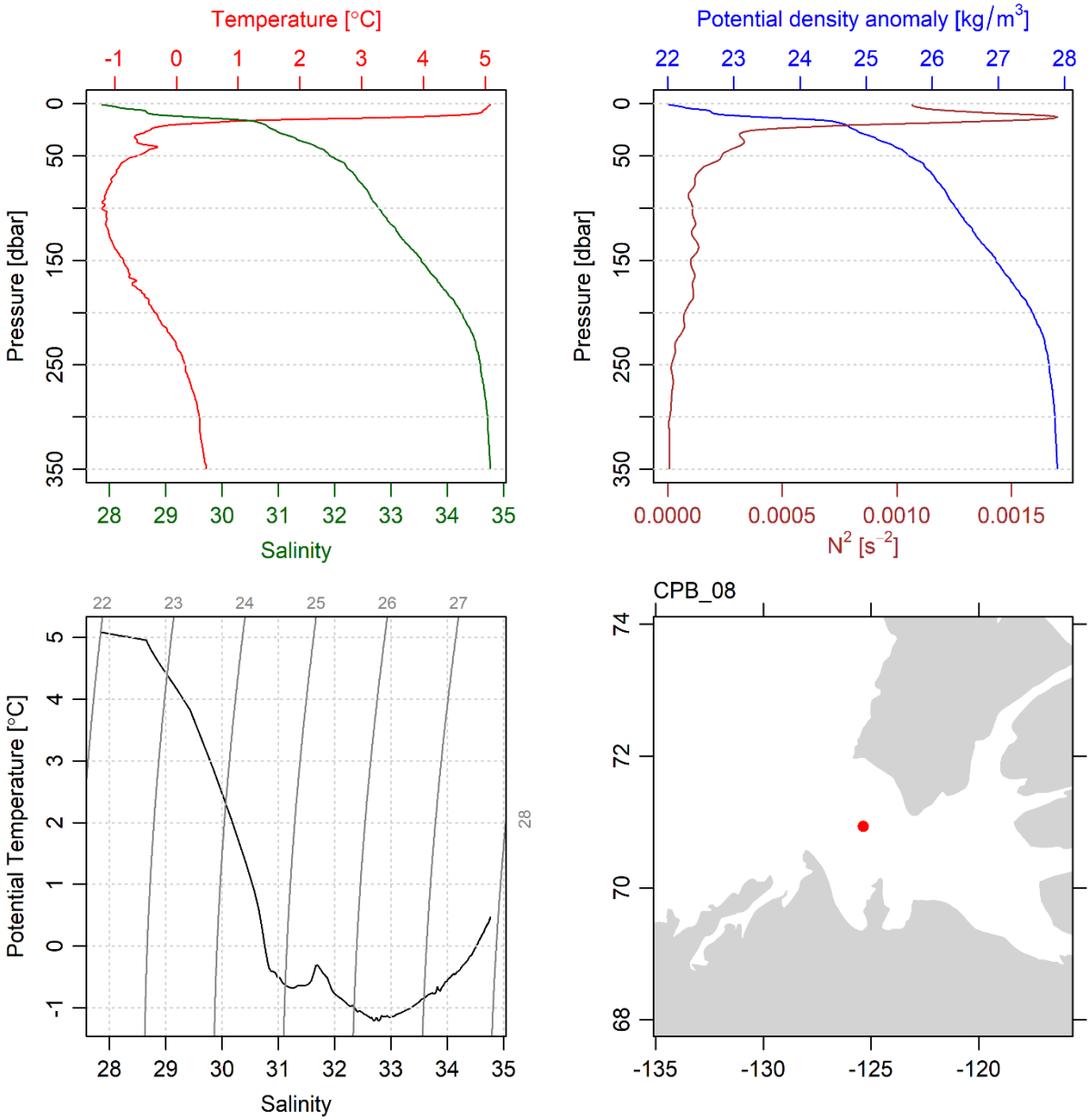
Temperature [°C]
-1 0 1 2 3 4 5
Pressure [dbar]
0 50 150 250 350
28 29 30 31 32 33 34 35
Salinity
Potential density anomaly [kg/m3]
22 23 24 25 26 27 28
0.0000 0.0005 0.0010 0.0015
N2 [s−2]
22 23 24 25 26 27
Potential Temperature [°C]
-1 0 1 2 3 4 5
28
CPB_08
74 72 70 68
-135 -130 -125 -120

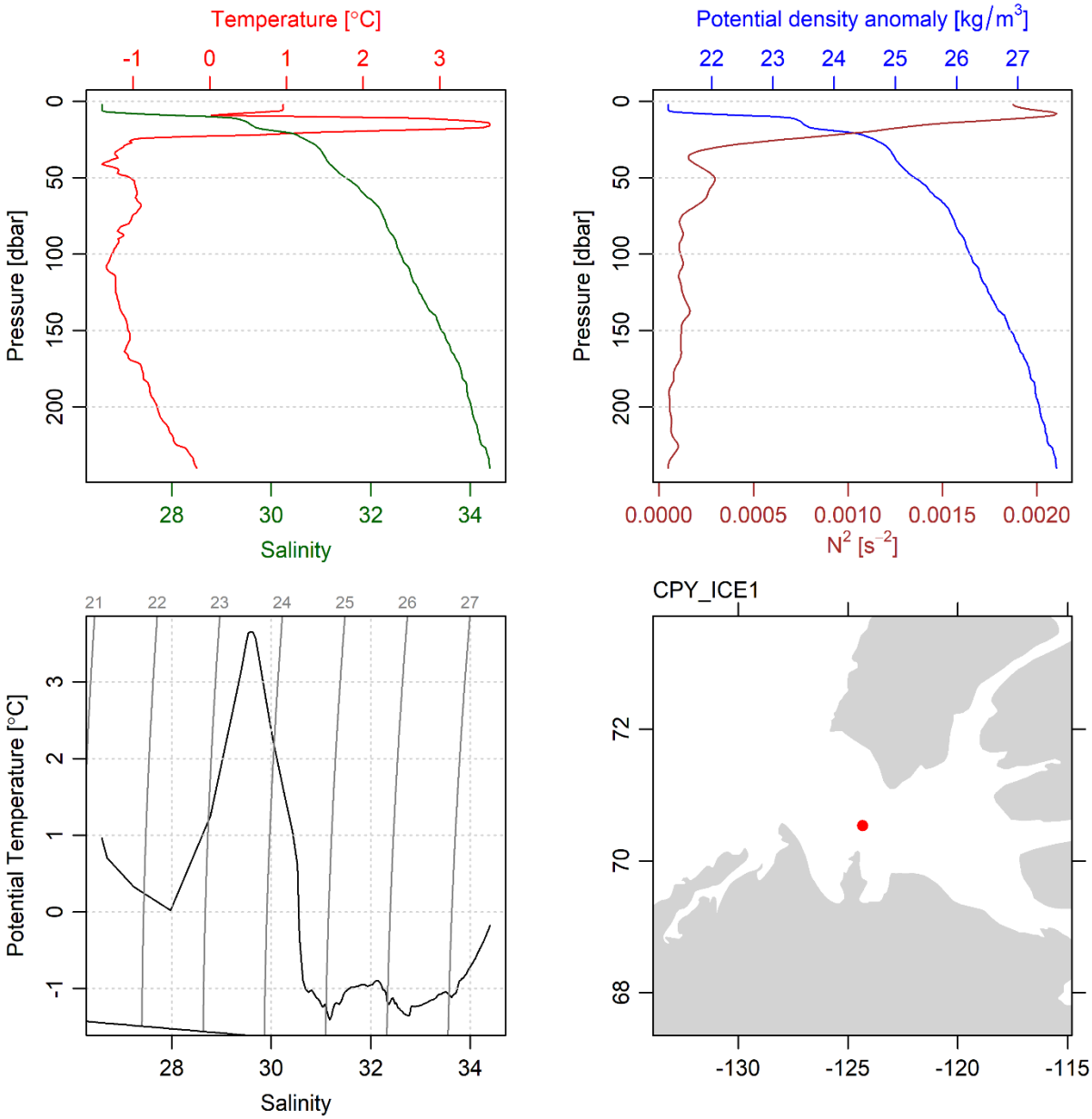
Temperature [°C]
-1
0
1
2
3
Pressure [dbar]
0
50
100
150
200
28
30
32
34
Salinity
Potential density anomaly [kg/m3]
22
23
24
25
26
27
0.0000
0.0005
0.0010
0.0015
0.0020
N2 [s−2]
Potential Temperature [°C]
21
22
23
24
25
26
27
-1
0
1
2
3
CPY_ICE1
72
70
68
-130
-125
-120
-115

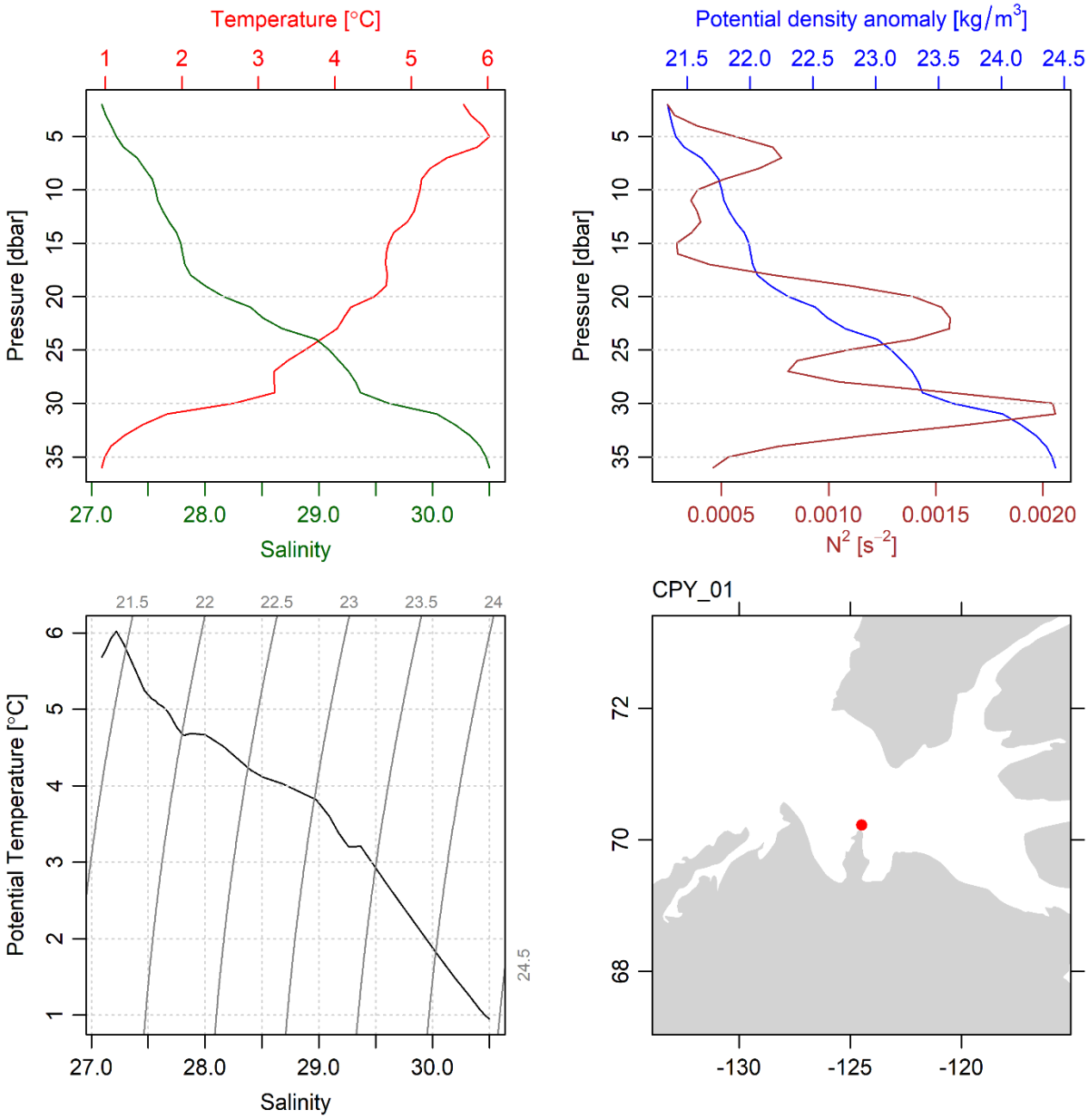
Temperature [°C]
1 2 3 4 5 6
Pressure [dbar]
5 10 15 20 25 30 35
27.0 28.0 29.0 30.0
Salinity
Potential density anomaly [kg/m3]
21.5 22.0 22.5 23.0 23.5 24.0 24.5
Pressure [dbar]
5 10 15 20 25 30 35
0.0005 0.0010 0.0015 0.0020
N2 [s−2]
21.5 22 22.5 23 23.5 24
Potential Temperature [°C]
1 2 3 4 5 6
24.5
27.0 28.0 29.0 30.0
Salinity
CPY_01
68 70 72
-130 -125 -120

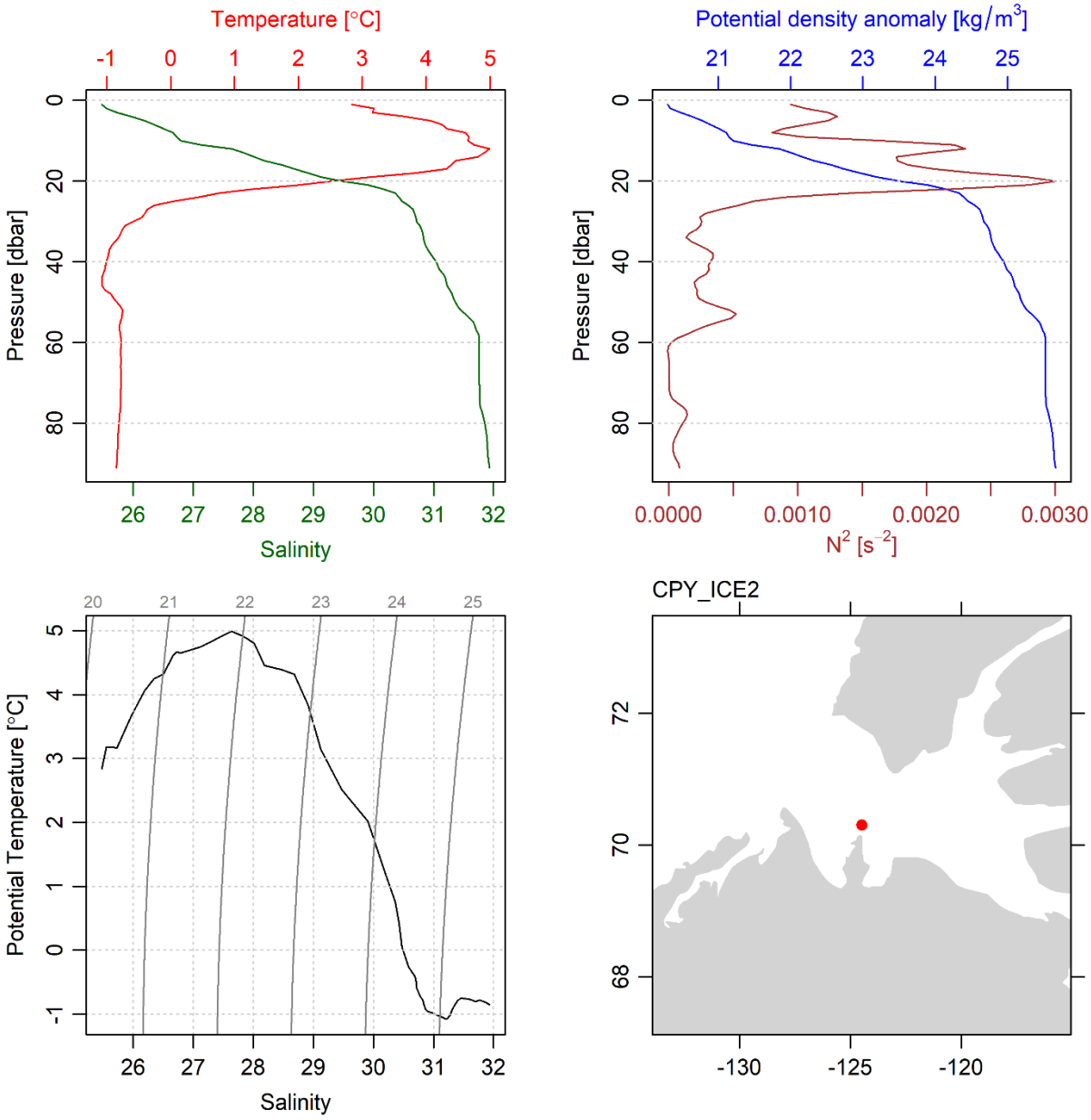
Temperature [°C]
-1 0 1 2 3 4 5
Pressure [dbar]
0 20 40 60 80
26 27 28 29 30 31 32
Salinity
Potential density anomaly [kg/m3]
21 22 23 24 25
0.0000 0.0010 0.0020 0.0030
N2 [s−2]
20 21 22 23 24 25
Potential Temperature [°C]
-1 0 1 2 3 4 5
CPY_ICE2
68 70 72
-130 -125 -120

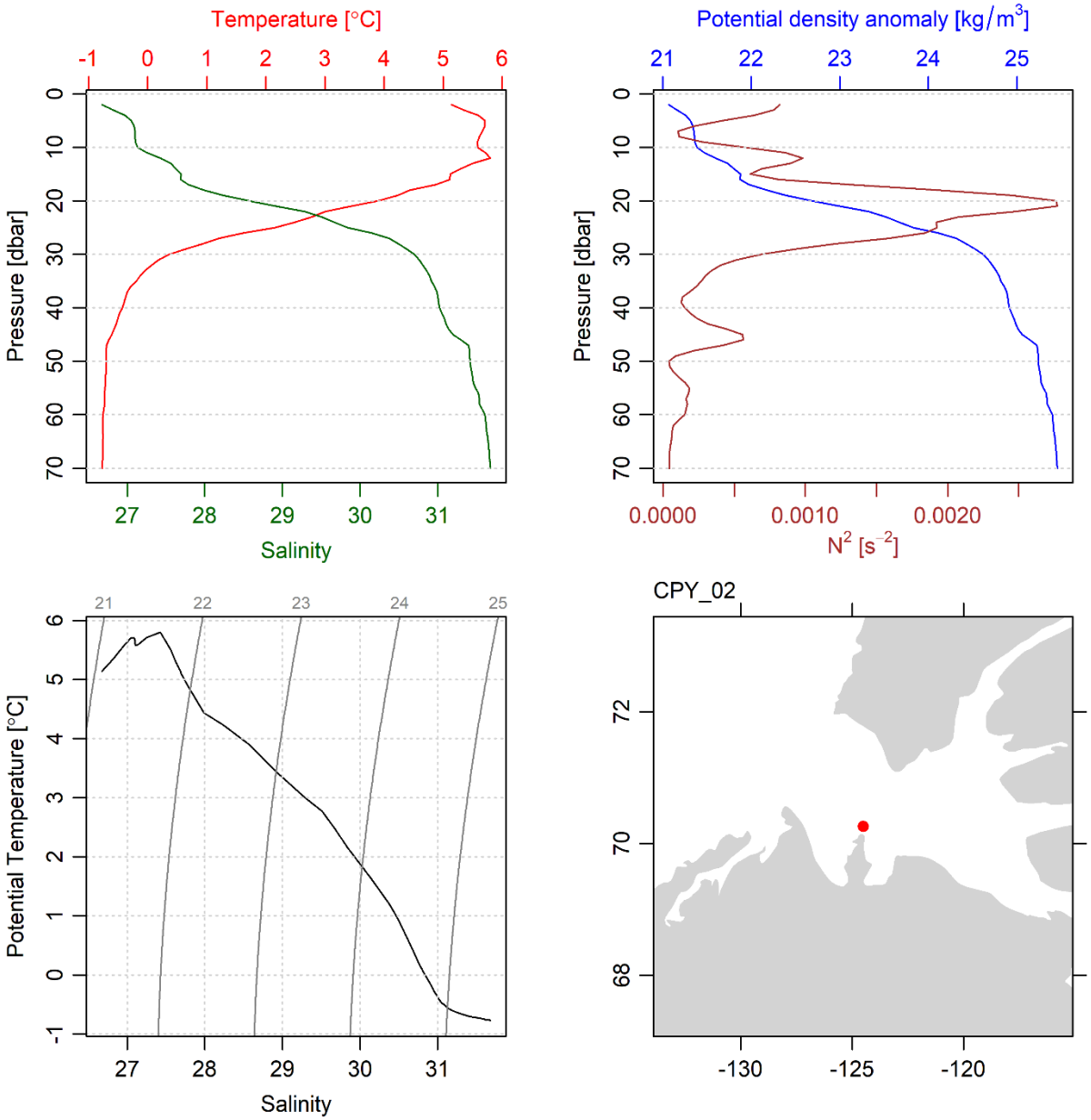
Temperature [°C]
-1 0 1 2 3 4 5 6
Pressure [dbar]
0 10 20 30 40 50 60 70
27 28 29 30 31
Salinity
Potential density anomaly [kg/m3]
21 22 23 24 25
0.0000 0.0010 0.0020
N2 [s−2]
Potential Temperature [°C]
-1 0 1 2 3 4 5 6
CPY_02
68 70 72
-130 -125 -120

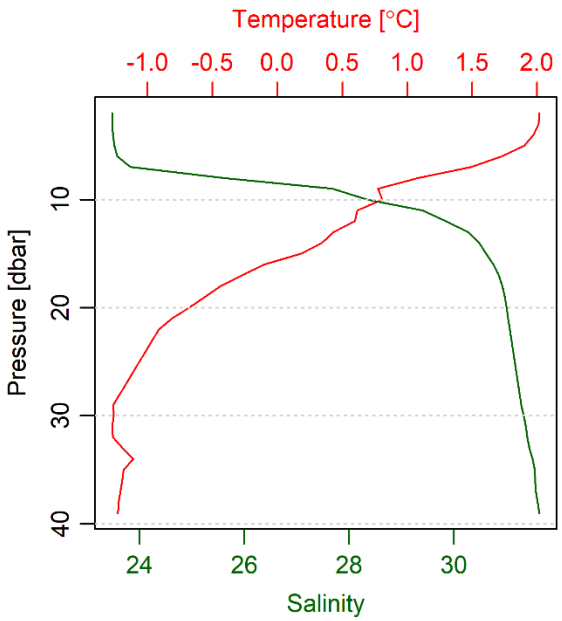
Temperature [°C]
-1.0 -0.5 0.0 0.5 1.0 1.5 2.0
Pressure [dbar]
10 20 30 40
24 26 28 30
Salinity

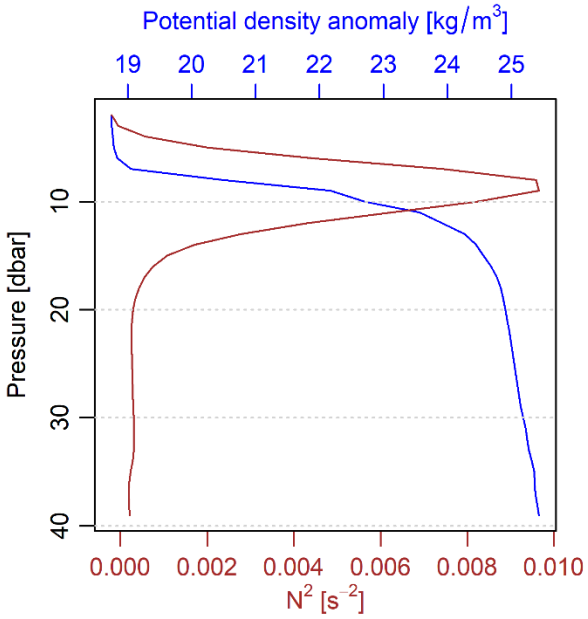
Potential density anomaly [kg/m3]
19 20 21 22 23 24 25
Pressure [dbar]
10 20 30 40
0.000 0.002 0.004 0.006 0.008 0.010
N2 [s−2]

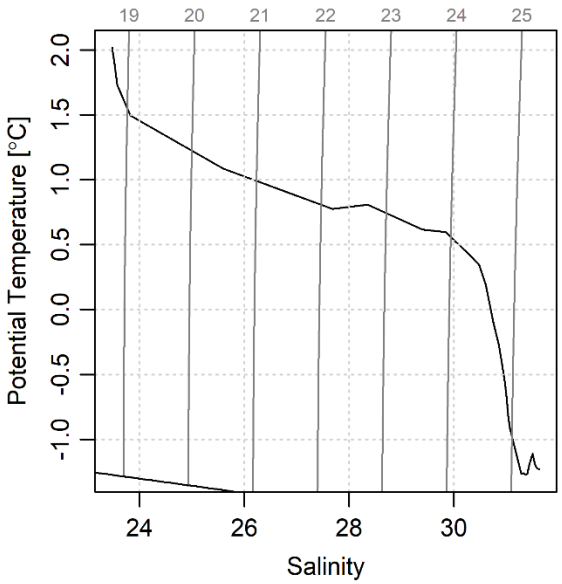
19 20 21 22 23 24 25
Potential Temperature [°C]
-1.0 -0.5 0.0 0.5 1.0 1.5 2.0
24 26 28 30
Salinity

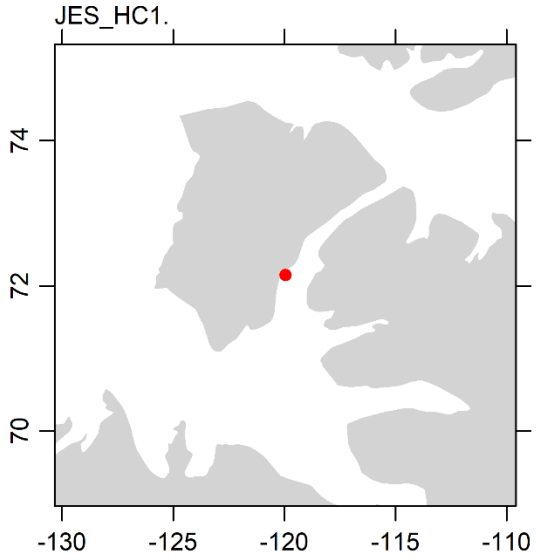
JES_HC1.
74
72
70
-130 -125 -120 -115 -110

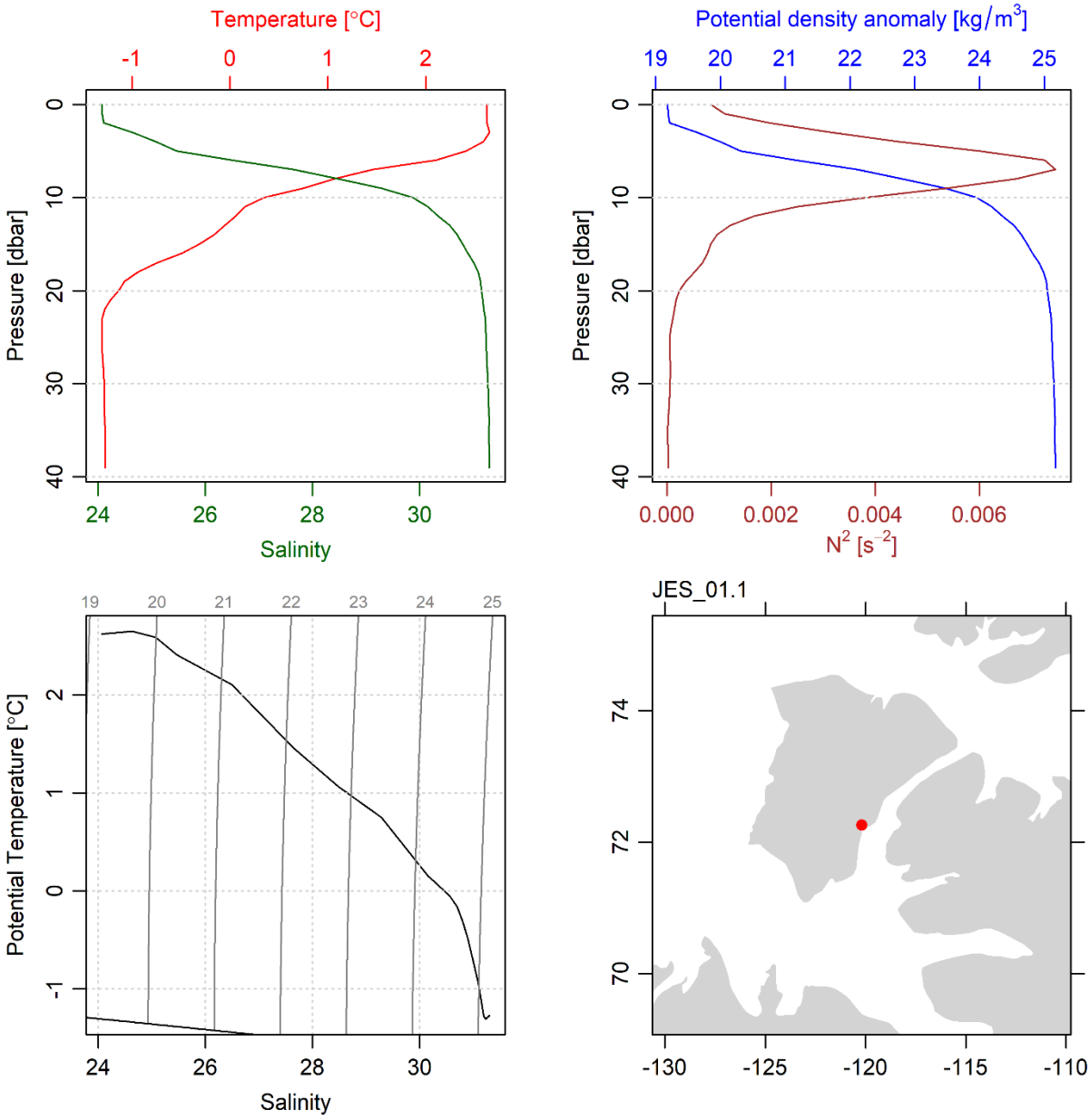
Temperature [°C]
-1
0
1
2
Pressure [dbar]
0
10
20
30
40
24
26
28
30
Salinity
Potential density anomaly [kg/m3]
19
20
21
22
23
24
25
0.000
0.002
0.004
0.006
N2 [s−2]
Potential Temperature [°C]
JES_01.1
74
72
70
-130
-125
-120
-115
-110